Johanna Breininger, BSc

# Synthesis of novel "on-off" fluorescent azaBODIPY indicators and their application in optical pH and $CO_2$ sensing materials

**MASTER'S THESIS**

to achieve the university degree of

Diplom-Ingenieurin

Master's degree programme: Technical Chemistry

submitted to

**Graz University of Technology**

Supervisor

Assoc. Prof. kand. Sergey Borisov

Institute of Analytical Chemistry and Food Chemistry

Graz, January, 2018

## Abstract

pH as well as $CO_2$ are among the most important parameters in industrial, environmental and medical monitoring. Therefore, there is an increasing demand for precise and reliable measuring devices in these fields. Optical sensors represent a promising alternative to conventional electrochemical sensors for these parameters. In this thesis the synthesis and the photophysical properties of novel pH sensitive $BF_2$-chelated tetraarylazadipyrromethene (azaBODIPY) dyes, which show suitable characteristics for indicators in pH and $CO_2$ sensors, were investigated. Moreover, their applicability for optical pH as well as $CO_2$ sensing was examined.

In contrast to most previously reported azaBODIPY dyes in pH sensors, which are based on PET (photoinduced electron transfer) as well as ICT (internal charge transfer), the dyes investigated in this thesis are purely based on PET and therefore absorption and emission wavelengths are nearly independent of pH. This facilitates the design of light harvesting systems with a pH insensitive azaBODIPY as antenna dye resulting in significant enhancement of sensor brightness. Consequently, film thicknesses can be reduced for faster response times.

The novel dyes show absorption and emission maxima in the red/NIR range (in the so-called "optical window"), excellent quantum yields and high molar absorption coefficients. These properties make the new dyes excellent candidates for pH sensors.

The $pK_a$ of the dyes was tuned by incorporation of electron donating or electron withdrawing substituents. Dyes with $pK_a$ values ranging from 7.8 to 12 were synthesized enabling applications in various fields like biology, medical applications or marine monitoring. While the dyes with low $pK_a$ are perfectly suitable for pH sensing, azaBODIPYs with such high $pK_a$ values were not reported before and are especially attractive for applications in carbon dioxide sensing via "plastic-type" $CO_2$ sensors. Fluorescence-based "on-off" $CO_2$ sensors for simple emission-based read-out were made.

New synthetic strategies for simple and versatile covalent immobilization of azaBODIPYs on polymer matrices were developed and investigated towards their applicability in sensors. Covalent coupling between the dye and the matrix was achieved by activation with $BCl_3$. In the future this method may not only enable covalent immobilization, but also various other substitution reactions on the boron center to alter the chemical and photophysical properties of the dye.

# Kurzfassung

Da pH und $CO_2$ wichtige Parameter in Industrie, Umweltanalyse und in der Medizin sind, besteht ein hoher Bedarf an präzisen und zuverlässigen Instrumenten für Messungen in diesen Bereichen. Optische Sensoren stellen eine vielversprechende Alternative für herkömmliche elektrochemische Sensoren dar. Der Fokus dieser Arbeit lag auf der Synthese und der Charakterisierung von neuen pH sensitiven $BF_2$-komplexierten tetraarylazadipyrromethene (azaBODIPY) Farbstoffen sowie deren Anwendung in optischen pH und $CO_2$ Sensoren.

Im Gegensatz zu den meisten bisher bekannten azaBODIPY Farbstoffen in pH Sensoren, welche sowohl auf PET (Photoinduced Electron Transfer) als auch auf ICT (Internal Charge Transfer) basieren, beruhen die neuen Farbstoffe ausschließlich auf dem PET-Effekt und haben daher beinahe pH-unabhängige Absorptions- und Emissionsspektren. Das ermöglicht ein einfaches Design von Light Harvesting Konzepten durch Zugabe eines pH-unempfindlichen Farbstoffes. Mit diesem Konzept konnte die Helligkeit der Sensoren signifikant erhöht werden. Dadurch können wiederum Schichtdicken verringert, und somit Ansprechzeiten der Sensoren verkürzt werden.

Die neuen Farbstoffe haben Absorptions- und Emissionsmaxima im roten/NIR Bereich (im sogenannten „optischen Fenster“), haben hervorragende Quantenausbeuten und hohe molare Absorptionskoeffizienten, wodurch sie bestens als Indikatoren in pH Sensoren geeignet sind.

Der $pK_a$ der Farbstoffe wurde durch elektronenziehende oder elektronendrückende Substituenten verändert. Farbstoffe mit $pK_a$ Werten zwischen 7,8 und 12 wurden hergestellt, wodurch Nutzungen in verschiedensten Anwendungsbereichen wie zum Beispiel in der Biologie, in der Medizin oder in Messungen von Meerwasser ermöglicht werden. Einerseits eignen sich die Farbstoffe mit niedrigem $pK_a$ hervorragend für pH Messungen, andererseits stellen die Farbstoffe mit hohem $pK_a$ vielversprechende Indikatoren für Kohlenstoffdioxid-Messungen in „plastic type“ $CO_2$ Sensoren dar. Ein unkompliziertes read-out wird durch den einfachen „On-Off“ Mechanismus der Fluoreszenz ermöglicht.

Für eine kovalente Immobilisierung der azaBODIPY Farbstoffe in Polymermatrizen wurden neue Synthesewege mit $BCl_3$ entwickelt. In der Zukunft könnte diese Methode nicht nur für die kovalente Bindung der Farbstoffe an Matrixmaterialien genutzt werden, sondern auch für unterschiedlichste Substitutionsreaktionen am Bor-Zentrum der Farbstoffe, um somit deren chemischen und photophysikalischen Eigenschaften zu verbessern.

**EIDESSTATTLICHE ERKLÄRUNG**

Ich erkläre an Eides statt, dass ich die vorliegende Arbeit selbstständig verfasst, andere als die angegebenen Quellen/Hilfsmittel nicht benutzt, und die den benutzten Quellen wörtlich und inhaltlich entnommenen Stellen als solche kenntlich gemacht habe. Das in TUGRAZonline hochgeladene Textdokument ist mit der vorliegenden Masterarbeit identisch.

**AFFIDAVIT**

I declare that I have authored this thesis independently, that I have not used other than the declared sources/resources, and that I have explicitly indicated all material which has been quoted either literally or by content from the sources used. The text document uploaded to TUGRAZonline is identical to the present master‘s thesis.

| Datum/Date | Unterschrift/Signature |
|---|---|

## Danksagung

An dieser Stelle möchte ich einen herzlichen Dank an all jene Menschen aussprechen, die mich im Laufe meines Studiums und während des Verfassens meiner Masterarbeit begleitet und unterstütz haben.

Danke, Ingo Klimant, für die Möglichkeit meine Masterarbeit in einer so tollen Arbeitsgruppe verfassen zu können. Danke auch für die vielen wertvollen Inputs, Ideen und Ratschläge.

Ein großer Dank gilt auch Sergey Borisov für die großartige Betreuung meiner Masterarbeit und die Unterstützung mit Ratschlägen, Ideen und Anregungen während meiner Arbeit.

Danke, Christoph, für deine unglaubliche Geduld und Hilfsbereitschaft, die du als Betreuer meiner Masterarbeit für mich aufgebracht hast. Danke, dass du dein Wissen mit mir geteilt hast und mir stets mit Rat und Tat zur Seite gestanden bist.

Außerdem möchte ich mich bei der gesamte ACFC Arbeitsgruppe bedanken. Durch das gute und freundliche Arbeitsklima hier am Institut wurden selbst die anstrengendsten Momente während der Masterarbeit zum Positiven gewendet. Es ist wunderschön in einer so freundlichen und wertschätzenden Gesellschaft Zeit zu verbringen.

Meinen Freunden und Freundinnen danke ich sehr für die schönen und unvergesslichen Momente in den letzten Jahren. Besonders möchte ich den $A^6$ Mädels für ihre lange und tiefe Freundschaft und für ihre motivierenden Worte und ihren Zuspruch während des Verfassens der Arbeit danken.

Und schließlich möchte ich mich herzlich bei meiner Familie, insbesondere bei meinen Eltern Helga und Walter, bedanken, die mir dieses Studium ermöglicht haben. Danke, dass ihr stets an mich glaubt, mich auf meinem Weg begleitet und mich in allen Entscheidungen meines Lebens unterstützt.

Johanna Breininger, BSc Graz, January, 2018

# Contents

# 1 Introduction

pH is an important parameter in many aspects of our life. pH monitoring in industrial processes, biomedical research, in health care or environmental monitoring are just a few examples to illustrate the importance of pH sensing. In most applications conventionally glass electrodes are used to monitor pH, but also recently established optical pH sensors have become an increasingly important tool due to several advantages over other conventional electrochemical devices: optical sensors have a high sensitivity within their dynamic range, they are not prone to electrochemical interferences, they allow for contactless measurement, possibilities of miniaturization and remote measurements in combination with fiber-optics. [1]

azaBODIPYs modified with PET (photoinduced electron transfer) groups are promising dyes for optical pH sensors and were numerously reported. [2–4] Previously reported azaBODIPYs carry a pH sensitive hydroxy group in para-position on a phenyl ring, which leads to incorporation of the hydroxy group into the $\pi$-system of the dye's core and consequently to pH dependent PET- and ICT-quenching. [5, 6] OH-substitution in meta-position however, does not connect the hydroxy group to the conjugated $\pi$-system, resulting in indicators purely base on PET-quenching. Thus, the new azaBODIPY dyes with m-OH substitution show a pH independent absorption and emission spectrum, whereas the intensity of emission spectra is pH dependent due to PET-quenching in the deprotonated state. Due to absorption and emission in the far-red/near infrared range of the light, high molar absorption coefficients, good quantum yields and excellent chemical stability and photostability azaBODIPY dyes are promising indicators for pH sensors. [3] The $pK_a$ of the dyes can be tuned by incorporation of electron donating or electron withdrawing substituents enabling applications in various fields. [2, 5]

While azaBODIPYs with $pK_a$ in the neutral to slightly basic pH range are suitable for pH sensors in marine monitoring, in biological or in medical applications, azaBOIDPYs with high $pK_a$ values are promising indicators in "plastic type" carbon dioxide sensors. In combination with a tetraoctylammonium hydroxide base $TOA^+OH^-$ the dye gets protonated in the presence of $CO_2$ which is in equilibrium with bicarbonate and carbonate ions. [7] Carbon dioxide sensors for applications in food packaging, medicine or environmental monitoring can be made with this approach.

Within the scope of this thesis a set of five novel indicator dyes with different electron donating and electron withdrawing substituents were synthesized, characterized and their applicability in pH as well as in carbon dioxide sensors for various pH and $CO_2$ ranges was examined. A pH insensitive azaBODIPY dye was used as an antenna dye (donor dye) in a light harvesting approach. Covalent immobilization of the dye in a polymer matrix (a copolymer consisting of polyacryloylmorpholine and polyhydroxyethyl acrylamide as well as cellulose acetate propionate) was achieved by formation of a B-O bond on the boron-center of the dye via activation with boron trichloride.

# 2 Theoretical Background

## 2.1 What is luminescence?

This chapter and the following subchapters are based on references [8] and [9]. Other references will be cited separately.

Luminescence is the emission of photons with energy in the ultraviolet, visible or infrared region of the light. The emission of a photon takes place after electronic excitation of the substance i.e. the excitation of an electron into an electronically higher state. Different types of luminescence can be categorized according to their mode of excitation (e.g. photoluminescence after absorption of a photon, electroluminescence by excitation in an electric field or chemoluminescence after a chemical process), however only photoluminescence will be considered in this thesis. De-excitation, i.e. the relaxation of the excited species back into the electronic ground state, can take place via emission of light, resulting in fluorescence or phosphorescence, but also via various other non-radiative processes (figure 2.1).

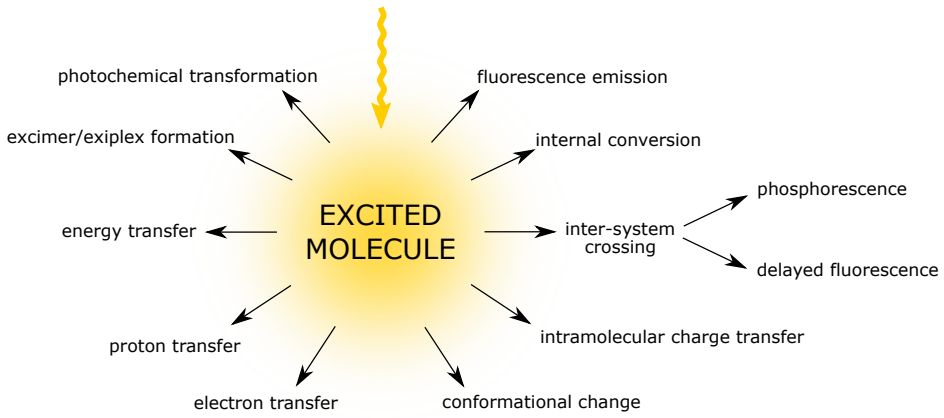


**Figure 2.1:** Possible relaxation processes of an excited species

## 2.2 Absorption of light

In photoluminescence, excitation of an electron from the ground state to an unoccupied orbital of higher energy is induced by absorption of a photon. Possible transitions of electrons between orbitals upon absorption of light to reach an excited states are shown in figure 2.2.

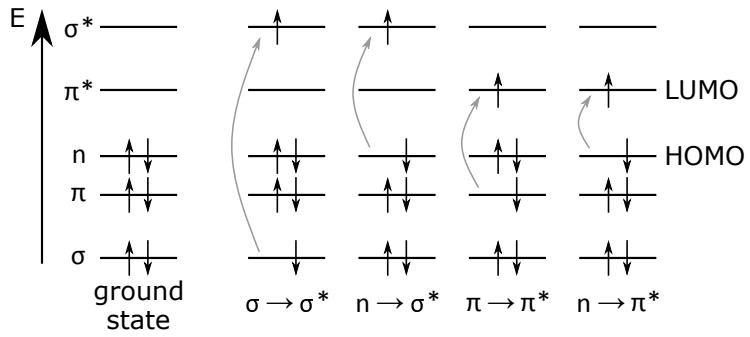


**Figure 2.2:** Possible transitions of electrons in a molecule to reach the excited state

A common transition is the excitation from HOMO (highest occupied molecular orbital) to LUMO (lowest unoccupied molecular orbital), which requires the least amount of energy. However, also other transitions are possible. The energies required for these transitions are of following order:

$$n \to \pi^* < \pi \to \pi^* < n \to \sigma^* < \sigma \to \pi^* < \sigma \to \sigma^*$$

In general, the spin of an excited electron remains unchanged during the transition from one molecular orbital to another (i.e. the total spin quantum number of the molecule $S = \sum s_i$, with $s_i = +\frac{1}{2}$ or $-\frac{1}{2}$ remains unchanged). Therefore, the multiplicity ($M = 2S + 1$) of ground state and excited state is 1. The excited state is called *singlet state* and the transition is a singlet-singlet transition. However, also transitions during which an electron changes its spin orientation are possible, resulting in a state of two unpaired electrons with parallel spin. The total spin quantum number is 1 and the multiplicity 3, therefore the excited state is called *triplet state*. Such transitions are spin forbidden, however, they occur due to "spin-orbit coupling".

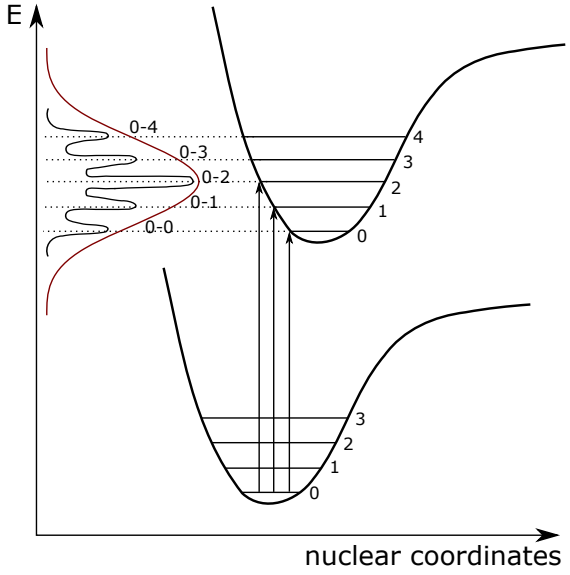


**Figure 2.3:** Franck-Condon principle

According to the *Franck-Condon* principle based on the *Born-Oppenheimer* approximation, the motional components of the nucleus and the electrons of a molecule can be considered as independent from each other. The motions of the electrons are much faster than those of the nuclei which means that electron transitions from one molecular orbital to another can be assumed to take place without change of the position of the nucleus. The transitions can be illustrated by use of Morse-like potential energy functions of the ground state $S_0$ and excited singlet state $S_1$. As shown in figure 2.3, the transitions in a diatomic molecule (with a shift representing the distance between the two nuclei) can be drawn as vertical lines between electronic level to reach the so called *Franck-Condon state* by a *vertical transition*.

Each electronic state has a set of sublevels representing the vibrational states, as showed in figure 2.3. Transitions take place between the various sublevels, resulting in a broadening of the absorption band. The maximum in the absorption spectrum is formed by an electronic transition from one electronic state to a vibrational level of higher state, which takes place with the highest probability. The rest of the shape of a spectrum is defined by transitions to other vibrational levels. The shape of the absorption band therefore depends of the shapes and positions of the involved potential energy curves as well as on the involved vibrational levels. Each transition is defined by the energy gap between the starting and the final energy level, which is described by $E = h\nu = hc/\lambda$ ($h$ is the Planck constant, $\nu$ th frequency, $c$ the speed of light and $\lambda$ the wavelength). Due to the contribution of the vibrational levels the absorption as well as the emission spectra do not consist of discrete lines, but of absorption and emission bands. [10]

The absorbance $A_\lambda$ can be described as the efficiency of absorption of light at a certain wavelength $\lambda$ by an absorbing medium, and is expressed by Lambert-Beer law:

$$A_\lambda = log\frac{I_\lambda^0}{I_\lambda} = \varepsilon_\lambda \cdot l \cdot c \tag{2.1}$$

where $I_\lambda^0$ is the intensity of the light entering the absorbing medium, $I_\lambda^0$ the intensity of the light leaving the medium, $\varepsilon_\lambda$ is the molar absorption coefficient in $L \cdot mol^{-1} \cdot cm^{-1}$, c the concentration of the medium in $mol \cdot L^{-1}$ and l is the thickness of the medium (typically cuvettes with 1 cm path length are used in absorption spectroscopy). The molar absorption coefficient $\varepsilon$ is usually calculated at the maximum of the absorption band $\lambda_{max}$. However, it is important to note, that the linear relationship between the absorbance and the concentration of a absorbing solution is only applicable for dilute solutions. At higher concentrations the actual absorbance could deviate from this linear relationship due to e.g. formation of aggregates.

## 2.3 The Perrin-Jablonski diagram

After absorption of light by a molecule and excitation to a higher electronic state (absorption takes place within a time span of about $10^{-15}$ s), the chromophore can return back to the

ground state by various intrinsic relaxation pathways under emission of energy (only intrinsic de-excitation process in absence of quenching substances are considered at this point). These pathways can be of radiative or non-radiative nature and can schematically be described in a *Perrin-Jablonski* diagram (figure 2.4). $S_0$, $S_1$ and $S_2$ are the singlet ground state, the first and the second singlet state, respectively, $T_1$ is the first triplet state. Each electronic state consists of various vibrational sublevels with different energies. Transitions between the energy levels are described by vertical lines.

As described above, absorption of a light (photon) induces excitation of an electron from the lowest vibrational level of the singlet ground state $S_0$, which is populated by most of the electrons at room temperature, to a vibrational state belonging to a singlet state of higher energy $S_n$. De-excitation can take place by radiative or non-radiative processes, which compete all with each other. The stronger the competing losses by non-radiative processes, the lower is the emission by fluorescence or phosphorescence. [10]

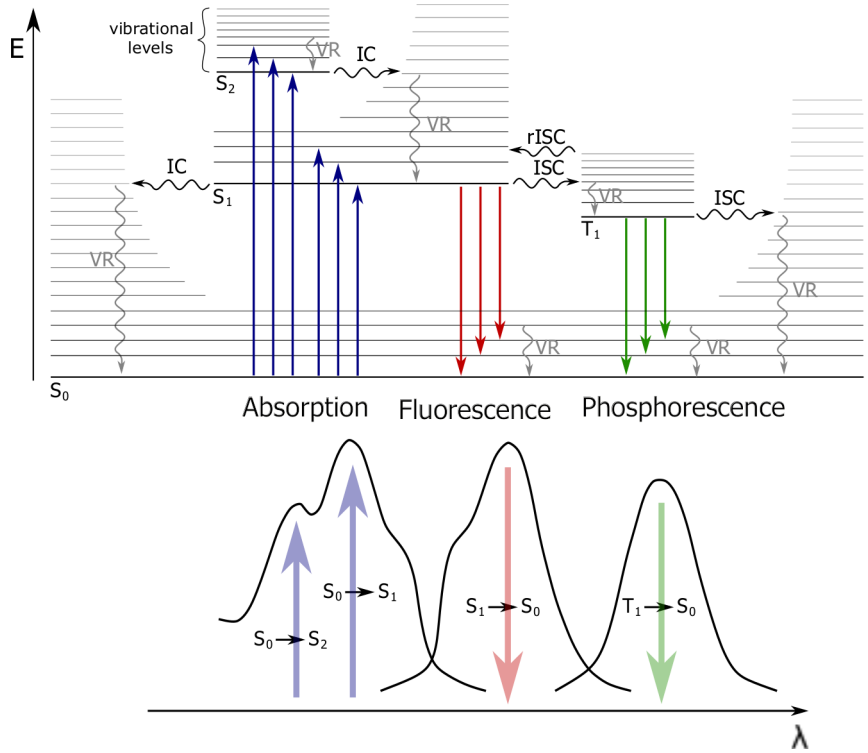


**Figure 2.4:** Perrin-Jablonski diagram

### 2.3.1 Possible intrinsic relaxation pathways

- After a molecule reached a vibrational level of a singlet state higher than 1 ($S_n, n > 1$), it quickly relaxes to the lowest vibrational level of $S_n$ and subsequently to the lowest vibrational level of the first excited state $S_1$ This pathway is called **internal conversion** and takes place in a time span of $10^{-13}$ s - $10^{-11}$ s. From there, fluorescence or other

relaxation processes can take place to reach the ground state $S_0$ (Kasha's rule). Internal conversion only takes place between electronic state with the same spin multiplicity (more precisely only between $S_2 \rightarrow S_1$, $S_1 \rightarrow S_0$ or $T_2 \rightarrow T_1$, but never between $S_1 \rightarrow T_1$).

- Relaxation from a vibrational level of $S_1$ to one of $S_0$ accompanied by emission of photons is called **fluorescence**. Internal conversion from $S_1$ to $S_0$ can take place as well, however the energy gap between the two levels is quite large, so this transition is hampered and fluorescence is favored over internal conversion. Therefore, fluorescence with a shorter lifetime ($10^{-10}$ - $10^{-7}$ s) can compete with the internal conversion relaxation from $S_1$ to $S_0$.

  An important characteristic of emission spectra is that they are often a mirror image of the absorption spectrum ("mirror image rule"). This can be explained by the fact that the energy gaps between the vibrational levels of the excited state $S_1$ and the ground state $S_0$ are similarly distributed. Absorption generally takes place from the lowest vibrational level of $S_0$ to a higher vibrational level of $S_1$, followed by vibrational relaxation. Vice versa, emission usually takes place from the lowest vibrational level of $S_1$ to a higher vibrational level of $S_0$ and subsequent vibrational relaxation. Therefore, emission spectra are shifted to higher wavelengths (lower energy) because energy is 'lost' to the environment during the vibrational relaxation in the excited $S_1$ and in the ground state. [11]

- Besides fluorescence, an alternative de-excitation pathway from $S_1$ is **inter-system crossing**, a transition between states with different spin multiplicities accompanied by spin reorientation (e.g. a transition from a vibrational level of $S_1$ to a vibrational level of the triplet state $T_1$ with the same energy). Even though these transitions are spin-forbidden, they can occur if spin-orbit coupling in the molecules is large enough to promote this transition. In some cases, if the energy gap is small enough and if the lifetime of $T_1$ is long enough, a transition back to the singlet state is also possible (**reverse inter-system crossing**).

- Return to the singlet ground state from a triplet state is called **phosphorescence**. Usually, phosphorescence has lower energy (longer wavelength) than fluorescence because $T_1$ is an energetically lower state than $S_1$. Because this transition is spin-forbidden (change of the spin multiplicity) emission of phosphorescent light takes much longer ($10^{-6}$ - 1 s) than fluorescence and therefore mostly relaxation by inter-system crossing and vibrational relaxation is favored.

- As described above, transition back to the $S_1$ from $T_1$ state is possible in some cases. From there, **delayed fluorescence**, emission at same energy as usual fluorescence takes place. However, the decay time of delayed fluorescence is longer than for normal fluorescence.

### 2.3.2 Characteristics of fluorescence emission

#### Stokes Shift

The fluorescence emission band is generally shifted to longer wavelength (lower energy) compared to the absorption band. This energy difference is called the Stokes Shift. It is defied as the energy gap between the maximum of the emission spectrum and the maximum of the first absorption band and is expressed in wavenumbers ($\Delta\bar{\nu} = \bar{\nu_a} - \bar{\nu_f}$). The Stokes Shift originates from the electrons being excited to higher vibrational levels of the $S_1$ state from where they rapidly relax to the lowest $S_1$ vibrational level associated with loss in energy. Additionally, during fluorescence emission electrons relax to various vibrational levels of $S_0$, which is again accompanied with energy loss. Other effects like energy transfer in the excited state, solvent effects or complex formation can influence the Stokes Shift.

#### Lifetime

A molecule stays in the excited state for a certain time, before it returns back to the ground state. This time, the fluorescence lifetime $\tau$, is the average time the species remains in the excited state. For deactivation from $S_1$, each process in the Jablonski diagram (2.4) can be depicted with a rate constant k, with $k_r^S$ representing the rate constant for radiative deactivation from $S_1$ by emission of fluorescent light, $k_{ic}^S$ representing the rate constant for internal conversion and $k_{isc}^S$ representing the rate constant of inter-system crossing to $T_1$. $k_{ic}^S$ and $k_{isc}^S$ can be combined to the rate constant for non-radiative de-excitation $k_{nr}^S$. Deactivation of a species A after promotion to the $S_1$ excited state can be described by the lifetime $\tau_S$ as the inverse of the sum of all de-excitation processes in the following way (note that only intrinsic de-excitation pathways will be considered in this section):

$$\tau_S = \frac{1}{k_r^S + k_{nr}^S} = \frac{1}{k_r^S + k_{isc}^S + k_{ic}^S} \tag{2.2}$$

$$-\frac{d[A^*]}{dt} = (k_r^S + k_{nr}^S)[A^*] \tag{2.3}$$

Integration and combination with equation 2.2 leads to equation 2.4, which describes the exponential decay back to the initial state after a light pulse:

$$[A^*] = [A^*]_0 \cdot exp(-\frac{t}{\tau_S}) \tag{2.4}$$

Or described with the fluorescence intensity $I_F$, which is decreasing mono exponentially after excitation with a pulsed light:

$$I_F(t) = I_{F,0} \cdot exp(-\frac{t}{\tau_F}) \tag{2.5}$$

The lifetime of a fluorophore can be measured by using time-resolved fluorimetry. Therefore, pulse fluorometry and phase-modulated fluorometry will be shortly described here.

### Time-resolved fluorometry

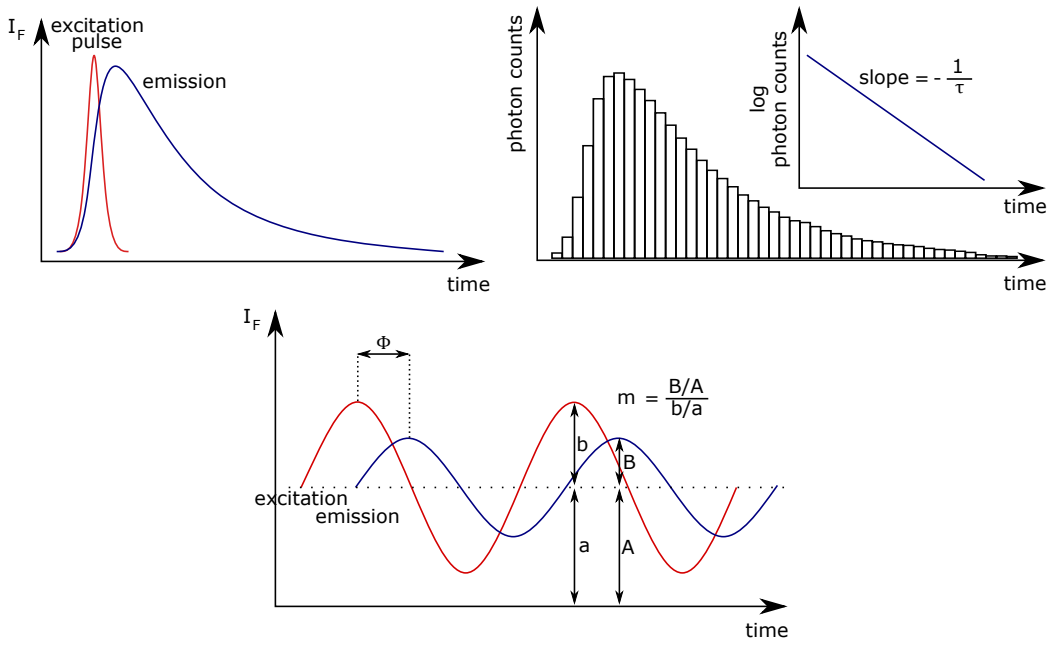


**Figure 2.5:** Principles of pulse fluorometry with time-correlated single photon counting (TCSPC) (top) and phase-modulated fluorometry (bottom)

In **pulse fluorometry** (or time-domain measurement) (figure 2.5, top) the fluorophore is excited with a short pulse of light, which should be shorter than the decay time of the excited species. The response of the fluorophore to this pulse, a (mostly) mono exponential decay, is recorded in the time-domain. One method for this type of lifetime measurements is time-correlated single photon counting (TCSPC). The detector settings are adjusted in a way, that only one emitted photon is detected following each excitation pulse. The time between the excitation pulse and the detection of the photon is recorded. Pile up of the recorded photons after each pulse can be shown in a cumulative histogram (time at which the photon is detected after the pulse vs. number of detected photons), which has a mono exponential decay. The lifetime can be calculated from the obtained data by least squares fit method.

In **phase-modulated fluorometry** (or frequency-domain measurement) (figure 2.5, bottom) the fluorophore is excited with an intensity-modulated light with sinusoidally modulated frequency. The response of the sample is a delayed sinusoidal signal with same frequency, but with a shifted phase (measured as the phase angle $\phi$) and an amplitude change (expressed as the modulation ratio $m = \frac{B/A}{b/a}$), which are both related to the modulation frequency $\omega$ and the decay time $\tau$. [12]

### Quantum yield

The fluorescence quantum yield $\Phi_F$ can be described as the ratio of photons emitted by an excited species to the number of photons absorbed. In other words, the fluorescence quantum yield is the efficiency to convert absorbed light into emitted light. Fluorescence competes with many other non-radiative de-excitation processes with the rate constant $k_{nr}$, which lower the quantum yield of a compound according to:

$$\Phi_F = \frac{emitted\,photons}{absorbed\,photons} = \frac{k_r^S}{k_r^S + k_{nr}^S} = k_r^S \tau_S \tag{2.6}$$

The product of the quantum yield and the molar absorption coefficient at the excitation wavelength yields the brightness B of a fluorophore ($B = \Phi_F \cdot \varepsilon(\lambda_{exc})$).

The quantum yield can be determined either by a relative method by comparison to a standard with known quantum yield or by an absolute method using an integrating sphere set-up. In the relative method a standard with spectral properties similar to the ones of the investigated sample has to be selected. Dilute solutions of the standard and the unknown compound are excited at the same wavelength. Absorption of the solutions at excitation wavelength should be smaller than 0.05 to avoid errors by inner filter effect. The quantum yield of the unknown dye $\Phi_f$ can be calculated according to equation 2.7.

$$\Phi_{f,x} = \Phi_{f,st} \cdot \frac{f_{st}}{f_x} \cdot \frac{F_x}{F_{st}} \cdot \frac{n_x^2}{n_{st}^2} \tag{2.7}$$

where $f$ is the absorption factor given by $1 - 10^{-A_{(\lambda_{exc})}}$, $F$ is the integrated area of the corrected emission spectrum and $n$ is the refractive index of the solvent. The indices $x$ and $st$ denote the sample $x$ and the standard, respectively. [13, 14]

For the absolute method an integrating sphere set-up is used, which allows detection of all absorbed photons and emitted photons of the sample. [13]

## 2.3.3 Fluorescence quenching

In the previous chapters only luminophores and their intrinsic properties were described (e.g. without influence of any intermolecular interactions). However, fluorescence emission can be influenced by various interactions of the excited species A* with a quencher molecule. As a result of these intermolecular de-excitation process, which compete with the intrinsic relaxation pathways, the fluorophore's properties like absorption and emission spectra, lifetimes or quantum yields are altered. The interaction can be due to diffusion of the quencher to the fluorophore (dynamic quenching) or due to formation of a complex (static quenching). Possible mechanisms could be photoinduced electron transfer, eximer or exiplex formation, photoinduced proton transfer or excitation energy transfer (see also figure 2.1). Intramolecular quenching can be achieved if the donor and acceptor are covalently linked, as for example in a

pH sensitive PET sensor, where a pH sensitive group (and hydroxy or amine group) is linked to an aromatic fluorophore. One quenching mechanism will be shortly described here:

In **photoinduced electron transfer** (PET) electrons are transferred from a donor molecule to an acceptor molecule. PET can be oxidative or reductive, depending on the redox potentials of the ground state and excited state of the donor and acceptor molecule, resulting in formation of a radical ion pair $A^{\cdot-}D^{\cdot+}$ and subsequent relaxation to the ground state via charge recombination.

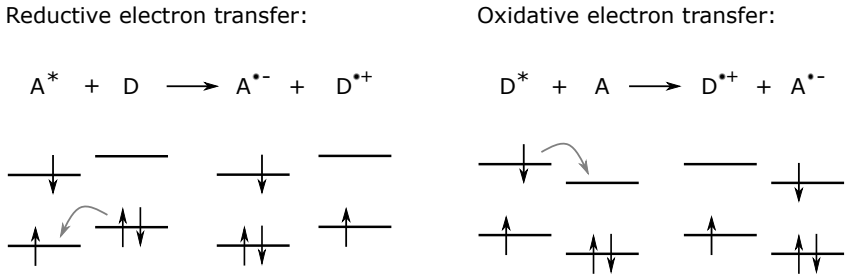


**Figure 2.6:** Schematic description of reductive and oxidative PET quenching

**Resonance energy transfer** is another possible relaxation mechanism, which can take place if the emission band of the donor overlaps with the absorption band of the acceptor molecule. The donor in excited state transfers its excitation energy to the acceptor according to $D^* + A \longrightarrow D + A^*$. An important feature of this type of fluorescence quenching is that energy transfer is a non-radiative process (in contrast to radiative transport, where emitted light from the donor is reabsorbed by the acceptor without direct interaction of the molecules). It takes place without emission of photons by interaction of dipoles with similar resonance energy, and therefore requires direct interaction of the donor and acceptor molecule, which can be due to long-range coulombic dipole-dipole interaction (Förster mechanism, FRET) and/or intermolecular orbital overlap involving electron exchange (Dexter mechanism). FRET is dependent on the distance $r$ of the interacting molecules in the following way:

$$k_T = \frac{1}{\tau_D^0}[\frac{R_0}{r}]^6 \tag{2.8}$$

$k_T$ is the rate constant of the transfer, $\tau_D^0$ the excited-state lifetime of the donor without transfer and $R_0$ the Förster critical radius, which is typically in the range between 20 and 90 Å.

## 2.4 Principles of chemosensors

A definition of chemical sensors can be phrased according to IUPAC: *"A chemical sensor is a device that transforms chemical information, ranging from the concentration of a specific sample component to total composition analysis, into an analytically useful signal. The chemical information, mentioned above, may originate from a chemical reaction of the analyte or from a physical property of the system investigated.*[...]*Chemical sensors contain two basic functional units: a receptor part and a transducer part. Some sensors may include a separator which is, for example, a membrane."* (IUPAC 1991, [15])

For clarification of this definition, the human nose can also be described as a very sensitive and selective sensor in a very abstract way. The olfactory membrane detects single chemical substances responsible for an odor (equivalent to the receptor of a chemical sensor), the nerve cells take on the role as transducer, and finally the brain can be compared to the measuring device and electronics as in sensors. A sensor as a whole consist of a recognition element (or receptor), a transducer and a read-out device. The recognition element is responsible for selective recognition and reaction to a specific analyte or a group of analytes, the transducer converts a response of the recognition element into a measurable signal. [16] An important feature of a chemical sensor, which is not included in the above mentioned definition, is its demand for reversibility and continuous measurements. Therefore, the definition should be extended by the so-called Cambridge definition: *"Chemical sensors are miniaturized devices that can deliver real-time and on-line information on the presence of specific compounds or ions in even complex samples."* [17]

A useful and often used classification of chemical sensors can be made according to the type of transduction involved [15]:

- Optical sensors are based on the principles of absorbance or reflectance of light, luminescence, refractive index, optothermal effects or light scattering.
- Electrochemical sensors are voltametric or potentiometric sensors or chemically sensitized field effect transistors.
- Electric sensors are e.g. metal oxide semiconductor based or organic semiconductor based sensors.
- Mass sensitive sensors detect a mass change at a surface.
- Magnetic sensors react to the paramagnetic properties of gases.
- Thermometric sensors are based on reaction heat or absorption of heat.

The following chapters are confined to only one group of chemosensors, the optical sensors. In molecular optical sensing, an indicator (mostly immobilized in or on a suitable polymer matrix) acts as a recognition element to detect the presence or absence of an analyte. The

indicator's optical properties are changed by interaction with the analyte and this information is converted into a measurable signal.A chemical sensor has to hold a few properties: a chemical signal is converted into an electrical signal, the response to a analyte change should be fast and reversible, they should have a long working life, they should be small, miniaturizeable and cheap, and react selectively to the desired analyte. [18]

The broad field of application make optical sensors such an important technology. In health care, the blood glucose level of patients could be continuously controlled by a sensor. Other metabolites could be controlled within seconds at the bedside instead of waiting for hours for a result from a centralized laboratory. In industrial processes, on-line and continuous monitoring of important process parameters such as pH, temperature, $CO_2$ or oxygen levels could be monitored. Another important application is environmental monitoring. Pollutants in air, water or soil can be monitored fast, decentralized and in real-time. [16] Moreover, the increasing technological progress in optoelectronics enable development of miniaturized and cost effective light sources and detector systems. Especially fluorescent sensors offer a number of advantages such as high sensitivity, selectivity, response time and possibility of spatial and temporal observations as well as remote sensing (via fiber optics). [8]

## 2.5 pH sensing

### 2.5.1 Principles of optical pH sensing

Due to the importance of pH in almost all fields of human life there is a huge interest in development of pH sensors. The applications of pH sensors range from analytical chemistry, bioanalytics, intracellular measurements, medical measurements to fluorescent microscopy for spatially resolved pH measurements. [8] Marine science, continuous monitoring of bioprocesses or fast and easy bedside metabolite control in health care are just a few examples.

Many different dyes act as pH indicator and can be used in pH sensitive sensors. Most dyes have only a small detection range of two to three pH units (compared to the large working range from 1 to 14 of pH electrodes). But for most physiological or environmental applications this narrow pH range is sufficient. Broad range pH sensors were also reported, which make use of a mix of dyes with different $pK_a$ values to achieve a larger working range. [6, 19]

pH is defined as the negative of the base 10 logarithm of the activity of protons, or simplified defined as:

$$pH \approx -log\, c\,(H^+) \tag{2.9}$$

(In aqueous solutions, protons are rather present as hydronium ions $H_3O^+$, however for convenience often $H^+$ is used.) For acids and bases in aqueous solutions, the following reactions can be defined: $HA + H_2O \rightleftharpoons A^- + H_3O^+$ and $B + H_2O \rightleftharpoons BH^+ + OH^-$, with

the equilibrium constants $K_a$ and $K_b$, respectively.

$$K_a = \frac{c(A^-) \cdot (H_3O^+)}{c(HA)} \tag{2.10}$$

$$K_b = \frac{c(BH^+) \cdot (OH^-)}{c(B)} \tag{2.11}$$

The Henderson-Hasselbach equation derives from the logarithmic form of equation 2.10

$$pH = pK_a + log\,\frac{[B]}{[A]} \tag{2.12}$$

and can be adapted for fluorometric signals to

$$pH = pK_a + log\,\frac{I - I_A}{I_B - I} \tag{2.13}$$

where A and B depict the acid and basic form of the fluorophore, respectively. [18]

Indicators for pH sensors are often weak organic acids or bases. Their optical properties can be changed by protonation or deprotonation. For choosing an indicator for pH sensing, several factors are crucial. The $pK_a$ of the dye should be in the appropriate range of interest (highest sensitivity and brightness is achieved close to the $pK_a$), the dye should have a high molar absorption coefficient and a good photostability. Moreover, it should exhibit thermal and chemical stability. For application as fluorescence indicator a large Stokes shift is preferred. In case of covalent immobilization, a functional group for bonding has to be present. Aside from that, not negligible are also factors like the indicator's toxicity, response time, sensitivity and selectivity. [1] It is important to keep in mind, that optical sensors measure the concentration of the pH indicator in the acidic and basic form, whereas the signal of electrochemical devices is directly linked to the activity of $H_3O^+$ ions. [1]

For most pH sensitive dyes absorption of the acidic and basic form differ, so distinction on color change via UV-Vis absorption spectroscopy can be made (colorimetric pH sensing, see figure 2.7, solid line). But also other optical properties of a dye can be exploited for pH sensing (reflectometry, fluorescence including lifetime, energy transfer or fluorescence quenching (see figure 2.7, dashed line)). Fluorescence-based indicators are preferred over absorption-based indicators for a few reasons: smaller dye concentrations are needed for pH sensing and less interferences may affect the results.

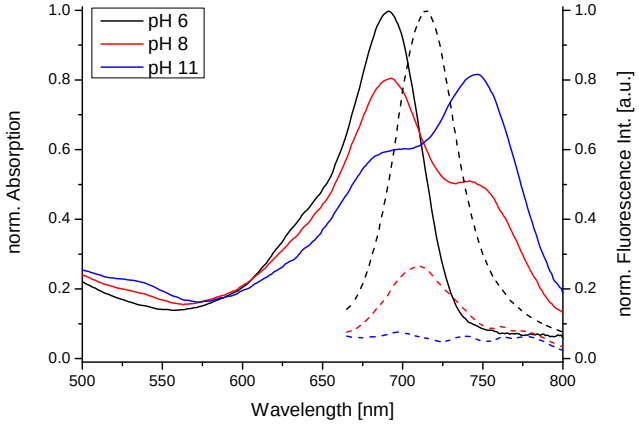


**Figure 2.7:** pH dependency of an exemplaric absorption and emission spectrum of azaBODIPY dyes

In order to determine the $pK_a$ of an indicator in optical sensors, the absorption or emission of the dye has to be measured at various pH vales. The maxima obtained from each spectrum is plotted versus the pH values of the corresponding measurements. The obtained curve is fitted with a Boltzmann equation, which is given by

$$y = \frac{A_1 - A_2}{1 + e^{(x-x_0)/d_x}} + A_2 \tag{2.14}$$

where $A_1$ is the maximum, $A_2$ the minimum of the curve, $x_0$ represents the point of inflection and $d_x$ the slope at the point $x_0$. The point of inflection of the fitted curve represents the $pK_a$ of the dye.

### 2.5.2 PET sensors

An important class of sensors for pH sensing uses the so-called PET (photoinduced electron transfer) effect. PET dyes usually carry a pH sensitive hydroxy or amino moiety, which is linked to a fluorophore by a methylene spacer. The spacer electronically disconnects the $\pi$-system of the fluorophore and the pH sensitive group. Intramolecular electron transfer from the HOMO of the proton free hydroxy or amino group to the excited fluorophore (so to say a radiation-less decay to the ground state) is enabled and induces quenching of the fluorescence by diminishing its population in the excited state. Protonation of the recognition group leads to a change of the redox potential and consequently to a shift of the energy levels involved. The HOMO of the recognition group become energetically lower than the one of the fluorophore, PET is blocked and consequently fluorescence emission is enabled. This process is schematically illustrated in figure 2.8. Indicators following this deactivation mechanism are also called "on-off" indicators. [8, 20]

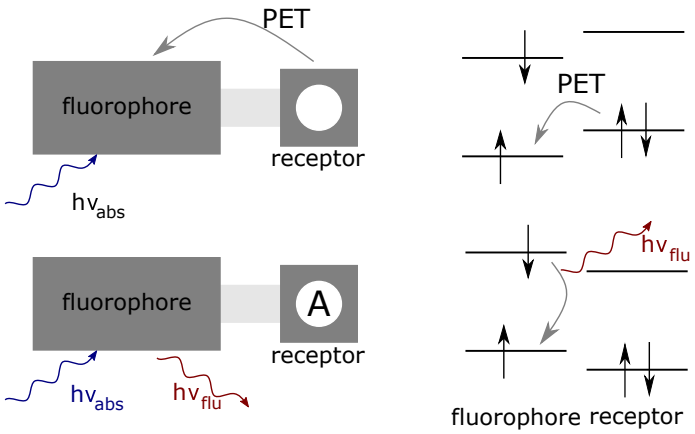


**Figure 2.8:** Principle of sensing via PET sensors

### 2.5.3 ICT sensors

Internal charge transfer can be observed in fluorophores in which two functionalities are connected directly with each other, one acting as an electron donor and the other acting as an electron acceptor. Upon excitation, an electron-hole pair is generated. This generates a "push–pull" $\pi$-electron system in the excited state with a dipole and charge redistribution within the $\pi$-system. Interaction of an analyte with the electron donating site of the fluorophore (which is the receptor in this case) diminishes the electron donating character of the dye, which leads to a change of the dipole and causes destabilization of the ICT state, which in turn leads to a blue shift of the spectrum. Vice versa, interaction of an analyte with the electron accepting site causes enhancement of ICT and stabilization and therefore a red shift of the spectrum is observed (figure 2.8). Additionally, altering of the quantum yields and lifetimes of ICT indicators can be observed. [21, 22]

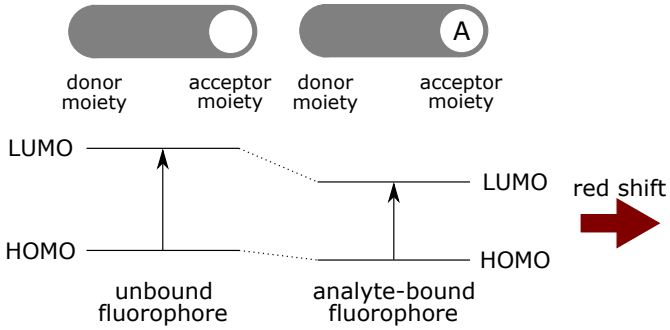


**Figure 2.9:** Principle of sensing via ICT sensors

### 2.5.4 Conventional pH sensing - glass electrode

The most common way to measure the pH in solution is measuring with a pH electrodes (glass electrode). Mostly, a combined electrode consisting of a reference electrode (Ag/AgCl) and a glass membrane electrode of the same type is used.

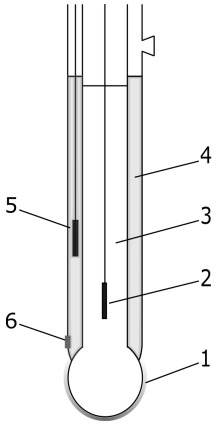


**Figure 2.10:** Schematic representation of a combination pH electrode

A schematic of the design of a combination pH electrode can be seen in figure 2.10. A thin membrane made of sodium silicate glass (1), which is selective to hydrogen ions, is used. An Ag/AgCl inner electrode (2) is incorporated within the glass membrane and surrounded by an internal buffer solution with typically pH 7 (3). The main electrode tube is incorporated in a second concentrically formed glass tube filled with a reference internal solution (KCl solution) (4) and embeds the reference electrode, which is usually also of Ag/AgCl type (5). A small frit (6) enables contact of the reference solution with the test solution. In solution, a gel layer at the surface of the glass membrane builds up. At the interface of the glass membrane and the test solution the following equilibrium reaction takes place:

$$SiO^-Na^+ + H_3O^+ \rightleftharpoons SiO^-H_3O^+ + {Na_{aq}}^+$$

A potential difference between the two electrodes, the one in contact with the internal buffer solution and the electrode in electric contact with the test solution via the diaphragm, is generated, which can be expressed in electrochemical way:

Ag/AgCl electrode | buffer solution | glass membrane || test solution | reference electrode

The measured signal is a potential difference at the glass membrane, originating from the difference of $H^+$ ion activities in the test solution and the reference solution.

A pH electrode is an inexpensive and easy tool and enables fast measurements over a wide working range. However, it can not be used for all sample solutions. Chemicals like alkaline solutions or fluoride ions may damage the electrode. Further drawbacks are its size, electromagnetical interferences, bad long-term stability and its limitation to single point measurements. Most of the mentioned limitations of glass electrodes can be eliminated by optical pH sensors. [18]

## 2.6 $CO_2$ sensing

Sensing of carbon dioxide is important in clinical as well as in environmental measurements, especially in marine monitoring in the context of greenhouse effect. Optical carbon dioxide sensors make use of the principle of pH sensors (see chapter 2.5). Sensors based on the Severinghaus electrode contain a hydrogencarbonate buffer entrapped behind a gas-permeable membrane additionally to the pH sensitive indicator. In the buffer, $CO_2$ is in balance with bicarbonate.

$$CO_2(g) \rightleftharpoons CO_2(aq)$$

$$CO_2(aq) + H_2O \rightleftharpoons H_2CO_3$$

$$H_2CO_3 \rightleftharpoons H^+ + HCO_3{}^-$$

The proton interacts with the basic form of the indicator, producing a color change or a change of a fluorescence signal.

$$H^+ + Ind^- \rightleftharpoons H^+Ind^-$$

The membrane is gas-permeable but impermeable to protons to prevent crosstalk to pH. Thus, the concentration of $CO_2$ can be detected indirectly as a change in proton concentration within the buffer solution via a pH probe. [7, 23, 24]

A drawback of these aqueous optical $CO_2$ sensors is the loss of water during storage and operating time and mostly long response times. Moreover, they often exhibit drifts caused by a change in osmotic pressure between the internal buffer solution and sample solution due to changes of sample ionic strength. [25] Dry $CO_2$ (or "plastic type" $CO_2$) sensors overcome these problems. The indicator as well as a lipophilic base (e.g. quaternary ammonium hydroxide) as phase transfer agent instead of the bicarbonate buffer are incorporated in a plastic layer, for example in ethyl cellulose. The deprotonated form of the indicator and the phase transfer agent form an ion pair.

$$Q^+ + Ind^- \rightleftharpoons Q^+Ind^-$$

Due to the solvation shell it is probably more appropriate to describe the ion pair as $Q^+Ind^- \, x\, H_2O$ rather than $Q^+Ind^-$.

$$Q^+Ind^- \, x\, H_2O + CO_2(g) \rightleftharpoons Q^+Ind^- \, x\, H_2O \cdot CO_2$$

$$Q^+Ind^- \, x\, H_2O \cdot CO_2 \rightleftharpoons Q^+Ind^- \, (x\text{-}1)\, H_2O \cdot H_2CO_3$$

$$Q^+Ind^- \, (x\text{-}1)\, H_2O \cdot H_2CO_3 \rightleftharpoons Q^+HCO_3{}^- + H^+Ind^-$$

The conversion of $Q^+Ind^-$ to $H^+Ind^-$ is associated with a detectable color change or change of the fluorescence properties. [7, 23, 26]

## 2.7 Fluorescence measuring methods - intensity vs. lifetime sensing

Direct measurement of the fluorescence intensity (so-called steady-state measurement) is the easiest and most straightforward method. However, it is prone to various errors, for example errors associated with leaching of the dye, photobleaching and variations in the intensity of the light source or sensitivity of the detector, scattering of the light or changing concentration of the indicator. Many of these errors can be eliminated by use of radiometric or time-resolved methods. Therefore, in many applications, steady-state measurements have been replaced by more sophisticated methods. [1, 27]

### 2.7.1 Principle of dual lifetime referencing (DLR)

DLR (dual lifetime referencing) is a type of time-resolved fluorometry and is a versatile method overcoming the usual limitations in direct fluorescence intensity measurements. It makes use of two luminophores, the indicator dye and a reference dye, which have to exhibit overlapping absorption and emission spectra in order to enable excitation of both lumiophores at one wavelength and detection of both emissions using only one detector. [1] Measurements can be done either in the frequency domain or in the time domain. The principles of frequency domain measurements are known from determinations of lifetimes of fluorophores (chapter 2.3.2). It requires an analyte sensitive indicator (fluorophore) and an inert luminophore with a much longer decay time than the fluorophore. Both dyes are incorporated in a matrix, for example in a hydrogel membrane. The two decay times can be measured as an overall sinusoidal signal, following a sinusoidal excitation. While the reference signal remains unchanged by the presence of an analyte, the presence of an analyte leads to a reduces phase angle and amplitude of the indicator and therefore to a reduction of the overall measured signal in respect to the sinusoidal excitation light. [28, 29] The phase angle of this overall signal is again a sinusoidal signal (assuming single exponential decay times for both luminophores) and results from the constant decay time of a reference luminophore and the variable decay time of an analyte sensitive fluorophore. According to equation 2.15

$$cot\,\Phi_m = cot\,\Phi_{ref} + \frac{1}{sin\,\Phi_{ref}} \cdot \frac{A_{ind}}{A_{ref}} \tag{2.15}$$

the measured phase angle reflects the referenced fluorescence signal, where $\Phi_m$ is the phase angle of the measured overall signal, $\Phi_{ref}$ the (known) phase angle of the reference luminophore and $A_{ind}$ and $A_{ref}$ the amplitudes of the fluorescence indicator and the reference, respectively. This method is a versatile tool because of its simplicity and a relatively cheap opto-electronic setup can be used. [30]

Another possibility of DLR is the measurement in the time domain. Therefore the sample consisting of an analyte sensitive fluorophore and a insensitive phosphorescent reference is excited with a light pulse. During the light pulse, the measured signal derives from both, the fluorophore and the reference phosphor. After the pulse, only luminescence arising from the long-lived phosphor is measured. In case of a single exponential decay, the following equation applies.

$$\frac{A_{ref,1} + A_{ind}}{A_{ref,2}} = (k_1 - 1) + k_2 \frac{I_{flu}}{I_{ref}} \tag{2.16}$$

where $A_{ref,1}$, $A_{ref,2}$ and $A_{ind}$ are the signal intensities of the reference dye during the pulse, after the pulse and the signal intensity of the fluorophore, respectively. $k_1$ and $k_2$ are constants, and $I_{ind}$ and $I_{ref}$ are the fluorescence intensities of the fluorophore indicator and the reference, respectively. [30]

## 2.8 Matrices

The selective element (in case of an optical sensor the dye) has to be immobilized and connected to the transducer in order to successfully pass on an analyte dependent response. Often used materials in pH sensors are cellulose acetate, ethyl cellulose, collagen, poly(vinyl alcohol), Nafion or hydrogels like polyurethane. [1] Immobilization can be done by simple adsorption on a surface. However, this method is not suitable for long-time measurements and should therefore be restricted to short-time explorative work. Another method is microencapsulation. In this method an analyte permeable membrane is used to immobilize the selective element on the surface of the transducer. The dye can furthermore be physically entrapment in a gel, paste or polymer solution such as polyacrylamide, starch gels or silastic gels, by mixing the dye with the matrix material and subsequent evaporation of the solvent. This is a simple and versatile method, however, sensor layer made with this method are not as stable as for example covalent immobilization due to possible leaching of the dye. Moreover, diffusion of the analyte to the dye is limited and therefore response times of the sensors are longer. Covalent immobilization is achieved by forming a covalent bond between a functional group of the dye, which is not essential for the recognition of analytes, and the matrix material. This method prevents dye leaching and aggregation of the dye, however finding a suitable immobilization approach often turns out to be a tricky task. Another method is cross-linking. In the last method the dye is first entrapped in a matrix and subsequently cross-linked with reagents such as multi isocyanate crosslinker to prevent the dye from leaching out. [16]

Some properties of the free and the immobilized indicator may differ depending on the type of immobilization. For example a covalently bound dye may have a slightly different $pK_a$ than a physically entrapped dye. For the special case of pH sensors, the matrix should be hydrophilic to enable proton diffusion within the matrix. Moreover, a matrix should exhibit chemical, mechanical and thermal stability. [1]

Covalent immobilization of azaBODIPYs on a polymer matrix was a central topic of this thesis. Functionalization and coupling on the boron center of the dyes was investigated. Functionalization of BODIPYs and azaBODIPYs opens up new possibilities not only to introduce groups for immobilization of the dye, but also for altering the fluorescence properties of the dyes, for bioconjugate chemistry, bio-labelling or to increase the solubility. [31]. Many procedures to substitute the boron center on $BF_2$-chelated dipyrromethenes (BODIPYs) to convert them into the corresponding C- and O-BODIPYs were reported. [32–34]

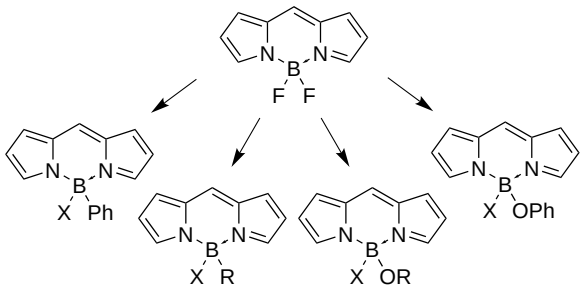


**Figure 2.11:** Synthesis of C- and O-BODIPYs starting from $BF_2$-chelated dipyrromethenes

Exchanging a fluorine atom at the boron center for a chlorine weakens the B-halogen bond in the order $F \gg Cl > Br > I$. Due to the weaker bond strength between boron and chlorine compared to the B-F bond strength, substitution on the boron center in Cl-BODIPYs is expected to be much easier than on the corresponding F-BODIPYs. The Cl-BODIPYs subsequently act as intermediates for further synthesis of C- and O-BODIPYs (BODIPYs carrying carbon- and oxygen-based moieties on the boron atom). Species like B-aryl, B-alkenyl, B-alkoxy or B-aryloxy BODIPYs were synthesized in good yields (figure 2.11). [35] Different approaches to activate the B-F bond were reported. Activation with $AlCl_3$ and subsequent treatment with methanol or phenol yields methoxy and phenoyloxy derivatives, respectively. These reactions are reported to work with relatively good yields of approximately 50 %. [36, 37] Using the Lewis acid $BCl_3$ F-BODIPYs were converted into Cl-BODIPYs, the intermediates were subsequently transformed into O- and C-substituted derivatives in an one-pot procedure with excellent yields. [38] Mono-alkoxy derivatives were synthesized by selectively removing one chlorine at the boron center with TMSOTf (timethylsilyl trifluoromethanesulfonate). This intermediate was reacted with alcohols to yield monoalkoxy derivatives. PEG-substituted BODIPYs were synthesized by treatment of $BF_2$-chelated dipyrromethenes with 2-[2-(2-methoxyethoxy)ethoxy]ethanol in the presence of $AlCl_3$. [39]

These procedures for BODIPYs were investigated on their applicability in substitution reactions of the B-F bond in azaBODIPYs (see also section 4.1.2).

## 2.9 Light harvesting

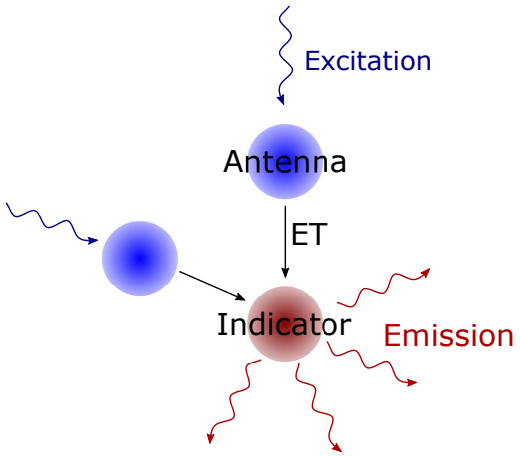


**Figure 2.12:** Principle of energy transfer from antenna dyes to the indicator dye with light harvesting

Signal enhancement of an optical sensor is significant in order to improve the signal-to-noise ratio, to reduce the influence of background fluorescence or to reduce the film thickness in a sensor. Especially in optical sensors, thin sensor layers (<500 nm) and nanometer-sized sensor particles are often required. Light harvesting is a versatile tool to increase the brightness of a dye and as a result to obtain an enhanced signal in reagent mediated sensors. The absorbed and emitted light of these sensors can be enhanced by adding a so-called antenna dye. The principle of this concept is illustrated in figure 2.12. Light harvesting appears in nature during photosynthesis, where auxiliary pigments like carotenoids absorb light and transfer the absorbed energy to reaction centers [40]. It is also exploited in dye sensitized solar cells for enhancement of excitation efficiency (in this context the antenna dye is referred to as sensitizer dye) [41]. In optical sensors, this approach requires an analyte insensitive dye (an antenna dye) with very high brightness added in a higher concentration than the anaylte sensitive indicator dye. The antenna dye efficiently absorbs the excitation light, through energy transfer (ET) [42] this excitation light is transferred to the indicator, which in turn emits fluorescent light. Since the antenna dye concentration is higher than the indicator concentration, one indicator molecule absorbs the energy of several antenna molecules in its proximity. This process leads not only to an enhanced signal intensity compared to the output achieved from the intrinsic absorption of the indicator, but also to an artificially enhanced Stokes shift. Absorption of the light takes place at the (energetically higher) excitation band of the donor and emission takes place at acceptor's emission band, increasing the Stokes shift by combination of two spectra. This facilitates the separation of absorption and emission light and provides a possibility to alter the excitation wavelength of a sensor in a way that inexpensive light sources can be used. [43]

## 2.10 Common fluorescent pH indicators

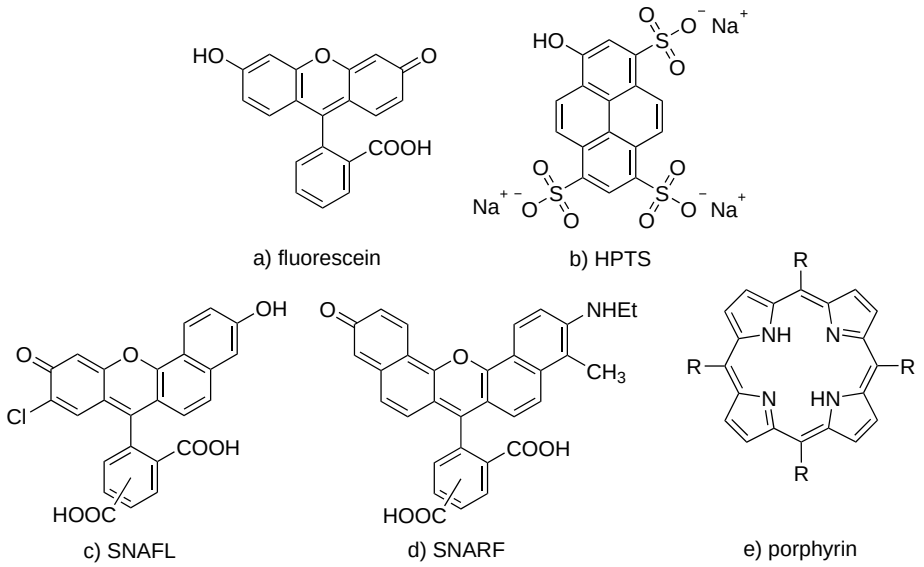


**Figure 2.13:** Structures of common optical pH indicators

As described earlier, optical pH sensors require an indicator dye, whose optical properties are changed upon pH change of the surrounding medium. This properties could be for example absorption, emission or lifetime changes.

Fluorescein was one of the first pH sensitive dyes used in pH sensors. Fluorescein exists in a neutral, monoanionic and dianionic form, depending on the pH of the environment, however, only the monoanionic and dianionic forms are fluorescent. Fluorescein was for example used for intralysosomal pH measurements. [44] The $pK_a$ of fluorescein is approximately 6.5, pH in cells is slightly higher though, so alternative pH sensitive dyes with higher $pK_a$ are preferential. Moreover, fluorescein rapidly leaks out of cells, limiting its application in biological applications. BCECF (2', 7'-bis(2-carboxyethyl)-5(6)-carboxyfluorescein), a highly charged derivative of fluorescein, exhibits a higher $pK_a$ close to 7.0, making it ideal for sensing of cytosolic pH. [45]

8-Hydroxypyrene-1,3,6-trisulfonate (HPTS) dyes typically absorb in the blue region and emit at around 520 nm. The $pK_a$ of HPTS is approximately 7.5, making it a convenient indicator for medical measurements or marine monitoring, as reported by Hulth *et al.* [46] Fluorescein and HPTS based indicators facilitate ratiometric sensing, which is a self-referencing measuring technique. Instabilities in the emission intensity can arise for example from leaching, photobleaching or fluctuations of the excitation light source. Ratiometric measurements can eliminate these errors by measuring at two different wavelengths. [1]

SNAFLs (seminaphthofluoresceins) and SNARFs (seminapthorhodafluors) are pH probes that contain benzene and naphthalene components. They have a pH dependent wavelength shift of both, absorption and emission spectra, with the protonated form emitting at around

550 nm and the basic form emitting at above 630 nm. Absorption and emission spectra have isosbestic points at 530 and 585 nm, which makes them suitable for dual-emission ratiometric sensing. The acidic as well as the basic forms are fluorescent, which makes probes based on lifetime measurements possible as well. The fluorescence response of SNAFLs and SNARFs is only slightly dependent on the ionic strength of the surrounding medium, which is an important advantage over the before mentioned fluorophores. However, SNAFLs and SNARFs have poor quantum yields and photostabilities, which limits their applications. Modifications of the SNARF structure to yield carboxy-SNARFS enhances their photostability and bathochromically shift their excitation wavelength. [9, 45]

Porphyrin based probes enable pH sensing due to protonation and deprotonation of the pyrrole protons in the porphyrin sturcture. They exhibit excitation at around 400–500 nm (Soret Band) and weaker excitation bands (Q-bands) at around 500-700 nm. Fluorescence maxima are observed between 600 nm and 800 nm, which can be quenched due to for example Förster resonance energy transfer. The Stokes shift is large enough for separation of the absorption and emission band which is advantageous for many sensing applications. [47]

Another class of optical pH indicators are BODIPYs and azaBODIPYs, which are addressed separately in the following section.

### 2.10.1 BODIPYs and azaBODIPYs

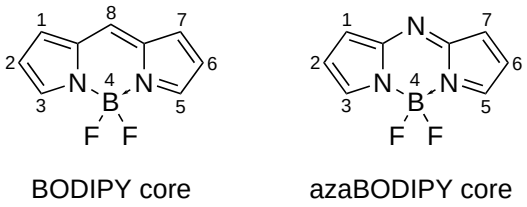


**Figure 2.14:** Structure of a BODIPY core and azaBODIPY core

Derivatives of 4,4-difluoro-4-bora-3a,4a-diaza-s-indacene (BODIPY) dyes belong to an important indicator class in optical sensing. BODIPYs exhibit typically sharp fluorescence peaks and good quantum yields. Moreover, they are reasonably stable in physiological conditions and exhibit an excellent photostability. BODIPYs emit in the region of 520 to 600 nm. [48] A bathochromic shift of the emission can be induced by modification of the BODIPY structure, for example by extension of the $\pi$-system, by rigidification or by introduction of electron donating groups.

A related dye class, azaBODIPYs, have a C-to-N substitution at the central carbon (the *meso*-carbon). The nitrogen lone pair alters the orbital level of the azaBODIPY in a way that causes reduction of the HOMO-LUMO energy gap in comparison to a BODIPY with similar substitution pattern, resulting in a bathochromic shift of absorption and emission bands. [49, 50] Almost all common azaBODIPYs have 1,3,5,7-aryl substituents ("tetraphenyl azaBODIPY"

structure). This compound emits at 695 nm, so a remarkable red-shift compared to the BODIPY analogues can be observed. Both absorption and emission spectra of azaBODIPY dyes strongly depend on the substituents pattern on the four aryl groups. Electron donating substitution in para-position result in a higher absorption coefficient as well as in a further bathocromic shift of the spectrum. Rigidification and extension of the $\pi$-system further enhances red shift of the emission spectrum. Solvent polarity does not have a large impact neither on the absorption nor on the emission spectra of azaBODIPYs.

Absorption and emission in the far-red and near-infrared (NIR) region of the light is preferential over UV, blue or green light excitation due to various reasons: NIR dyes are less prone to causing photo-damage to the biotissues, auto-absorption as well as auto-fluorescence of biomolecules is reduced in this region of the light, a deeper and more efficient tissue penetration can be achieved. Moreover, background noise can be reduced and signal-to-noise ratio magnified due to less excitation and emission light scattering. Excitation at shorter wavelength than in the so called "optical window" (650-950 nm) leads to more absorption of the light by hemoglobin or other endogenous chromophores and higher autofluorescence and scattering by tissue. On the other side, at higher wavelengths absorption by water becomes predominant. This makes this class of NIR emitting dyes particularly interesting for in vitro and in vivo biomedical applications. Apart from that, the development in the field of low-cost red and NIR region excitation sources and NIR detectors further promoted the development of far-red and NIR dyes. [3, 27, 51]

### 2.10.2 azaBODIPY dyes in pH sensors

Based on the PET (photoinduced electron transfer) mechanism, azaBODIPYs are a functional dye for pH sensing. They typically consist of a "fluorophore–spacer–receptor" design, where an amino or hydroxy group (an analyte recognition site) is incorporated in the structure of the azaBODIPY. An aliphatic spacer electronically disconnects the fluorophore and the receptor. Electron transfer from the amino or hydroxy group to the fluorophore followed by a non-radiative decay competes with radiative relaxation, and therefore quenches fluorescence in the deprotonated state (fluorescence "off"). Binding of a proton suppresses PET and fluorescence is restored (fluorescence "on"). [52]

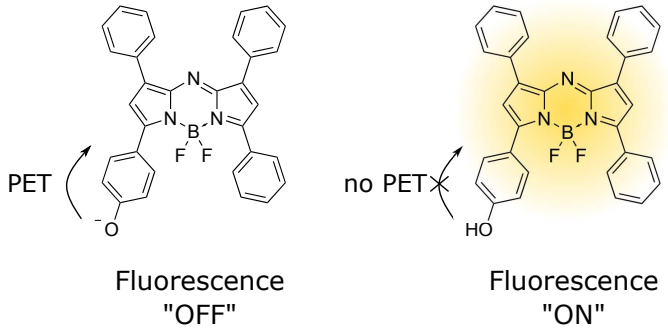


**Figure 2.15:** Operating principle of a fluorescent pH indicator based on azaBODIPYs

Favorable properties of azaBODIPYs are, among others, their high fluorescence quantum yields, sharp absorption and emission bands, good photostabilities and an ability to tune their photophysical properties by modifications of their structure.

Recent publications in this field include a publication by Murtagh *et al.*, whose pH sensitive NIR fluorescence probes show a pH response in the physiological pH range upon phenol/phenolate interconversion and absorption and emission properties above 680 nm. [4] A conjugation of the dye to a biomolecules via alkyne-azide cycloaddition was reported. [4] Jokic *et al.* reported on/off PET sensors based on azaBODIPYs with tuneable $pK_a$ values. The dyes show absorption in the range between 660 nm and 710 nm, fluorescence emission between 680 nm and 740 nm and high molar absorption coefficients of about 80 000. The $pK_a$ of the indicators can be tuned in the physiological and slightly alkaline range by introduction of electron donating ($CH_3$, $OCH_3$) or electron withdrawing (Cl) substituents on the 3- and 5-aryl ring of the azaBODIPY. A pH dependent shift of the absorption maximum due to internal charge transfer (ICT) and Förster resonance energy transfer (FRET) from the protonated to the deprotonated form of the dye can be observed. Emission spectra exhibit a decrease in fluorescence intensity due to PET quenching. [5] Schutting *et al.* reported the application of di-OH azaBODIPYs in $CO_2$ sensors. The pH sensitive dyes with two de-/protonatable hydroxy groups together with a tetraoctylammonium base absorb in the near-infrared region. Furthermore, tuning of the $pK_a$ of the dyes with electron donating or electron withdrawing groups enables different applications from marine science and environmental monitoring to food packaging. [53] Strobl *et al.* published a set of azaBODIPYs covering a large pH range from 1.5 to 13. By using a mixture of several pH indicators with different $pK_a$ values a broad-range sensor was made for pH-sensing over the entire pH range. [6]

The above mentioned dyes exhibit PET- as well as ICT-quenching. Due to ICT deprotonation of the dye leads to a bathochromic shift of the absorption maximum. Moreover, strong FRET induces energy transfer from the protonated (fluorescent) to the deprotonated (non-fluorescent) state of the dye, which reduces the brightness significantly. With a new approach of a m-OH substitution indicators purely based on PET-quenching are aimed to be synthesized in this thesis.

# 3 Experimental

## 3.1 Synthesis

### 3.1.1 Synthesis of azaBODIPY dyes

#### 3-Hydroxy-4'-butoxychalcone

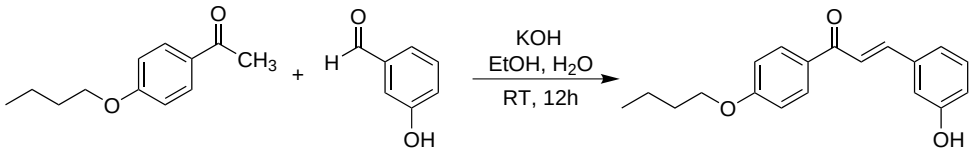


**Figure 3.1:** Synthesis of 3-hydroxy-4'-butoxychalcone

1.00 g 4'-butoxyacetophenone (5.20 mmol, 1.00 eq) and 651.0 mg 3-hydroxybenzaldehyde (5.33 mmol, 1.02 eq) were dissolved in 5 mL EtOH in a round bottom flask. 5 mL of an aqueous potassium hydroxide solution (875.5 mg, 15.60 mmol, 3.00 eq) were added dropwise. The solution was stirred for 12 h at room temperature during which the solution turned orange. The reaction mixture was added dropwise to 40 mL 1 M HCl solution to precipitate a yellow solid. The product was filtered, washed with water and dried. The obtained yellow solid was used for further synthesis without purification.

Crude yield: 1.34 g (87 %), yellow powder

#### 3-Hydroxy-4'-butoxynitrochalcone

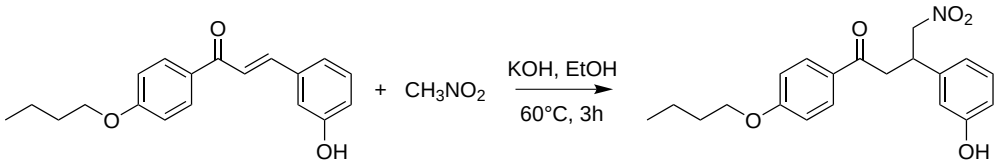


**Figure 3.2:** Synthesis of 3-hydroxy-4'-butoxynitrochalcone

In a round bottom flask equipped with a reflux condenser 1.34 g 3-hydroxy-4'-butoxychalcone (4.53 mmol, 1.00 eq) and 5.00 mL nitromethane (92.56 mmol, 20.45 eq) were mixed with 10 mL of a potassium hydroxide solution in EtOH (612.0 mg, 10.91 mmol, 2.41 eq) and stirred at

60 °C for 3 h. The reaction progress was monitored by adding a spatula tip of ammonium acetate to a few drops of the reaction mixture dissolved in BuOH in a glass vial and heating with a heat gun up to the boiling point. A blue coloration and TLC (DCM) of the solution indicates formation of the azaBODIPY ligand and therefore a successful reaction conversion to the desired nitrochalcone.
After cooling to room temperature the solvent was removed by rotary evaporation. The brown oily residue was dissolved in 50 mL EtOAc and washed with HCl solution (3 x 50 mL). After drying the organic phase over $Na_2SO_4$ and removing the solvent by rotary evaporation a brown oil was obtained, which was used for further synthesis without purification.

Crude yield: 2.19 g (135 %, product containing residual solvent), brown oil

**4,4'-Dibutoxychalcone**

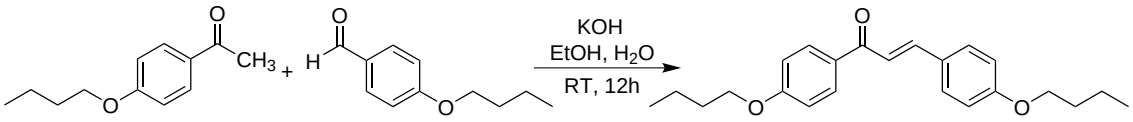


**Figure 3.3:** Synthesis of 4,4'-dibutoxychalcone

5.40 g 4'-butoxyacetophenone (28.07 mmol, 1.00 eq) and 5.00 g 4-butoxybenzaldehyde (28.08 mmol, 1.00 eq) were dissolved in 20 mL EtOH in a round bottom flask. 15 mL of an aqueous potassium hydroxide solution (4.77 g, 85.02 mmol, 3.03 eq) were added dropwise. The solution was stirred for 12 h at room temperature during which the solution turned orange. The reaction mixture was added dropwise to 150 mL 1 M HCl solution to precipitate a yellow solid. The product was filtered, washed with water and dried. The obtained yellow solid was used for further synthesis without purification.

Crude yield: 8.60 g (87 %), yellow powder

**4,4'-Dibutoxynitrochalcone**

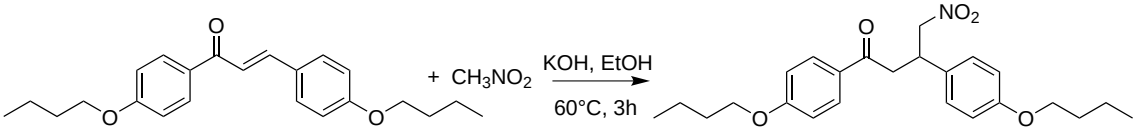


**Figure 3.4:** Synthesis of 4,4'-dibutoxynitrochalcone

In a round bottom flask equipped with a reflux condenser 1.01 g 4,4'-dibutoxychalcone (2.87 mmol, 1.00 eq) and 3.00 mL nitromethane (55.54 mmol, 19.35 eq) were mixed with 5 mL of a potassium hydroxide solution in EtOH (351.0 mg, 6.26 mmol, 2.18 eq) and stirred at 60 °C for 3 h. The reaction progress was monitored by adding a spatula tip of ammonium acetate to a few drops of the reaction mixture dissolved in BuOH in a glass vial and heating with a heat gun up to the boiling point. A blue coloration and TLC (DCM) of the solution indicates formation of the azaBODIPY ligand and therefore a successful reaction conversion to the desired product.
After cooling to room temperature the solvent was removed by rotary evaporation. The brown oily residue was dissolved in 100 mL EtOAc and washed with HCl solution (3 x 100 mL). After drying the organic phase over $Na_2SO_4$ and removing the solvent by rotary evaporation a brown oil was obtained, which was used for further synthesis without purification.

Crude yield: 1.29 g (109 %, product containing residual solvent), brown oil

**m-OH azaBODIPY ligand**

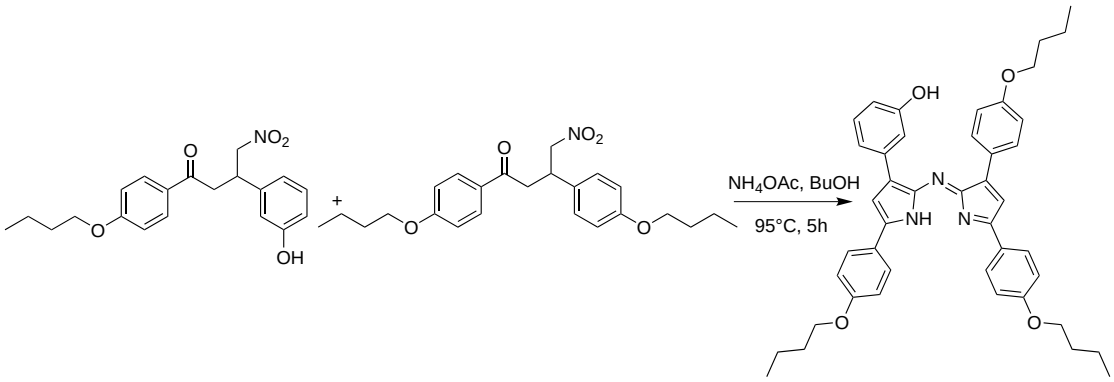


**Figure 3.5:** Synthesis of m-OH azaBODIPY ligand

474.2 mg 3-hydroxy-4'-butoxynitrochalcone (1.33 mmol, 1.00 eq), 507.2 mg 4,4'-dibutoxynitrochalcone (1.23 mmol, 0.92 eq) and 3.58 g ammonium acetate (46.66 mmol, 35.00 eq) were mixed with 25 mL BuOH in a round bottom flask equipped with a reflux condenser and stirred at 95 °C. The reaction conversion was monitored by TLC (DCM) and UV/VIS absorption spectroscopy. After 5 h the reaction mixture was cooled to room temperature and stirred over the weekend.
After removing the solvent by rotary evaporation the obtained solid was dissolved in DCM and washed with $H_2O$ (3 x 300 mL). The organic phase was dried over $Na_2SO_4$ and the solvent was removed. The crude product was purified by column chromatography (silica gel, DCM, detection by TLC with DCM and UV/VIS spectroscopy).

Yield: 44.6 mg (5 %), blue solid

**m-OHazaBODIPY complex (1)**

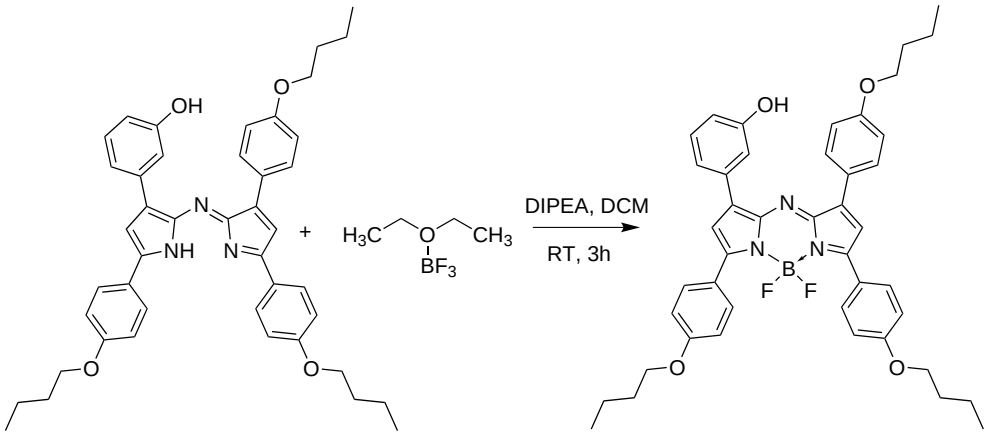


**Figure 3.6:** Synthesis of m-OH azaBODIPY complex (**1**)

44.6 mg m-OH azaBODIPY ligand (65.41 µmol, 1.00 eq) were dissolved in dry DCM under inert argon atmosphere in a Schlenk tube. 230 µl *N*,*N*-diisopropylethylamine (1.32 mmol, 20.19 eq) and 160 µl boron trifluoride diethyl etherate (1.30 mmol, 19.82 eq) were added dropwise. The solution was stirred at room temperature for 3 h during which the solution turned grey-blue. After a quantitative conversion was monitored by TLC (DCM : CH 3 : 1), the solution was partitioned between DCM and aqueous $NaHCO_3$ solution (3 x 25 mL), dried over $Na_2SO_4$ and the solvent was removed by rotary evaporation.
The crude product was purified by column chromatography (silica gel, DCM:CH 3:1, detection by TLC with DCM:CH 3:1 and UV/VIS spectroscopy) and recrystallization from MeOH to yield red-purple crystals.

Yield: 26.1 mg (55 %), red-purple crystals

$^1$H NMR (300 MHz, chloroform-d): $\delta = 8.04$ (t, J = 7.9 Hz, 6H), 7.61 (s, 1H), 7.50 (d, J = 7.5 Hz, 1H), 7.30 (d, J = 7.8 Hz, 1H), 7.06 – 6.90 (m, J = 8.0 Hz, 8H), 6.86 (d, J = 7.4 Hz, 1H), 5.06 (s, 1H), 4.13 – 3.90 (m, 6H), 1.88 – 1.70 (m, 6H), 1.51 (dd, J = 14.9, 7.4 Hz, 6H), 0.99 (t, J = 7.3 Hz, 9H). See figure 9.2 on page 101.
APT NMR (76 MHz, chloroform-d): $\delta = 161.83$, 161.44, 160.73, 159.26, 156.72, 155.91, 145.83, 144.78, 143.58, 141.34, 134.28, 131.83, 131.54, 131.01, 129.76, 125.12, 124.23, 123.94, 121.49, 118.24, 117.44, 116.42, 116.01, 114.83, 77.16, 67.97, 31.35, 19.38, 13.98. See figure 9.3 on page 101.

**2-Chloro-3-hydroxy-4'-butoxychalcone**

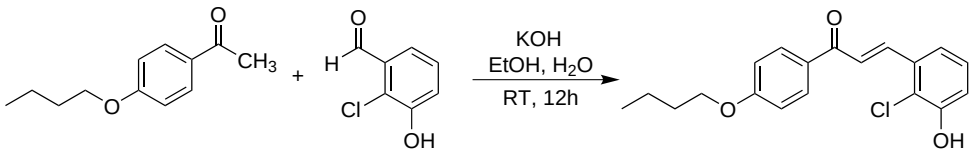


**Figure 3.7:** Synthesis of 2-chloro-3-hydroxy-4'-butoxychalcone

613.9 mg 4'-butoxyacetophenone (3.20 mmol, 1.01 eq) and 498.0 mg 2-chloro-3-hydroxybenzaldehyde (3.18 mmol, 1.00 eq) were dissolved in 3 mL EtOH in a round bottom flask. 3 mL of an aqueous potassium hydroxide solution (539.5 mg, 9.62 mmol, 3.02 eq) were added dropwise. The solution was stirred for 12 h at room temperature during which the solution turned orange. The reaction mixture was added dropwise to 40 mL 1 M HCl solution to precipitate a yellow solid. The product was filtered, washed with water and dried. The obtained yellow solid was used for further synthesis without purification.

Crude yield: 907.9 mg (86 %), yellow powder

**2-Chloro-3-hydroxy-4'-butoxynitrochalcone**

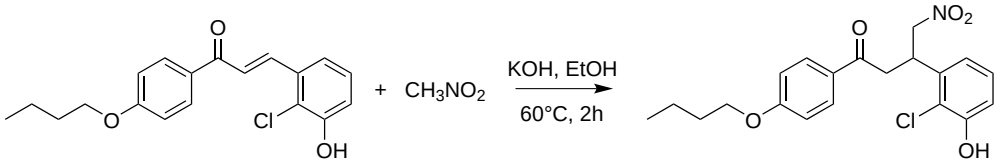


**Figure 3.8:** Synthesis of 2-chloro-3-hydroxy-4'-butoxynitrochalcone

In a round bottom flask equipped with a reflux condenser 907.9 mg 2-chloro-3-hydroxy-4'-butoxychalcone (2.74 mmol, 1.00 eq) and 3.00 mL nitromethane (55.54 mmol, 20.24 eq) were mixed with 5 mL of a potassium hydroxide solution in EtOH (337.0 mg, 6.01 mmol, 2.19 eq) and stirred at 60 °C for 2 h. The reaction progress was monitored by adding a spatula tip of ammonium acetate to a few drops of the reaction mixture dissolved in BuOH in a glass vial and heating with a heat gun up to the boiling point. A blue coloration and TLC (DCM) of the solution indicates formation of the azaBODIPY ligand and therefore a successful reaction conversion to the desired 2-chloro-3-hydroxy-4'-butoxynitrochalcone.
After cooling to room temperature the solvent was removed by rotary evaporation. The brown oily residue was dissolved in 50 mL EtOAc and washed with HCl solution (3 x 40 mL). After drying the organic phase over $Na_2SO_4$ and removing the solvent by rotary evaporation a brown oil was obtained, which was used for further synthesis without purification.

Crude yield: 1.34 g (125 %, product containing residual solvent), brown oil

### m-OH Cl azaBODIPY ligand

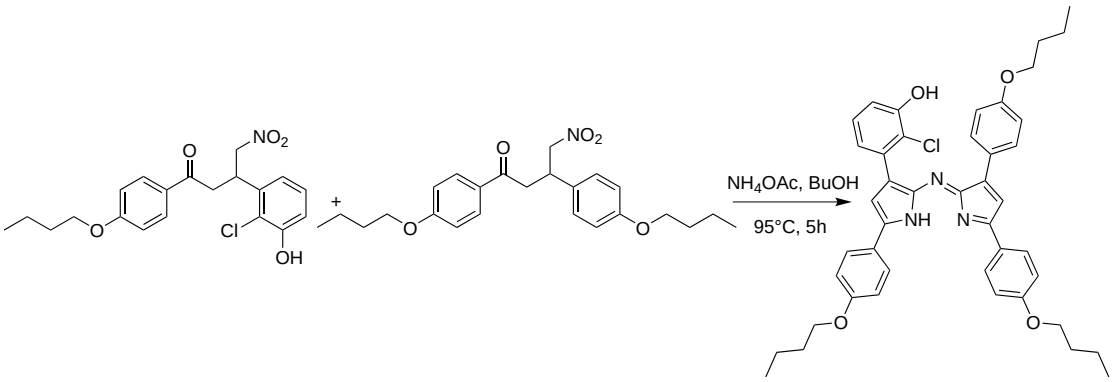


**Figure 3.9:** Synthesis of m-OH Cl azaBODIPY ligand

522.1 mg 2-chloro-3-hydroxy-4'-butoxynitrochalcone (1.33 mmol, 1.00 eq), 542.3 mg 4,4'-dibutoxynitrochalcone (1.31 mmol, 0.98 eq) and 4.09 g ammonium acetate (53.06 mmol, 39.82 eq) were mixed with 25 mL BuOH in a round bottom flask equipped with a reflux condenser and stirred at 95 °C. The reaction conversion was monitored by TLC (DCM : CH 2 : 1) and UV/VIS absorption spectroscopy. After 5 h the reaction mixture was cooled to room temperature and stirred overnight.
After removing the solvent by rotary evaporation the obtained solid was dissolved in DCM and washed with $NaHCO_3$ solution (3 x 300 mL). The organic phase was dried over $Na_2SO_4$ and the solvent was removed. The crude product was purified by column chromatography (silica gel, DCM, detection by TLC with DCM : CH 2 : 1 and UV/VIS spectroscopy).

Yield: 62.0 mg (7 %), blue metallic solid

### m-OH Cl azaBODIPY complex (2)

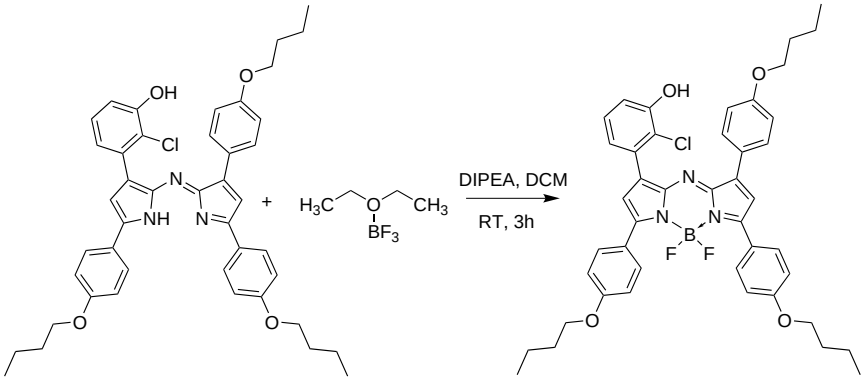


**Figure 3.10:** Synthesis of m-OH Cl azaBODIPY complex (**2**)

62.0 mg m-OH Cl azaBODIPY ligand (68.55 µmol, 1.00 eq) were dissolved in dry DCM under inert argon atmosphere in a Schlenk tube. 230 µl *N,N*-diisopropylethylamine (1.32 mmol, 15.26 eq) and 160 µl boron trifluoride diethyl etherate (1.30 mmol, 14.98 eq) were added dropwise. The solution was stirred at room temperature for 3 h during which the solution turned grey-blue. After a quantitative conversion was monitored by TLC (DCM), the solution was partitioned between DCM and aqueous $NaHCO_3$ solution (3 x 25 mL), dried over $Na_2SO_4$ and the solvent was removed by rotary evaporation.
The crude product was purified by column chromatography (silica gel, DCM : CH 2 : 1, detection by TLC with DCM : CH 2 : 1 and UV/VIS spectroscopy) and recrystallized from MeOH to yield red crystals.

Yield: 25.8 mg (39 %), red crystals

$^1$H NMR (300 MHz, chloroform-d): $\delta = 8.19 - 7.98$ (m, J = 18.0, 8.9 Hz, 6H), 7.39 – 7.28 (m, J = 13.0, 6.9 Hz, 2H), 7.17 – 7.07 (m, 2H), 7.05 – 6.93 (m, 5H), 6.87 (d, J = 8.7 Hz, 2H), 5.84 (s, 1H), 4.03 (dt, J = 12.5, 6.3 Hz, 6H), 1.88 – 1.71 (m, J = 7.8, 5.7 Hz, 6H), 1.57 – 1.47 (m, J = 15.0, 7.5 Hz, 6H), 1.00 (t, J = 7.3 Hz, 9H). See figure 9.4 on page 102.
APT NMR (76 MHz, chloroform-d): $\delta = 162.06$, 161.42, 160.80, 160.40, 155.51, 152.15, 146.41, 144.96, 144.00, 138.75, 132.20, 131.97, 131.60, 130.85, 127.23, 125.77, 124.80, 124.27, 123.82, 121.77, 119.60, 117.60, 116.11, 114.84, 77.16, 67.96, 31.37, 19.38, 13.97. See figure 9.5 on page 102.

**2,4-Dichloro-3-hydroxy-4'-methoxychalcone**

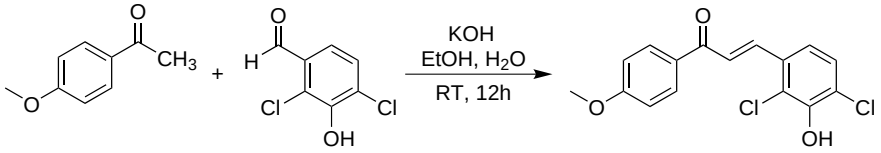


**Figure 3.11:** Synthesis of 2,4-dichloro-3-hydroxy-4'-methoxychalcone

412.7 mg 4'-methoxyacetophenone (2.75 mmol, 1.12 eq) and 469.0 mg 2,4-dichloro-3-hydroxybenzaldehyde (2.46 mmol, 1.00 eq) were dissolved in 5 mL EtOH in a round bottom flask. 5 mL of an aqueous potassium hydroxide solution (649.00 mg, 11.57 mmol, 4.71 eq) were added dropwise. The solution was stirred for 12 h at room temperature during which the solution turned orange and a precipitate was formed. The reaction mixture was added to 30 mL 1 M HCl solution to precipitate the yellow product. The solid was filtered, washed with water and dried. The obtained yellow product was used for further synthesis without purification.

Crude yield: 691.7 mg (87 %), yellow powder

**2,4-Dichloro-3-hydroxy-4'-methoxynitrochalcone**

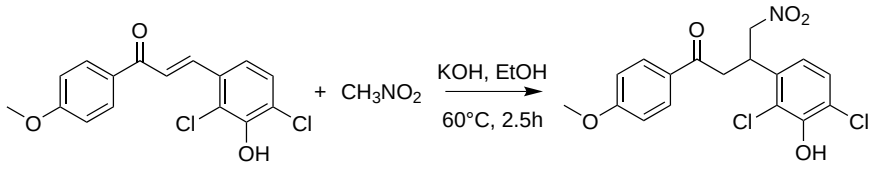


**Figure 3.12:** Synthesis of 2,4-dichloro-3-hydroxy-4'-methoxynitrochalcone

In a round bottom flask equipped with a reflux condenser 691.7 mg 2,4-dichloro-3-hydroxy-4'-methoxychalcone (2.14 mmol, 1.00 eq) and 2.5 mL nitromethane (46.28 mmol, 21.62 eq) were mixed with 3 mL of a potassium hydroxide solution in EtOH (340.0 mg, 6.06 mmol, 2.83 eq) and stirred at 60 °C for 2.5 h. The reaction progress was monitored by adding a spatula tip of ammonium acetate to a few drops of the reaction mixture dissolved in BuOH in a glass vial and heating with a heat gun up to the boiling point. A blue coloration and TLC (DCM) of the solution indicates formation of the azaBODIPY ligand and therefore a successful reaction conversion.
After cooling to room temperature the solvent was removed by rotary evaporation. The brown oily residue was dissolved in 50 mL EtOAc and washed with HCl solution (3 x 40 mL). After drying the organic phase over $Na_2SO_4$ and removing the solvent by rotary evaporation a brown oil was obtained, which was used for further synthesis without purification.

Crude yield: 1.08 g (131 %, product containing residual solvent), brown oil

**4,4'-Dimethoxychalcone**

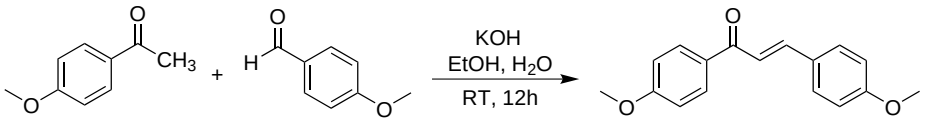


**Figure 3.13:** Synthesis of 4,4'-dimethoxychalcone

998.6 mg 4'-methoxyacetophenone (6.65 mmol, 1.00 eq) and 810 µl *p*-anisaldehyde (6.66 mmol, 1.00 eq) were dissolved in 5 mL EtOH in a round bottom flask. 5 mL of an aqueous potassium hydroxide solution (1.12 g, 19.97 mmol, 3.00 eq) were added dropwise. The solution was stirred for 12 h at room temperature during which the solution turned orange and a solid was formed. The reaction mixture was added dropwise to 40 mL 1 M HCl solution to precipitate the yellow product. The solid was filtered, washed with water and dried. The obtained product was used for further synthesis without purification.

Crude yield: 1.60 g (90 %), yellow powder

**4,4'-Dimethoxynitrochalcone**

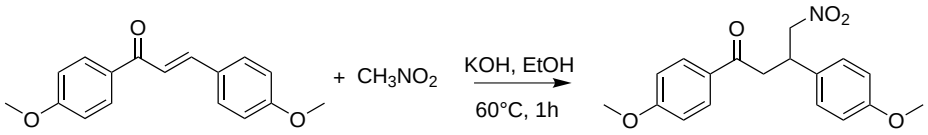


**Figure 3.14:** Synthesis of 4,4'-dimethoxynitrochalcone

In a round bottom flask equipped with a reflux condenser 1.60 g 4,4'-dimethoxychalcone (5.96 mmol, 1.00 eq) and 6.5 mL nitromethane (120.33 mmol, 20.18 eq) were mixed with 10 mL of a potassium hydroxide solution in EtOH (740.0 mg, 13.19 mmol, 2.21 eq) and stirred at 60 °C for 1 h. During heating the reaction mixture turned brown. The reaction progress was monitored by adding a spatula tip of ammonium acetate to a few drops of the reaction mixture dissolved in BuOH in a glass vial and heating with a heat gun up to the boiling point. A blue coloration and TLC (DCM) of the solution indicates formation of the azaBODIPY ligand and therefore a successful reaction conversion to the desired nitrochalcone.
After cooling to room temperature the solvent was removed by rotary evaporation. The brown oily residue was dissolved in 100 mL EtOAc and washed with HCl solution (3 x 70 mL). After drying the organic phase over $Na_2SO_4$ and removing the solvent by rotary evaporation a brown oil was obtained, which was used for further synthesis without purification.

Crude yield: 2.41 g (123 %, product containing residual solvent), brown oil

**m-OH diCl azaBODIPY ligand**

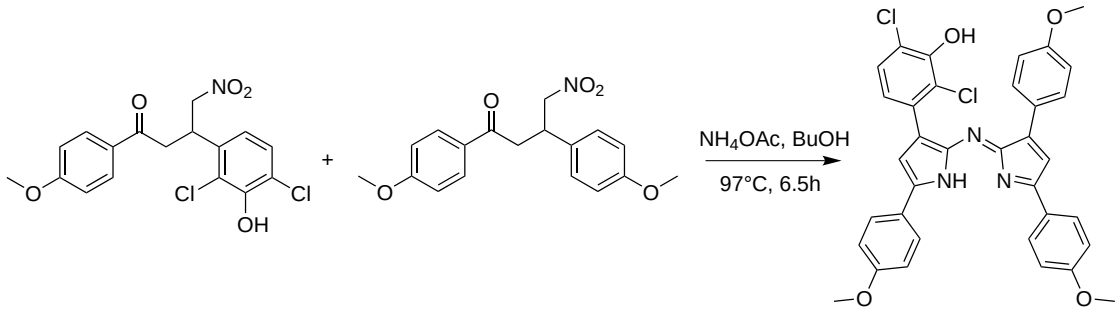


**Figure 3.15:** Synthesis of m-OH diCl azaBODIPY ligand

492.3 mg 2,4-dichloro-3-hydroxy-4'-methoxynitrochalcone (1.28 mmol, 1.00 eq), 441.9 mg 4,4'-dimethoxynitrochalcone (1.34 mmol, 1.05 eq) and 3.69 g ammonium acetate (47.35 mmol, 36.95 eq) were mixed with 25 mL BuOH in a round bottom flask equipped with a reflux condenser and stirred at 97 °C. The reaction conversion was monitored by TLC (DCM) and UV/VIS absorption spectroscopy. After 6.5 h, during which the solution turned blue, the reaction mixture was cooled to room temperature and stirred overnight.

After removing the solvent by rotary evaporation the obtained blue solid was dissolved in DCM and washed with $H_2O$ (3 x 100 mL). The organic phase was dried over $Na_2SO_4$ and the solvent was removed. The crude product was purified by column chromatography (aluminum oxide, EA + 1 % acetic acid, detection by TLC with DCM and UV/VIS spectroscopy).

Yield: 60.2 mg (8 %), metallic blue solid

**m-OH diCl azaBODIPY complex (3)**

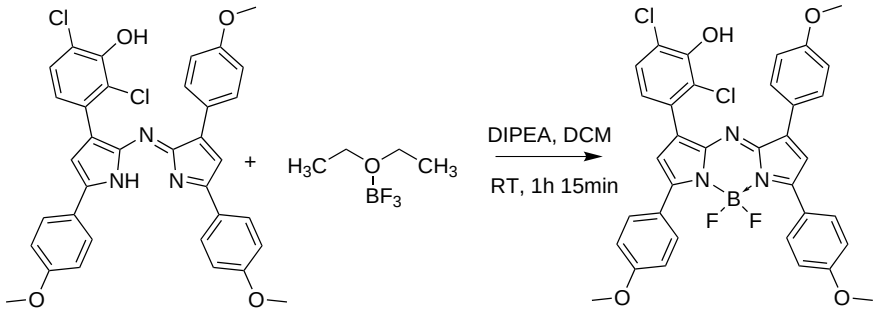


**Figure 3.16:** Synthesis of m-OH diCl azaBODIPY complex (**3**)

60.2 mg m-OH diCl azaBODIPY ligand (96.39 µmol, 1.00 eq) were dissolved in dry DCM under inert argon atmosphere in a Schlenk tube. 250 µl *N,N*-diisopropylethylamine (1.44 mmol, 14.89 eq) and 180 µl boron trifluoride diethyl etherate (1.46 mmol, 15.13 eq) were added dropwise. The solution was stirred at room temperature for 1 h and 15 min. After a quantitative conversion was monitored by TLC (DCM : CH 3 : 1), the solution was partitioned between DCM and aqueous $NaHCO_3$ solution (3 x 25 mL), dried over $Na_2SO_4$ and the solvent was removed by rotary evaporation.
The crude product was purified by column chromatography (aluminum oxide, EA + 2 % MeOH + 0.5 % acetic acid, detection by TLC with DCM : CH 3 : 1 and UV/VIS spectroscopy) and precipitated in CH.

Yield: 41.3 mg (63 %), green crystals

$^1$H NMR (300 MHz, chloroform-d): $\delta = 8.20 - 7.95$ (m, 6H), 7.35 (d, J = 5.7 Hz, 2H), 7.15 (s, 1H), 7.08 – 6.97 (m, J = 10.8, 4.0 Hz, 5H), 6.91 (d, J = 8.4 Hz, 2H), 3.89 (d, J = 3.2 Hz, 9H).
See figure 9.6 on page 103.
APT NMR spectrum could not be recorded due to insufficient solubility of the compound.

**2,6-Difluoro-3-hydroxy-4'-butoxychalcone**

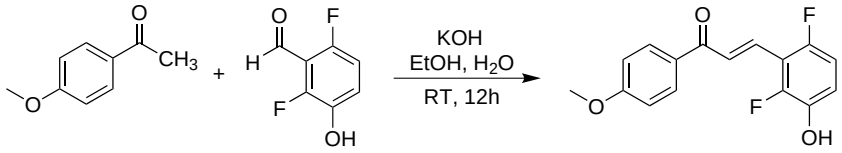


**Figure 3.17:** Synthesis of 2,6-difluoro-3-hydroxy-4'-butoxychalcone

953.7 mg 4'-methoxyacetophenone (6.35 mmol, 1.04 eq) and 964.8 mg 2,6-difluoro-3-hydroxybenzaldehyde (6.10 mmol, 1.00 eq) were dissolved in 5 mL EtOH in a round bottom flask. 5 mL of an aqueous potassium hydroxide solution (1.06 g, 18.89 mmol, 3.10 eq) were added dropwise. The solution was stirred for 12 h at room temperature during which the solution turned brown. The reaction mixture was added dropwise to 40 mL 1 M HCl solution to precipitate a brown-orange product. The solid was filtered, washed with water and dried. The obtained brown product was used for further synthesis without purification.

Crude yield: 1.62 g (91 %), brown powder

**2,6-Difluoro-3-hydroxy-4'-butoxynitrochalcone**

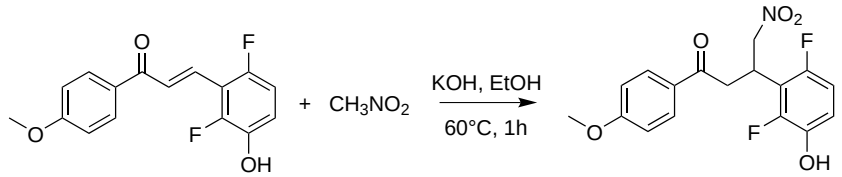


**Figure 3.18:** Synthesis of 2,6-difluoro-3-hydroxy-4'-butoxynitrochalcone

In a round bottom flask equipped with a reflux condenser 1.62 g 2,6-difluoro-3-hydroxy-4'-butoxychalcone (5.58 mmol, 1.00 eq) and 6.00 mL nitromethane (111.07 mmol, 19.90 eq) were mixed with 10 mL of a potassium hydroxide solution in EtOH (618.00 mg, 11.02 mmol, 1.97 eq) and stirred at 60 °C for 1 h. The solution turned red-brown and a brown precipitate was formed. The reaction progress was monitored by adding a spatula tip of ammonium acetate to a few drops of the reaction mixture dissolved in BuOH in a glass vial and heating with a heat gun up to the boiling point. A blue coloration and TLC (DCM + MeOH 95 + 5) of the solution indicates formation of the azaBODIPY ligand and therefore a successful reaction conversion to the desired 2,6-difluoro-3-hydroxy-4'-butoxynitrochalcone.
After cooling to room temperature the solvent was removed by rotary evaporation. The brown oily residue was dissolved in 50 mL EtOAc and washed with HCl solution (3 x 50 mL). After

drying the organic phase over $Na_2SO_4$ and removing the solvent by rotary evaporation a brown oil was obtained, which was used for further synthesis without purification.

Crude yield: 1.36 g (120 %, product containing residual solvent), brown oil

**m-OH diF azaBODIPY ligand**

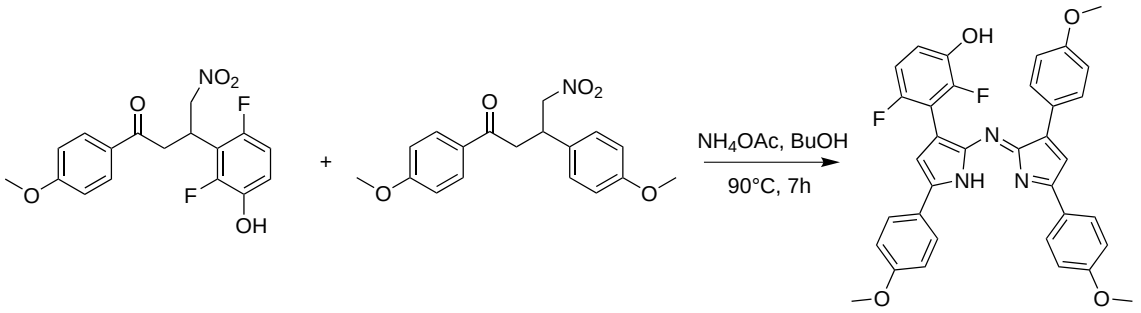


**Figure 3.19:** Synthesis of m-OH diF azaBODIPY ligand

1.13 g 2,6-difluoro-3-hydroxy-4'-butoxynitrochalcone (3.23 mmol, 1.00 eq), 1.11 g 4,4'-dimethoxynitrochalcone (3.38 mmol, 1.05 eq) and 9.06 g ammonium acetate (117.54 mmol, 36.39 eq) were mixed with 50 mL BuOH in a round bottom flask equipped with a reflux condenser and stirred at 90 °C. The reaction conversion was monitored by TLC (DCM) and UV/VIS absorption spectroscopy. After 7 h, during which the solution turned dark blue, the reaction mixture was cooled to room temperature and stirred over the weekend.
After removing the solvent by rotary evaporation the obtained blue solid was dissolved in DCM and washed with $H_2O$ (3 x 300 mL). The organic phase was dried over $Na_2SO_4$ and the solvent was removed. The crude product was purified by column chromatography (silica gel, DCM + 1 % THF, detection by TLC with DCM and UV/VIS spectroscopy).

Yield: 74.7 mg (4 %), metallic blue solid

**m-OH diF azaBODIPY complex (4)**

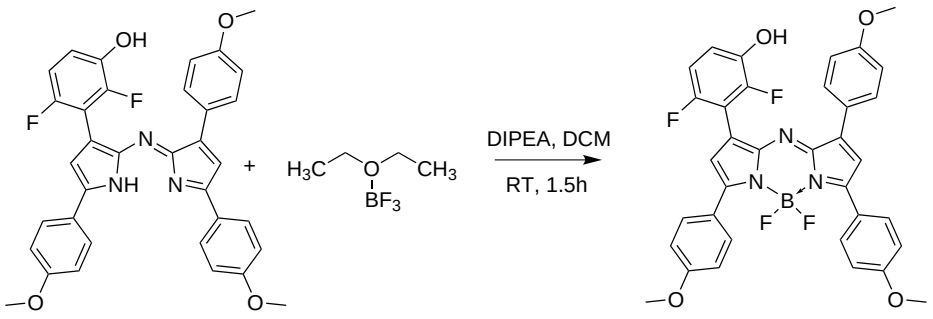


**Figure 3.20:** Synthesis of m-OH diF azaBODIPY complex (**4**)

64.7 mg m-OH diF azaBODIPY ligand (109.36 µmol, 1.00 eq) were dissolved in dry DCM under inert argon atmosphere in a Schlenk tube. 286 µl *N*,*N*-diisopropylethylamine (1.64 mmol, 15.01 eq) and 202 µl boron trifluoride diethyl etherate (4.64 mmol, 14.97 eq) were added dropwise. The solution was stirred at room temperature for 1.5 h. After a quantitative conversion was monitored by TLC (CH : EA 1 : 1), the solution was partitioned between DCM and aqueous $NaHCO_3$ solution (3 x 25 mL), dried over $Na_2SO_4$ and the solvent was removed by rotary evaporation.
The crude product was purified by column chromatography (silica gel, DCM : Tol 3 : 1, detection by TLC with DCM : CH 3 : 1 and UV/VIS spectroscopy) and recrystallization from MeOH.

Yield: 36.9 mg (53 %), purple metallic crystals

$^1$H NMR (300 MHz, chloroform-d): $\delta = 8.16 - 7.97$ (m, 6H), 7.09 – 6.82 (m, 10H), 3.96 – 3.78 (m, 9H). See figure 9.7 on page 103.
APT NMR (76 MHz, chloroform-d): $\delta = 162.56$, 161.68, 161.44, 161.30, 155.61, 152.16, 149.69, 146.58, 146.40, 144.55, 140.68, 140.43, 132.10, 131.49, 130.89, 130.10, 124.98, 124.53, 123.97, 122.12, 118.02, 117.13, 117.01, 114.48, 114.37, 114.26, 111.47, 111.15, 77.16, 55.54. See figure 9.8 on page 104.

**3-Hydroxy-4,4'-dimethoxychalcone**

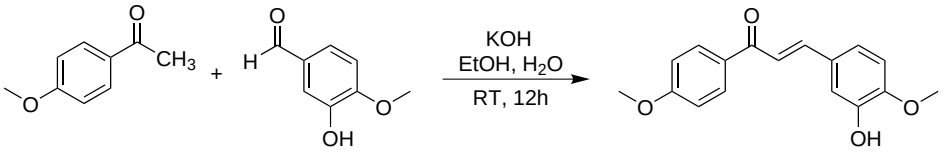


**Figure 3.21:** Synthesis of 3-hydroxy-4,4'-dimethoxychalcone

998.3 mg 4'-methoxyacetophenone (6.65 mmol, 1.00 eq) and 1.02 g isovanillin (6.69 mmol, 1.01 eq) were dissolved in 5 mL EtOH in a round bottom flask. 5 mL of an aqueous potassium hydroxide solution (1.17 g, 20.85 mmol, 3.14 eq) were added dropwise. The solution was stirred for 12 h at room temperature during which the solution turned orange. The reaction mixture was added dropwise to 25 mL 1 M HCl solution to precipitate the yellow product. The solid was filtered, washed with water and dried. The obtained yellow solid was used for further synthesis without purification.

Crude yield: 1.49 g (79 %), yellow powder

### 3-Hydroxy-4,4'-dimethoxynitrochalcone

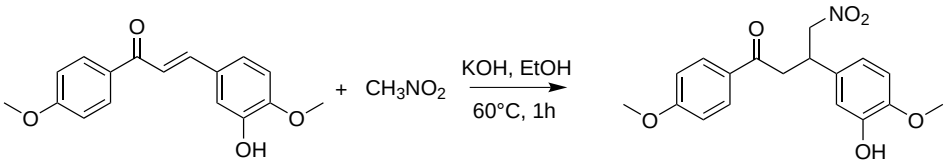


**Figure 3.22:** Synthesis of 3-hydroxy-4,4'-dimethoxynitrochalcone

In a round bottom flask equipped with a reflux condenser 1.49 g 3-hydroxy-4,4'-dimethoxychalcone (5.25 mmol, 1.00 eq) and 5.70 mL nitromethane (105.52 mmol, 20.11 eq) were mixed with 10 mL of a potassium hydroxide solution in EtOH (612.0 mg, 10.91 mmol, 2.08 eq) and stirred at 60 °C. The reaction progress was monitored by adding a spatula tip of ammonium acetate to a few drops of the reaction mixture dissolved in BuOH in a glass vial and heating with a heat gun up to the boiling point. After 1 h a blue coloration and TLC (DCM) of the solution indicates formation of the azaBODIPY ligand and therefore a successful reaction conversion.
The solution was stirred at room temperature overnight, then the solvent was removed by rotary evaporation. The brown oily residue was dissolved in 50 mL EtOAc and washed with HCl solution (3 x 50 mL). After drying the organic phase over $Na_2SO_4$ and removing the solvent by rotary evaporation a brown oil was obtained, which was used for further synthesis without purification.

Crude yield: 2.19 g (121 %, product containing residual solvent), brown oil

### m-OH MeO azaBODIPY ligand

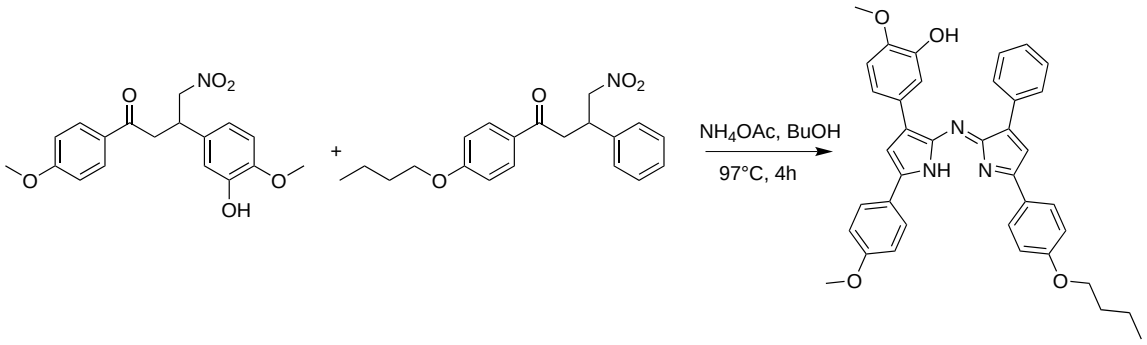


**Figure 3.23:** Synthesis of m-OH MeO azaBODIPY ligand

493.4 mg 3-hydroxy-4,4'-dimethoxynitrochalcone (1.43 mmol, 1.00 eq), 493.8 mg 4'-butoxynitrochalcone (1.45 mmol, 1.01 eq) and 4.11 g ammonium acetate (53.32 mmol, 37.32 eq) were mixed with 25 mL BuOH in a round bottom flask equipped with a reflux condenser and

stirred at 90 °C. The reaction conversion was monitored by TLC (DCM : CH 1 : 1) and UV/VIS absorption spectroscopy. After 4 h the reaction mixture was cooled to room temperature and stirred overnight.
After removing the solvent by rotary evaporation the obtained solid was dissolved in DCM and washed with NaCl solution (3 x 300 mL). The organic phase was dried over $Na_2SO_4$ and the solvent was removed. The crude product was purified by column chromatography (silica gel, DCM : CH 1 : 1, detection by TLC with DCM : CH 1 : 1 and UV/VIS spectroscopy) and recrystallized from MeOH.

Yield: 62.0 mg (7 %), dark green powder

**m-OH MeO azaBODIPY complex (5)**

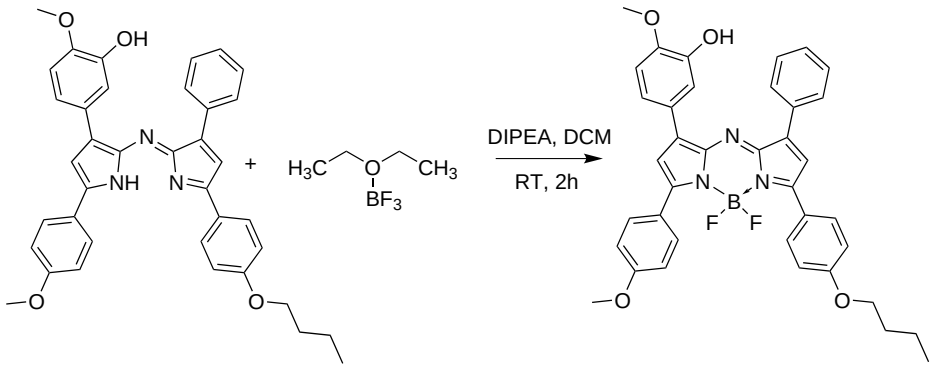


**Figure 3.24:** Synthesis of m-OH MeO azaBODIPY complex (**5**)

62.0 mg m-OH MeO azaBODIPY ligand (103.73 µmol, 1.00 eq) were dissolved in dry DCM under inert argon atmosphere in a Schlenk tube. 310 µl *N*,*N*-diisopropylethylamine (1.78 mmol, 17.16 eq) and 220 µl boron trifluoride diethyl etherate (1.78 mmol, 17.19 eq) were added dropwise. The solution was stirred at room temperature for 2 h. After a quantitative conversion was monitored by TLC (CH : EA 1 : 1), the solution was partitioned between DCM and aqueous $NaHCO_3$ solution (3 x 25 mL), dried over $Na_2SO_4$ and the solvent was removed by rotary evaporation.
The crude product was purified by column chromatography (silica gel, DCM + 1 % MeOH, detection by TLC with DCM : CH 3 : 1 and UV/VIS spectroscopy) and precipitated in CH to yield purple metallic crystals.

Yield: 66.4 mg (98 %), purple metallic crystals

$^1$H NMR (300 MHz, chloroform-d): $\delta = 8.17 - 8.00$ (m, J = 8.6, 3.5 Hz, 6H), 7.79 (d, J = 1.8 Hz, 1H), 7.64 (dd, J = 8.4, 1.7 Hz, 1H), 7.49 (t, J = 7.3 Hz, 2H), 7.42 (d, J = 7.0 Hz, 1H), 7.07 –

6.87 (m, 7H), 5.64 (s, 1H), 4.05 (t, J = 6.4 Hz, 2H), 3.97 (s, 3H), 3.89 (s, 3H), 1.86 – 1.74 (m, J = 14.5, 6.6 Hz, 2H), 1.56 (s, 2H), 0.99 (t, J = 7.3 Hz, 3H). See figure 9.9 on page 104.
APT NMR spectrum could not be recorded due to insufficient solubility of the compound.

### 3.1.2 Synthesis of polymers as sensor matrices

**Copolymer PAMcoHEAA with 1% hydroxy groups**

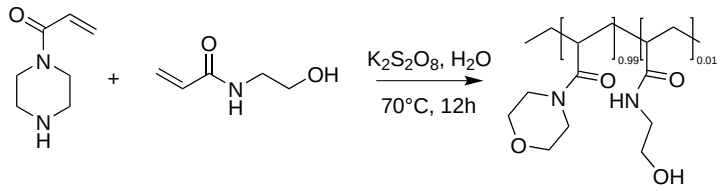


**Figure 3.25:** Synthesis of copolymer PAMcoHEAA with 1% hydroxy groups

The two monomers 4-acryloylmorpholine (4.43 mL, 35.15 mmol, 1.00 eq) (filtered through aluminum oxide to remove the monomethyl ether hydroquinone inhibitor before usage), and *N*-hydroxyethyl acrylamide (37 µl, 356.7 µmol, 0.01 eq) were dissolved in 50 mL $H_2O$ in a Schlenk tube under inert argon atmosphere. A spatula tip of potassium peroxodisulfate was added. The solution was flushed with nitrogen for 10 min and degassed by freeze-pump-thaw method (3 x). The solution was stirred at 70 °C for 12 h.
The viscous reaction mixture was added dropwise to 400 mL THF to precipitate a white polymer. The polymer was dried in a vacuum drying oven, dissolved in DCM and repeatedly precipitated in 400 mL Tol (2 x). Finally, the polymer was dissolved in DCM and precipitated in 400 mL CH to obtain a voluminous white polymer, which was dried in a vacuum drying oven.

Yield: 4.43 g (89 %)

**Copolymer PAMcoHEAA with 2% hydroxy groups**

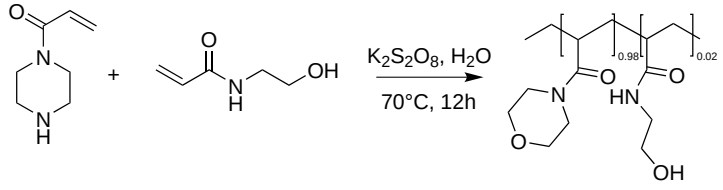


**Figure 3.26:** Synthesis of copolymer PAMcoHEAA with 2% hydroxy groups

The two monomers 4-acryloylmorpholine (4.38 mL, 34.71 mmol, 1.00 eq) (filtered through aluminum oxide to remove the monomethyl ether hydroquinone inhibitor before usage), and *N*-hydroxyethyl acrylamide (73 µl, 708.4 µmol, 0.02 eq) were dissolved in 50 mL $H_2O$ in a

Schlenk tube under inert argon atmosphere and 1 mg potassium peroxodisulfate was added. The solution was flushed with nitrogen for 10 min, degassed by freeze-pump-thaw method (3 x) and stirred at 70 °C for 12 h.
The viscous reaction mixture was added dropwise to 400 mL THF to precipitate a white polymer. The polymer was dried in a vacuum drying oven, dissolved in DCM and repeatedly precipitated in 400 mL Tol (2 x). Finally, the polymer was dissolved in DCM and precipitated in 400 mL CH to obtain a voluminous white polymer, which was dried in a vacuum drying oven.

Yield: 4.29 g (75 %)

### 3.1.3 Covalent immobilization of azaBODIPY dyes on a polymer matrix

**Protection of the hydroxy group on p-OH BuO azaBODIPY**

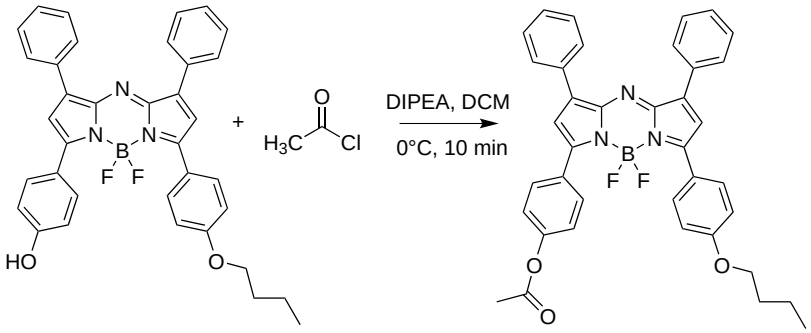


**Figure 3.27:** Synthesis of the protected p-OH BuO azaBODIPY

The p-OH BuO azaBODIPY (100.0 mg, 170.8 µmol, 1.00 eq) was dissolved in dry DCM in a Schlenk tube under inert argon atmosphere and cooled to 0 °C in an ice bath. 45 µl *N*,*N*-diisopropylethylamine (258.34 µmol, 1.51 eq) and 18 µl acetyl chloride (253.16 µmol, 1.48 eq) were added. The reaction conversion was monitored by TLC (DCM). After 10 min the solution was washed with $H_2O$, dried over $Na_2SO_4$ and the solvent was removed under reduced pressure. The crude product was purified by column chromatography (silica gel, DCM, detection by TLC with DCM).

Yield: 103.6 mg (97 %), purple metallic crystals

$^1$H NMR (300 MHz, chloroform-d): $\delta = 8.21 - 7.99$ (m, 8H), 7.46 (t, J = 6.0 Hz, 6H), 7.23 (d, J = 8.7 Hz, 2H), 7.12 (s, 1H), 7.07 – 6.90 (m, 3H), 4.06 (t, J = 6.4 Hz, 2H), 2.34 (s, 3H), 1.90 – 1.69 (m, 2H), 1.49 (dd, J = 14.9, 7.5 Hz, 2H), 1.00 (t, J = 7.3 Hz, 3H). See figure 9.10 on page 105.

**Protection of the hydroxy group on m-OH diCl azaBODIPY**

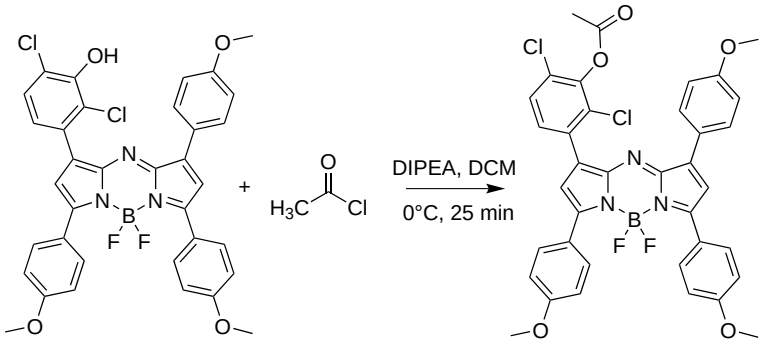


**Figure 3.28:** Synthesis of the protected *o*, *p*-diCl m-OH trimethoxy azaBODIPY

The m-OH diCl azaBODIPY (**3**) (20.0 mg, 29.75 µmol, 1.00 eq) was dissolved in dry DCM in a Schlenk tube under inert argon atmosphere and cooled to 0 °C in an ice bath. 11 µl *N*,*N*-diisopropylethylamine (63.15 µmol, 2.21 eq) and 4 µl acetyl chloride (56.26 µmol, 1.89 eq) were added. The reaction conversion was monitored by TLC (DCM : CH 3 : 1). After 25 min the solution was washed with $H_2O$, dried over $Na_2SO_4$ and the solvent was removed under reduced pressure. The crude product was purified by column chromatography (silica gel, DCM, detection by TLC with DCM : CH 3 : 1).

Yield: 20.6 mg (94 %), green solid

$^1$H NMR (300 MHz, chloroform-d): $\delta = 8.11$ (d, J = 8.8 Hz, 2H), 8.03 (t, J = 9.0 Hz, 4H), 7.64 (d, J = 8.5 Hz, 1H), 7.44 (d, J = 8.6 Hz, 1H), 7.16 (s, 1H), 7.01 (dd, J = 9.0, 3.4 Hz, 5H), 6.94 (d, J = 8.8 Hz, 2H), 3.89 (d, J = 3.4 Hz, 9H), 2.46 (s, 3H). See figure 9.11 on page 105.

**General procedure of the reaction of p-OH BuO azaBODIPY dye with hexaethylene glycole**

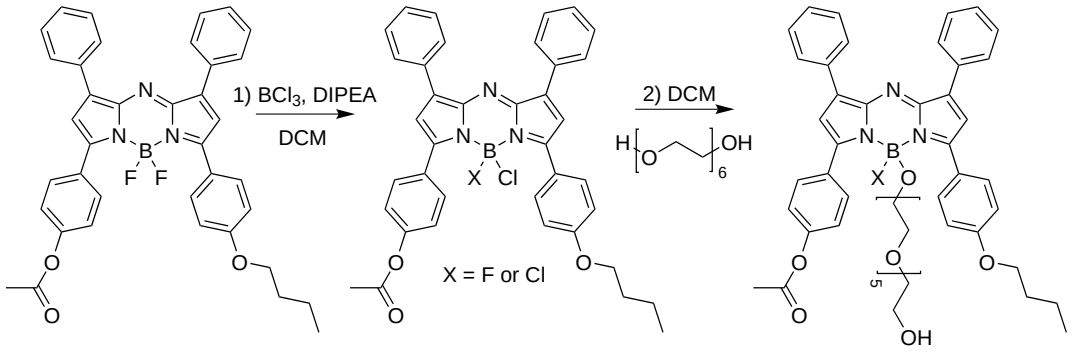


**Figure 3.29:** Reaction scheme of the coupling reaction of p-OH BuO azaBODIPY with hexaethyleneglycol

1.0 mg protected p-OH BuO azaBODIPY dye (1.59 µmol, 1.00 eq, see section 3.1.3) was dissolved in dry DCM in a Schlenk tube under inert argon atmosphere. 3 µl of a 1 M solution of $BCl_3$ in DCM (3.0 µmol, 1.88 eq) were added. The solution was stirred for 10 min at room temperature, then a solution of 20 µl hexaethylene glycol (79.8 µmol, 50.0 eq) and 3.0 µl DIPEA (17.2 µmol, 10.8 eq) in 1 ml dry DCM were added to the reaction mixture and stirred for another 10 min. The solution was partitioned between DCM and water. The resulting solution was analyzed with TLC (with DCM + MeOH 30 + 5), UV/VIS spectroscopy or $^1$H NMR (see section 4).

### Coupling of p-OH BuO azaBODIPY dye to a PAMcoHEAA polymer matrix with 1 % OH groups

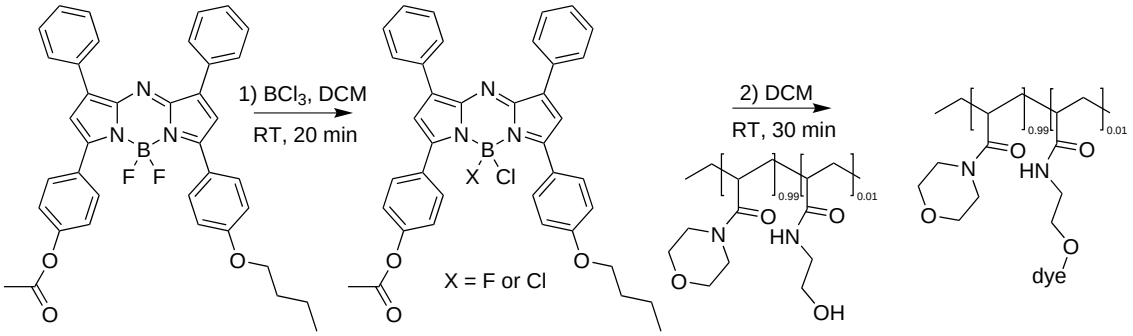


**Figure 3.30:** Reaction scheme of the covalent immobilization of p-OH BuO azaBODIPY on PAMcoHEAA polymer matrix with 1 % hydroxy groups

5.0 mg protected p-OH BuO azaBODIPY dye (7.97 µmol, 1.00 eq, see section 3.1.3) were dissolved in dry DCM in a Schlenk tube under inert argon atmosphere. 96 µl of a 0.1 M solution of $BCl_3$ in Tol (9.6 µmol, 1.20 eq) were added. The solution was stirred for 20 min at room temperature, then the reaction mixture was added to a solution of 500 mg PAMcoHEAA polymer (see section 3.1.2) in DCM under inert argon atmosphere and stirred for another 30 min. The solution was partitioned between DCM and aqueous $NaHCO_3$ solution (2 x 200 mL). The solvent was evaporated under reduced pressure up to a few milliliters which were precipitated in 200 mL CH : Tol 2 : 1. (2 x) to remove the unbound dye. The obtained light green polymer was dried in a vacuum oven. The amount of the bound dye was estimated by dissolving 5 mg of polymer in 1 ml DMSO and measuring the absorption of the solution.

Yield: 346 mg light green polymer with approximately 0.05 wt.% dye bound to the polymer matrix

### Coupling of p-OH BuO azaBODIPY dye to a PAMcoHEAA polymer matrix with 2 % OH groups

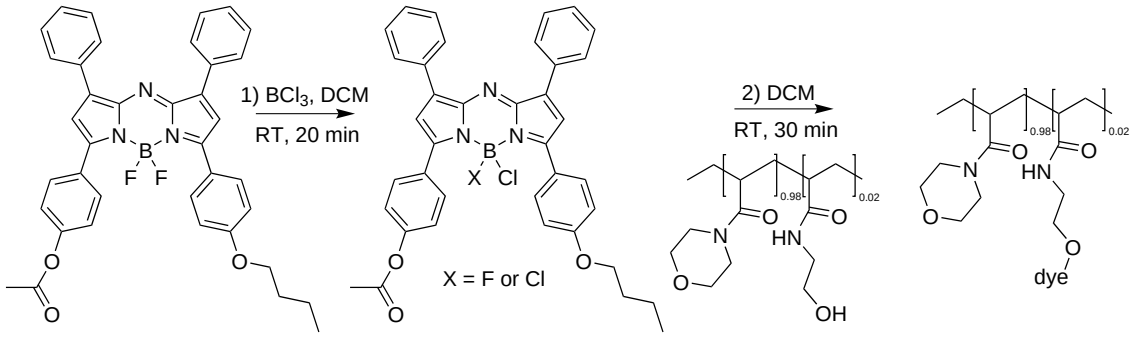


**Figure 3.31:** Reaction scheme of the covalent immobilization of p-OH BuO azaBODIPY on PAMcoHEAA polymer matrix with 2 % hydroxy groups

3.0 mg protected p-OH BuO azaBODIPY dye (4.78 µmol, 1.00 eq, see section 3.1.3) were dissolved in dry DCM in a Schlenk tube under inert argon atmosphere. 57 µl of a 0.1 M solution of $BCl_3$ in Tol (5.7 µmol, 1.19 eq) were added. The solution was stirred for 20 min at room temperature, then the reaction mixture was added to a solution of 300 mg PAMcoHEAA polymer (see section 3.1.2) in DCM under inert argon atmosphere and stirred for another 30 min. The solution was partitioned between DCM and $NaHCO_3$ solution (2 x 150 mL). The solvent was evaporated under reduced pressure up to a few milliliters which were precipitated in 200 mL CH : Tol 2 : 1. (2 x) to remove the unbound dye. The obtained light green polymer was dried in a vacuum oven. The amount of the bound dye was estimated by dissolving 5 mg of polymer in 1 ml DMSO and measuring the absorption of the solution.

Yield: 235 mg light green polymer with approximately 0.055 wt.% dye bound to the polymer

### Coupling of m-OH diCl azaBODIPY dye to a PAMcoHEAA polymer matrix with 1 % OH groups

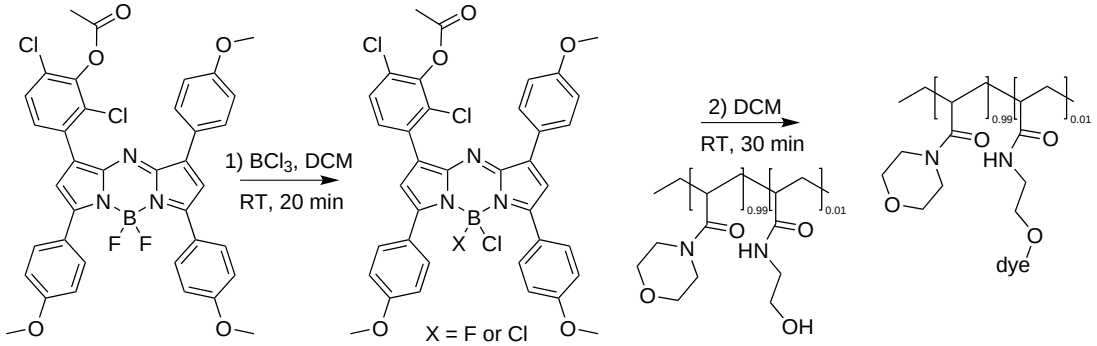


**Figure 3.32:** Reaction scheme of the covalent immobilization of m-OH diCl azaBODIPY on PAMcoHEAA polymer matrix with 1 % hydroxy groups

3.0 mg protected m-OH diCl azaBODIPY dye (4.20 µmol, 1.00 eq, see section 3.1.3) were dissolved in dry DCM in a Schlenk tube under inert argon atmosphere. 50 µl of a 0.1 M solution of $BCl_3$ in Tol (5.0 µmol, 1.19 eq) were added. The solution was stirred for 20 min at room temperature, then the reaction mixture was added to a solution of 300 mg PAMcoHEAA polymer (see section 3.1.2) under inert argon atmosphere and stirred for another 30 min. The solution was partitioned between DCM and $NaHCO_3$ solution (2 x 150 mL). The solvent was evaporated under reduced pressure up to a few milliliters which were precipitated in 200 mL CH : Tol 2 : 1. (2 x) to remove the unbound dye. The obtained light green polymer was dried in a vacuum oven. The amount of the bound dye was estimated by dissolving 5 mg of polymer in 1 ml DMSO and measuring the absorption of the solution.

Yield: 221 mg light green polymer with approximately 0.03 wt.% dye bound to the polymer matrix

**Coupling of p-OH BuO azaBODIPY dye to a cellulose acetate propionate matrix**

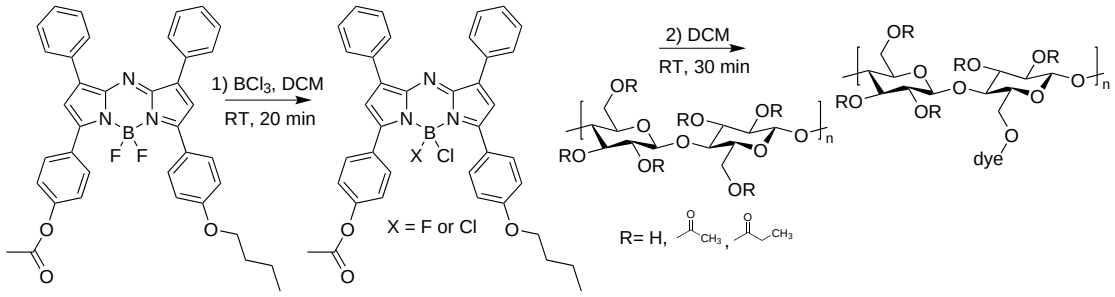


**Figure 3.33:** Reaction scheme of the covalent immobilization of p-OH BuO azaBODIPY on a cellulose acetate propionate matrix

3.0 mg protected p-OH BuO azaBODIPY dye (4.78 µmol, 1.00 eq, see section 3.1.3) were dissolved in dry DCM in a Schlenk tube under inert argon atmosphere. 24 µl of a 1 M solution of $BCl_3$ in Tol (24 µmol, 5.02 eq) were added. The solution was stirred for 20 min at room temperature, then the reaction mixture was added to a solution of 300 mg cellulose acetate propionate in DCM under inert argon atmosphere and stirred for another 30 min. Most of the solvent was evaporated in a $N_2$ stream up to a few milliliters which were precipitate in 45 mL CH : Tol 2 : 1. (2 x) to remove the unbound dye. The precipitate was dried, dissolved in acetone and precipitated in 45 mL CH : Tol 2 : 1 two more times. The obtained light green cellulose acetate proprionate was dried in a vacuum oven. The amount of the bound dye was estimated by dissolving 5 mg of polymer in 1 ml DMSO and measuring the absorption of the solution.

Yield: 220 mg light green stained cellulose acetate proprionate with approximately 0.33 wt.% dye bound to the matrix

## 3.2 Sensor film preparation

### 3.2.1 Preparation of stock solutions

Compounds **1**, **2**, **3**, **4** and **5** as well as p-OH C12 azaBODIPY, unsubstituted tetraphenyl azaBODIPY and diCl tert-butyl BODIPY were weighed in 3 mL vials and dissolved in THF to obtain solutions with concentrations of 2 mg/mL. For the D4 stock solution hydrogel D4 and THF were weighted in a 20 mL vial and stirred overnight to yield a 10 wt. % solution of polymer in THF. Ethyl cellulose (ethyloxy content 50 %) and Tol : EtOH 3 : 2 were weighed in a 20 mL vial to yield a stock solution of 5 wt.% EC. A Hyflon® AD 60 stock solution was prepared by dissolving the polymer in perfluordecalin (washed with aqueous $K_2CO_3$ solution and dried over $Na_2SO_4$ before use) to yield a 5 wt.% solution.

### 3.2.2 Preparation of D4 sensor films for pH calibration

Sensor "cocktails" containing 100 mg D4 (using a stock solution in THF) and 0.2 mg dye (0.2 % relative to the polymer, using stock solutions of compounds **2**, **3**, **4** and **5** in THF) were prepared by mixing and homogenizing the solution of the polymer and the dye. The "cocktails" were knife coated on a dust-free PET foil with a 3 mil coating knife and dried at room temperature to obtain sensor films with a thickness of approximately 7.6 µm.

### 3.2.3 Preparation of D4 sensor films for quantum yield measurements

Sensor "cocktails" containing 25 mg D4 (using a stock solution in THF) and 12.5 µg, 50 µg, 125 µg or 250 µg of compound **3** (0.05 %, 0.2 %, 0.5 % or 1 % in respect to the polymer, using stock solutions in THF) were prepared by mixing and homogenizing the solution of the polymer and the dyes. The "cocktails" were knife coated on dust-free PET foils with a 3 mil (in case of the 0.05 % sensor film), 1 mil (in case of the 0.2 % sensor film) or 0.5 mil (in case of the 0.5 % and 1 % sensor film) coating knife. After evaporation of the solvent, sensor layers with thicknesses of approximately 7.6, 2.5 and 1.3 µm were obtained.

The same way sensor films with a reference dye p-OH C12 azaBODIPY were prepared. In addition, blank foils solely based on D4 hydrogel were knife coated on a PET support with the film thicknesses of 3, 1 or 0.5 mil. For the quantum yield measurements sensor spots with a diameter of 11 mm were punched out of each sensor foil.

### 3.2.4 Preparation of D4 sensor films for concentration dependency measurements

Sensor films consisting of 25 mg D4 and 12.5 µg, 50 µg, 125 µg or 250 µg of compound **3** (0.05 %, 0.2 %, 0.5 % or 1 % in respect to the polymer) were prepared by mixing the corresponding amount of dye and D4 (by using stock solutions in THF) in a vial and knife coating the "cocktails" on a dust-free PET foil with a 0.5 mil coating knife. Additionally, sensor foils

with the same compositions, but using a reference dye p-OH C12 azaBODIPY instead, were prepared. After evaporation of the solvent sensor foils with a film thickness of approximately 1.3 µm were obtained.

### 3.2.5 Preparation of D4 sensor films for light harvesting experiments

For the investigations of a light harvesting concept, sensor films with a pH insensitive donor dye (an unsubstituted tetraphenyl azaBODIPY dye, donor 1) and an acceptor dye (compound **3**, m-OH diCl azaBODIPY) in different ratios were prepared (see table 3.1). 12.5 mg D4 (using a stock solution in THF) were mixed with the corresponding amount of donor and acceptor dye (by using stock solutions in THF), homogenized by vigorous stirring and knife coated on a dust-free PET foil with a film thickness of 0.5 mil, obtaining a final film thickness of approximately 1.3 µm after evaporation of the solvent. The same way sensor films with diCl tert-butyl BODIPY as donor dye (donor 2) were prepared.

**Table 3.1:** Composition of the sensor films for light harvesting measurements

| | amount of donor (wt.% relative to the polymer) | amount of acceptor (wt.% relative to the polymer) |
|---|---|---|
| 12.5 mg D4 + | - | 25 µg (0.2 %) |
| | 25 µg (0.2 %) | 25 µg (0.2 %) |
| | 50 µg (0.4 %) | 25 µg (0.2 %) |
| | 50 µg (0.4 %) | 12.5 µg (0.1 %) |
| | 50 µg (0.4 %) | - |

### 3.2.6 Preparation of PAMcoHEAA polymer sensor films for pH calibration

25 mg of m-OH diCl azaBODIPY (compound **3**) immobilized on polymer PAMcoHEAA (see section 3.1.3 on page 46) were mixed with 5 mg Egyptian blue and dissolved in 250 µl dioxane in the glove box. 1.4 µl di-n-butlydilauryltin (catalyst) and 1.4 µl DESMODUR N 75 MPA/X (aliphatic polyisocyanate crosslinker) were added and stirred vigorously before the "cocktail" was knife coated on a dust-free PET foil with a 3 mil coating knife and cured for 1 h at 80 °C in the glove box. A final film thickness of approximately 7.6 µm was obtained after curing. The acetyl protection group on the hydroxy groups of the dyes were cleaved off by stirring in 0.01 M aqueous NaOH solution for 30 minutes.

### 3.2.7 Preparation of ethyl cellulose sensor films for $CO_2$ calibration

For the indicator layer, a "cocktail" consisting of 25 mg ethyl cellulose (using a stock solution in Tol : EtOH 3 : 2), 25 µg m-OH diF azaBODIPY (0.1 % relative to the polymer) and 2 mg Egyptian blue were mixed and homogenized by vigorous stirring. The "cocktail" was purged

with $CO_2$ before 10 µl tetraoctylammonium hydroxide solution (20% in MeOH) were added and knife coated on a PET foil using a 1 mil coating knife. A $CO_2$ permeable Hyflon layer was knife coated onto the first layer with a 1 mil coating knife after the first layer was completely dry. The final sensor film has a thickness of approximately 2.4 µm.

With the same procedure a sensor film containing 25 mg ethyl cellulose, 25 µg m-OH azaBODIPY (0.1 % relative to the polymer) and 2 mg Egyptian blue, as well as a sensor film containing 25 mg ethyl cellulose, 25 µg m-OH MeO azaBODIPY (0.1 % relative to the polymer) and 2 mg Egyptian blue on a PET support was prepared. For a light harvesting attempt a "cocktail" consisting of 25 mg ethyl cellulose, 50 µg m-OH azaBODIPY (0.2 % relative to the polymer), 100 µg unsubstituted tetraphenyl azaBODIPY (as light harvesting donor, 0.4 %) and 2 mg Egyptian blue was knife coated on a dust-free glass support with a 0.5 mil coating knife, followed by a Hyflon layer, obtaining a film thickness of approximately 1.3 µm in the dry state.

## 3.3 Structural characterization

### 3.3.1 Nuclear magnetic resonance spectroscopy (NMR)

$^1$H, COSY and APT NMR spectra of the synthesized dyes were recorded on a 300 MHz Brucker instrument (www.bruker.com) in deuterated chloroform as solvent using TMS (tetramethylsilane) as reference signal. For analysis of the data MestReNova software from Mestrelab (www.mestrelab.com) was used.

### 3.3.2 High resolution mass spectrometry (HR-MS)

Mass spectra of the five synthesized dyes were recored on a Micromass TofSpec 2E Time-of-Flight Mass Spectrometer by Bruker (www.bruker.com). The data were analyzed with MassLynx software V4.1 by Waters (www.waters.com). External calibration was done with a suitable mixture of poly(ethyleneglycol)s (PEG). These measurements were conducted by Karin Bartl from the Institute of Chemistry and Technology of Materials at TU Graz.

## 3.4 Photophysical characterization

### 3.4.1 Preparation of buffer solutions

Buffer solutions with concentrations of 100 mM and pH values ranging from 5 to 13 were prepared with piperazine, MES, bis-TRIS, TRIS, CHES or CAPS buffer by using a pH meter (SevenEasy™, Mettler Toledo, www.mt.com) using a glass electrode (SenTix® HW, WTW, www.wtw.com) to adjust the pH. The pH meter was calibrated by using standard buffer solutions with a pH of 4.01, 7.01 and 10.01 (Hanna instruments, www.hannainstruments.at). The pH of the buffer solutions was adjusted by adding 1 M HCl or 1 M NaOH solution.

The ionic strength of the buffer solutions was set to 100 mM by using NaCl as background electrolyte.

### 3.4.2 Absorption measurements

Absorption spectra were recorded on a Varian Cary® 50 UV-Vis spectrophotometer by Agilent (www.agilent.com) using Cary WinUV software. The spectra were recorded using fast scan mode with baseline correction (using the corresponding solvent as blank sample) in a range between 900 nm and 300 nm. 100-OS precision cuvettes from Hellma Analytics with a light path of 10 mm were used (www.hellma-analytics.com).

#### Molar absorption coefficients

For determining the molar absorption coefficients of the synthesized dyes, stock solutions with concentrations of approximately $5 \cdot 10^{-6}$ M were prepared by dissolving a defined amount of dye in a defined volume of THF and recording the absorption spectra (triple determination, see equation 2.1 on page 5).

#### Determination of the amount of dye bound to the polymer matrix

In order to describe the efficiency of the coupling reactions 5 mg of each indicator stained polymer was dissolved in 1 ml DMSO and absorption of the solution was measured. The amount of dye bound to the polymer was calculated using Lambert-Beer law (2.1 on page 5).

### 3.4.3 Emission and excitation measurements

Emission and excitation spectra were recorded on a Fluorolog® 3 Spectrofluorometer from Horiba Scientific (www.horiba.com) equipped with a R2658 photomultiplier tube by Hamamatsu (www.hamamatsu.com) or on a fluorescence spectrophotometer F-7000 from Hitachi (www.hitachi-hightech.com). 100-OS precision cuvettes from Hellma Analytics with a light path of 10 mm were used (www.hellma-analytics.com).

#### pH calibration

pH calibration of the synthesized azaBODIPY dyes was conducted for all dyes in solution as well as for the indicators entrapped in a hydrogel D4 matrix or covalently immobilized on a PAMcoHEAA polymer matrix. For the measurements in solution, stock solutions of each dye of approximately 0.5 mg/mL in THF were prepared. The stocks were diluted in EtOH, and subsequently mixed with buffer solutions with pH values ranging from 5 to 13 in a ratio of 1 : 1 to obtain solutions with concentrations of approximately $1.5 \cdot 10^{-6}$ M. Emission spectra of the resulting solutions were recorded from 660 to 850 nm with excitation at 650 nm. The maxima of the obtained fluorescence spectra were plotted versus the pH values of the buffer, which was used for the corresponding measurements, and fitted with a Boltzmann equation (see equation 2.14 on page 15) to calculate the $pK_a$.

pH calibration of the dyes physically entrapped in a hydrogel D4 matrix was conducted with sensor films prepared according to the procedure described in section 3.2.2 on page 48. The sensor layers on PET foil were cut into rectangular stripes which fit exactly diagonally into a glass cuvette. The cuvette was filled with buffer solutions ranging from pH 5 to pH 13 and washed with water after each pH change. Emission spectra were recorded from 660 nm to 800 nm with excitation at 650 nm for each pH step. The sigmoidal curves resulting from plotting the maxima of the spectra versus the pH were fitted with a Boltzmann equation. The point of inflection of the fitted curve represents the $pK_a$ of the physically entrapped dye.

The sensor film consisting of m-OH diCl azaBODIPY (**3**) covalently immobilized on the polymer matrix PAMcoHEAA (see section 3.2.6 on page 49) was measured in an analogous manner, with excitation wavelength set to 620 nm and emission spectra recorded from 650 nm to 850 nm.

### Quantum yields

Quantum yields were measured relatively to a fluorescent dye with a known fluorescence quantum yield as well as employing an absolute method by using an integrating sphere set up (see section 2.3.2 on page 10).

For determining the relative quantum yields, first the absorption and emission spectra of a $1.5 \cdot 10^{-6}$ M solution of diBuO azaBODIPY standard dye in chloroform, which has a quantum yield of 36 % (in chloroform) [54, 55], were recorded with $\lambda_{exc} = 650$ nm from 655 nm to 900 nm. Subsequently, absorption and emission spectra of $1.5 \cdot 10^{-6}$ M solutions of compounds **1**, **2**, **3**, **4** and **5** in THF were recorded with the identical instrument settings. The relative quantum yields were calculated according to equation 2.7 on page 10. [13, 14]

For determining the absolute quantum yields of the immobilized dyes, a Fluorolog® 3 Spectrofluorometer equipped with a Quanta-$\varphi$ integrating sphere from Horiba Scientific (www.horiba.com) was used. Excitation spectra were recorded from 600 nm to 650 nm with excitation wavelength set to 625 nm, and placing a neutral density 5 % transmission filter (actual transmission $\lambda_{exc}(625\,nm) = 4.74\,\%$, balance factor = 21, see figure 9.19 on page 113) in front of the detector. Emission spectra were recorded with $\lambda_{exc} = 625$ nm from 645 nm to 900 nm. Sensor films containing 0.05 %, 0.2 %, 0.5 % and 1 % m-OH diCl azaBODIY dye (compound **3**) or p-OH C12 azaBODIPY dye in a D4 matrix as well as blank films consisting of only D4 were prepared according to the procedure described in section 3.2.3 on page 48. Sensor spots with a diameter of 11 mm were punched out and placed in a pH 5 buffer in the sample holder of the device. The quantum yields of the dyes were calculated using FluorEssence™ software by Horiba.

### Concentration dependency of emission in D4

In order to investigate the impact of various concentrations of PET dyes physically entrapped in a D4 matrix, sensor films of compound **3** (m-OH diCl azaBODIPY) and p-OH C12 azaBODIPY

in hydrogel D4 were prepared as described in 3.2.4 on page 48. The sensor films were cut into rectangular stripes to fit diagonally into a glass cuvette filled with buffer solutions ranging from pH 5 to pH 11 and measured, rinsing the cuvette with water after each pH step. Emission spectra were recorded from 650 nm to 850 nm with excitation at 620 nm. $pK_a$ values were determined in an analogues manner as for pH calibrations. Additionally, absorption spectra from 300 nm to 900 nm were recorded at pH 5 and pH 11.

### Light harvesting concept in D4

A concept of light harvesting was investigated by using the sensor films as described in section 3.2.5 on page 49. Emission spectra ($\lambda_{em} = 635$ nm to 900 nm, $\lambda_{exc} = 624$ and $\lambda_{em} = 660$ nm to 900 nm, $\lambda_{exc} = 650$) and excitation spectra ($\lambda_{exc} = 400$ nm to 730 nm, $\lambda_{em} = 740$ nm) were recorded at pH 5 and 10.

The sensor films in dry state were also examined using a FireStingO2 from PyroScience (www.pyro-science.com).

### Fluorescence lifetime

Fluorescence lifetimes $\tau$ were determined by TCSPC (time-correlated single photon counting) using a Fluorolog® 3 Spectrofluorometer equipped with a NanoLED light source N-635L (for excitation at $\lambda_{exc}$= 635 nm) controlled by a DeltaHub module from Horiba Scientific. Data analysis was performed with DAS6 decay analysis software from Horiba Scientific (www.horiba.com). A scattering suspension of poly(1-vinylpyrrolidone-co-styrene) in water was used to record the prompt fluorescence signal (with emission monochromator set to 643 nm). The lifetimes of compounds **1**, **2**, **3**, **4** and **5** were measured in THF with emission monochromator set to 700 nm. Moreover, the sensor films for concentration dependency measurements in D4 (see section 3.2.4 on page 48) were measured with emission wavelength set to 700 nm in buffer solution with pH 5.7. Furthermore, decay times of the dyes in the sensor films prepared for light harvesting measurements (see section 3.2.5 on page 49) were measured in a buffer solution with pH 5.7 at $\lambda_{em} = 660$ nm (emission maximum of the donor) and at 730 nm (emission maximum of the acceptor). The measured data were fitted with a mono-exponential or bi-exponential fit.

### $CO_2$ calibration

$CO_2$ measurements were performed on a set-up consisting of four Piccolo2-OEM modules from Pyro Science (www.pyro-science.com) and mass flow controllers (MFCs) red-y from Vögtlin Instruments (www.voegtlin.com) controlled by SenGasChar software from Pyro Science. The $CO_2$ sensitive foils prepared as described in section 3.2.7 on page 49 were cut into rectangular stripes to fit into the sample holder of the device. A gas mix of nitrogen and test gas (20, 5 or 0.2 % $CO_2$) was produced by the MFCs, the gas mix was humidified to 100 % relative

humidity by bubbling through water before the gas stream entered the sample chamber. All measurements were performed at room temperature. The measurements were performed with maximum LED intensity, 8 ms measuring time and a modulation frequency of 2000 Hz. Each cycle consisted of 5 or 7 calibration steps, with a duration of 15 min up to 60 min, from 0 hPa to 189.6 hPa $CO_2$ (using the 20 % $CO_2$ gas mix), from 0 hPa to 49 hPa $CO_2$ (using the 5 % $CO_2$ gas mix) or from 0 hPa to to 1.9 hPa $CO_2$ (using the 0.2 % $CO_2$ gas mix), performing multiple cycles.

# 4 Results and Discussion

azaBODIPYs exhibit a couple of favorable properties, which make them ideal indicators for pH sensing: they have high molar absorption coefficients, high fluorescence quantum yields, sharp absorption and emission bands and they are extremely photostable. Moreover, they absorb and emit in the red/ near infrared region of the light, which is preferential for many applications of fluorescence-based sensors. Previously reported azaBODIPYs in pH sensors are based on on/off PET-quenching and ICT. [5, 6] They carry a pH sensitive hydroxy group in para-position on the phenyl group, which leads to incorporation of the OH-group into the $\pi$-system of the dye's core. Consequently, absorption spectra show a pH dependent shift to higher wavelengths upon deprotonation. With a new approach, azaBODIPYs with meta-OH substitution were synthesized. Due to the meta-hydroxy group, the pH sensitive group is no longer incorporated into the $\pi$-system and the dye is purely based on PET-quenching.

In the first section of this chapter the synthesis of the novel azaBODIPY dyes as well as new synthetic strategies for covalent immobilization of the dyes on a matrix material will be discussed. In the second section the photophysical properties of the new dyes will be examined. And finally, the sensing properties and the applicability of the new dyes in pH and $CO_2$ sensors will be discussed.

## 4.1 Synthetic considerations

### 4.1.1 Synthesis of azaBODIPY dyes

For the synthesis of tetraarylazadipyrromethenes, the precursors of azaBODIPYs, two different approaches are commonly used. The first approach uses 2,4-diaryl-5-nitroso-pyrroles and 2,4-diarylpyrroles as educts, which are condensed to yield a tetraarylazadipyrromethene. This synthetic strategy allows for unsymmetrical tetraarylazadipyrromethenes with four distinct aryl substituents. The condensation reaction is tolerant to a wide range of different aryl substituents, however, the commercially available choice of pyrroles for this reaction is limited. [56]

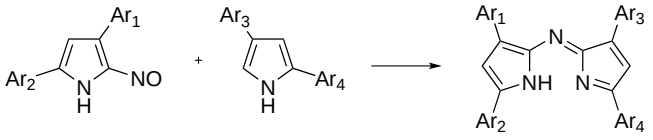


**Figure 4.1:** Method 1 for the synthesis of tetraarylazadipyrromethenes

In the second approach diaryl $\alpha,\beta$-unsaturated ketones (chalcones) are used as educts. The chalcones are converted into the corresponding 1,3-diaryl-4-nitrobutan-1-ones (nitrochalcones) via Michael addition of nitromethane. Condensation of to nitrochalcones with ammonium acetate yields the tetraarylazadipyrromethene. [54] When two nitrochalcones with distinct substituents are used for this reaction generally three main products are formed: two symmetrical tetraarylazadipyrromethenes and one asymmetrical tetraarylazadipyrromethene.

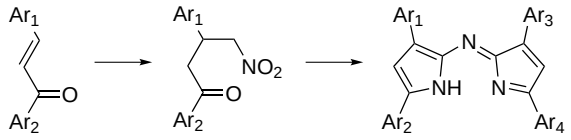


**Figure 4.2:** Method 2 for the synthesis of tetraarylazadipyrromethenes

The second approach was used to synthesize the azaBODIPY dyes **1-5**. $\alpha,\beta$-unsaturated ketones with the desired aryl substitution are not commercially available, therefore a previous reaction step, the synthesis of the chalcones from an acetophenone and a benzaldehyde, was necessary. A disadvantage of this reaction method is the limited availability of the corresponding benzaldehydes for the azaBODIPY synthesis. An overview of the four reaction steps is illustrated in figure 4.3.

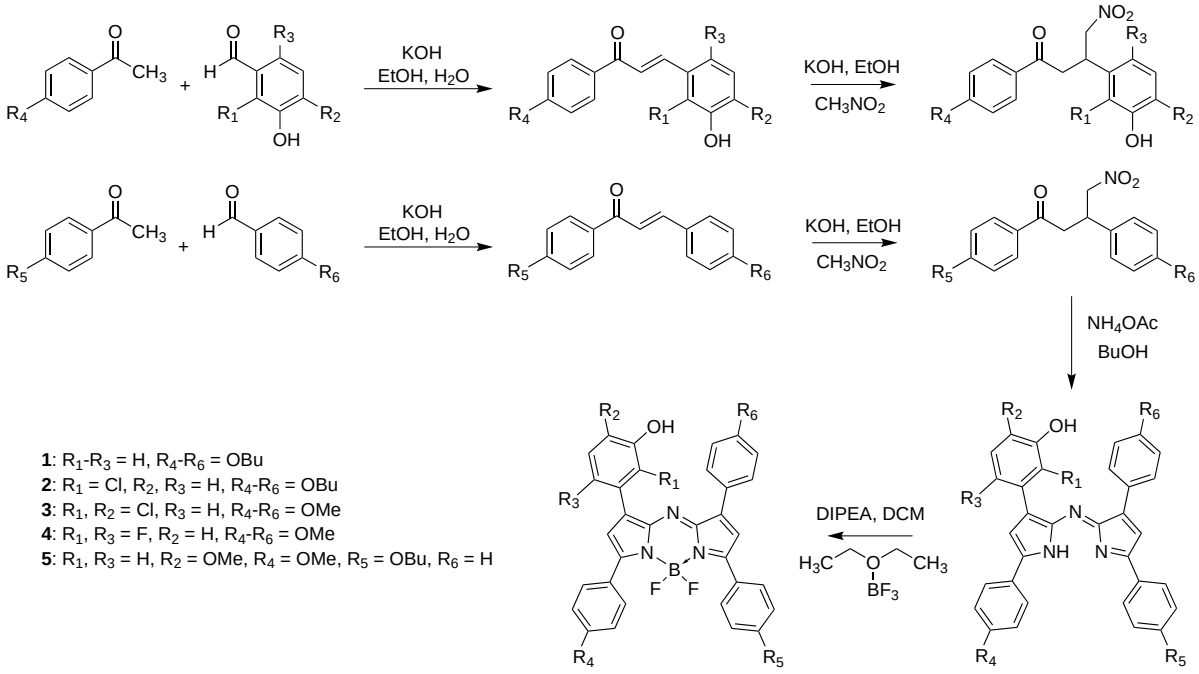


**Figure 4.3:** Overview of the reaction steps for the synthesis of compounds **1-5**

AzaBODIPYs with the substitution pattern as shown in figure 4.3 and a pH sensitive group in meta-position on the $Ar_1$ were chosen due to several reasons: azaBODIPYs with similar structure, but pH sensitive group in para-position of the $Ar_2$ ring show absorption shifts to higher wavelength in the deprotonated form because the hydroxy group is fully integrated into the conjugated $\pi$-system of the dye's core. [6] OH-substitution on meta-position prevents the integration of the hydroxy group into the $\pi$-system and therefore the absorption spectrum is nearly independent of pH. Such a meta-OH substitution on $Ar_2$ was reported by Jokic *et al.*. However, this m-OH-substituted dye shows very low quantum yields. [5] With a new approach azaBODIPY dyes carrying a hydroxy group in meta-position on the $Ar_1$ were synthesized. They are promising pH indicators with pH independent absorption, exhibiting emission quenching due to sufficient PET quenching. Methoxy and butoxy groups were introduced to enhance the hydrophobic character of the dye, to enhance its solubility in organic solvents and its stability in matrix materials to prevent migration and aggregation. Different electron donating and electron withdrawing substituents on $Ar_1$ offer a possibility to tune the $pK_a$ of the dye. In general, the more electron withdrawing a substituent on the aryl moiety is, the lower the $pK_a$ of the indicator.

The procedure and reaction conditions for the synthesis of compounds **1-5** were adapted from Jokics *et al.* [5]

**Step 1: Chalcone**

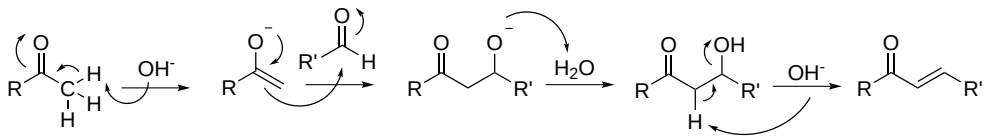


**Figure 4.4:** Reaction mechanism of the Claisen-Schmidt reaction

In the first reaction step an acetophenone and a benzaldehyde are coupled via Claisen-Schmidt condensation by using KOH as base. The reaction was run overnight at room temperature. The reaction worked with excellent yields of approximately 80-90 % (crude yields). The obtained yellow solid was used for the next reaction step without purification.

**Step 2: Nitrochalcone**

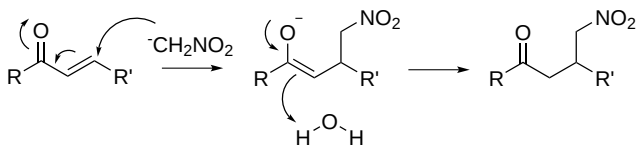


**Figure 4.5:** Reaction mechanism of the Michael addition with nitromethane

In a Michael addition with nitromethane the chalcone was converted into the corresponding nitrochalcone. The nitromethane, which acts as Michael-donor, is deprotonated by a base (KOH) to yield a carbanion. The nitromethanide anion intermediate couples to the Michael-acceptor, an $\alpha,\beta$-unsaturated ketone, followed by uptake of a proton to yield the product.

The reaction time was between 1 and 4 hours. After a complete conversion of the chalcone to the nitrochalcone the reaction mixture was washed with aqueous HCl solution and the solvent was removed by rotary evaporation. Oily products with crude yields of more than 100 % were obtained, which were used in the following reaction steps without further purification. It is assumed that not all of the nitromethane was completely removed, resulting in an oily instead of a solid crude product with yields over 100 %. That made it difficult to weigh out an accurate amount for the following reaction step, and consequently impossible to define an exact ratio of the two nitrochalcones for the ligand-forming reaction. Complete drying of the crude product could therefore possibly increase the yields of the follow up reaction step.

### Step 3: Tetraarylazadipyrromethene

Two nitromethanes with different aryl substituents were joined by a condensation reaction with ammonium acetate. Studies using isotope-labelled compounds, mass spectrometry and $^{15}$N NMR techniques suggest a possible reaction mechanism via an in situ formation of a pyrrole and the corresponding nitrosopyrrole followed by a condensation reaction. [57] The reaction yields a mixture of three different products, two symmetric products and one asymmetric product. The desired asymmetric tetraarylazadipyrromethene could be easily separated and purified via column chromatography with silica gel (or aluminum oxide in case of compound **3**). However, only low yields of less than 10 % could be achieved in this reaction step.

### Step 4: $BF_2$-chelated tetraarylazadipyrromethene

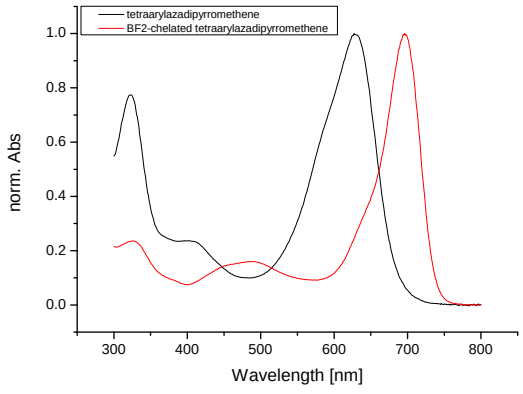


**Figure 4.6:** Absorption of the tetraarylazadipyrromethene vs. $BF_2$-chelated tetraarylazadipyrromethene using the example of compound **1**

Finally, in the last step of the azaBODIPY synthesis, complexation of the tetraarylazadipyrromethenes with boron trifluoride diethyl etherate and *N,N*-diisopropylethylamine yields the $BF_2$-chelated tetraarylazadipyrromethene (azaBODIPY) in good yields. Purification of the final product was done by column chromatography with silica gel (or aluminum oxide in case of compound **3**) and subsequent recrystallization from MeOH. The bathochromic shift of the absorption from a tetraarylazadipyrromethene to a $BF_2$-chelated tetraarylazadipyrromethene by using the example of compound **1** can be seen in figure 4.6.

Concluding, the following set of five azaBODIPY dyes was synthesized (figure 4.7).

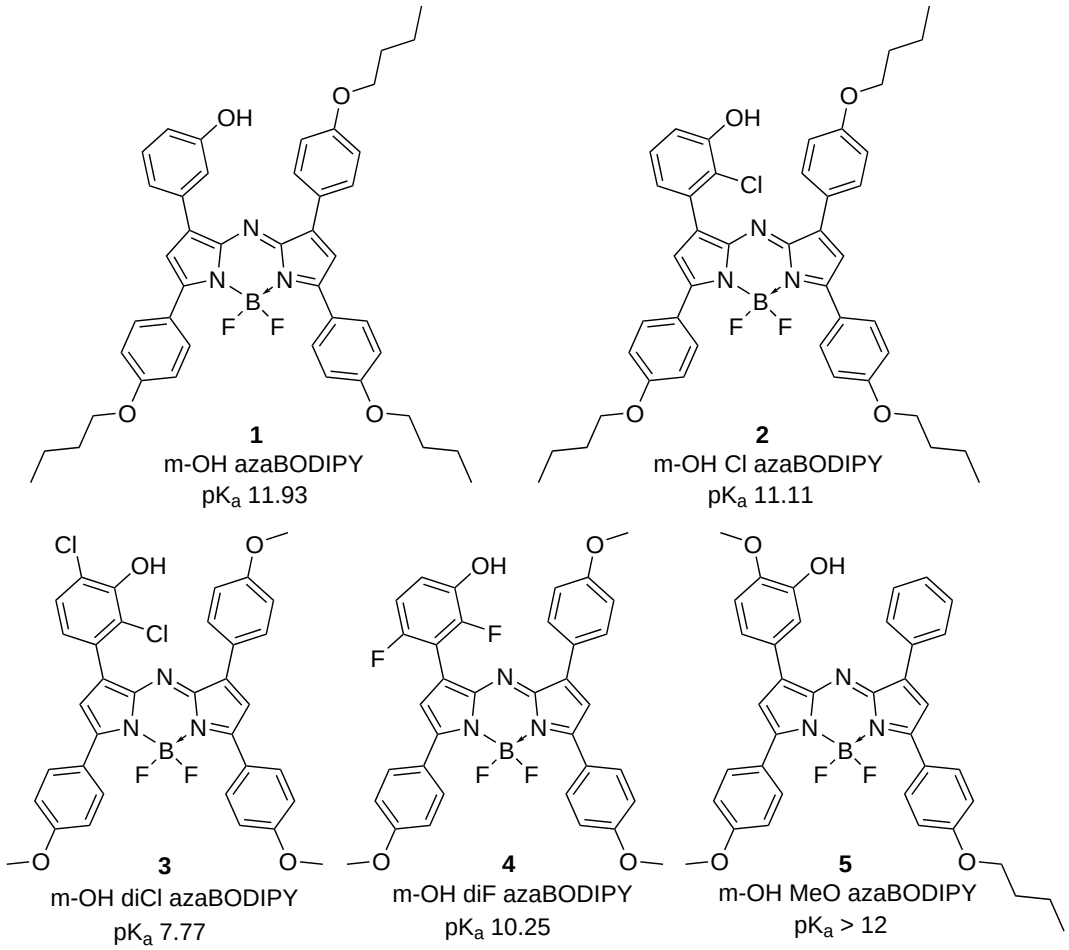


**Figure 4.7:** Set of five synthesized azaBODIPY dyes and their $pK_a$ in EtOH/$H_2O$ 1 : 1 (**1** m-OH azaBODIPY, **2** m-OH Cl azaBODIPY, **3** m-OH diCl azaBODIPY, **4** m-OH diF azaBODIPY and **5** m-OH MeO azaBODIPY)

### 4.1.2 Covalent immobilization of azaBODIPY dyes on a polymer matrix

The covalent immobilization of azaBODIPYs on two different matrix materials was investigated. Firstly, immobilization on a copolymer of polyacryloylmorpholine and polyhydroxyethylacrylamide (PAMcoHEAA) was investigated, and secondly, cellulose acetate propionate was examined as matrix material. Covalent immobilization of the dye on a matrix material can be beneficial over physically entrapped dye molecules: that way leaching and aggregation of the dye within the matrix can be prevented.

The bonding of the dye to the matrix should be achieved via a B-O bond on the boron center of the dye. Many procedures for substitution reactions on the boron center on $BF_2$-chelated dipyrromethenes (BODIPYs) to convert them into the corresponding C- and O-BODIPYs were reported (see section 2.8). [32–34] These procedures are adopted for the functionalization of azaBODIPYs.

The aim of this task is to couple azaBODIPY dyes to the N-hydroxyethyl acrylamide moiety of a polymer and to the hydroxy group of cellulose acetate propionate. The in section 2.8 mentioned functionalization reactions were examined for this purpose. However, the bond formation on the boron center of azaBODIPYs seems to be a much more delicate reaction than the functionalization on the BODIPY analogues. Prior to the coupling reaction the hydroxy group of the azaBODIPY needs to be protected to prevent dimerization or polymerization of the azaBODIPY molecules during treatment with $BCl_3$ or reaction of the hydroxy group with the crosslinker during the curing step (see section 3.2.6). Protection with acetyl chloride was conducted in DCM at room temperature under inert atmosphere in a 10 minute reaction with quantitative yields. p-OH BuO azaBODIPY was chosen for the investigation of this reaction mechanism because it was available in large amounts. In the p-OH azaBODIPY molecule the pH-sensitive hydroxy group is connected to the $\pi$-system of the dye which leads to pH dependent absorption.

#### Coupling of azaBODIPYs to HEG

First experiments were conducted with hexaethylene glycol (HEG) instead of the polymer for easier handling and simpler analysis by TLC, $^1$H NMR and UV/VIS spectroscopy (figure 4.8). Reaction with TMSOTf in various amounts (5 - 10 eq), 50 eq HEG and various amounts of DIPEA (approximately 10 or 50 eq) were conducted at 0 °C and at room temperature (according to the general procedure described in section 3.1.3). TLC of a reaction at 0 °C for 10 min with 7.5 eq TMSOTf, 50 eq HEG and 10 eq DIPEA showed a spot, presumably the product spot, besides the educt spot. However, the educt spot is predominant with only very little conversion. Longer reaction times (20 min) and large excess of DIPEA (50 eq) leads to decomposition of the azaBODIPY to the corresponding ligand, indicated by a color change of the solution from green to blue. The conclusion can be drawn that TMSOTf is not a suitable reagent for this reaction.

Reaction with 10 eq $BCl_3$ (using a 1 M solution in DCM), 50 eq HEG and 15 eq DIPEA leads to conversion of the azaBODIPY besides an unknown side-product (see figure 4.8, TLC on the right).

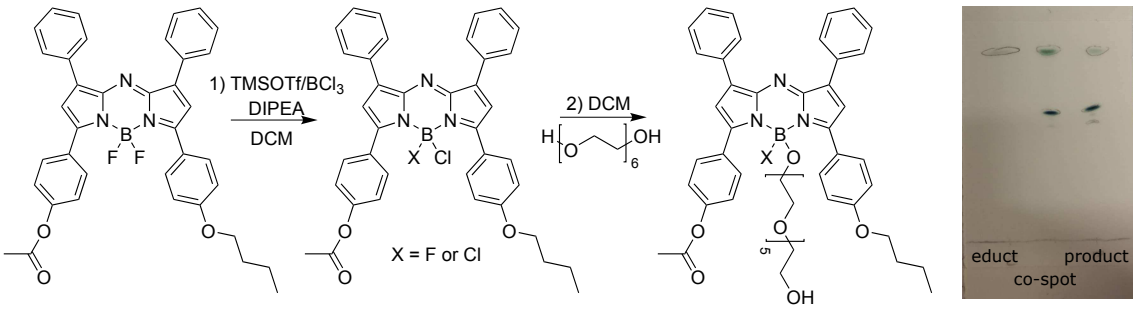


**Figure 4.8:** Reaction pathway and TLC of the coupling reaction of p-OH BuO azaBODIPY and hexaethylene glycol with $TMSOTf/BCl_3$

The fractions can be easily separated by column chromatography (on silica gel with DCM : CH 1 : 1). A blue side product elutes first, which is supposedly a degradation product of the dye, the ligand. After elution of a green product, presumably the unbound azaBODIPY dye, the desired product elutes, the HEG-coupled azaBODIPY. $^1$H NMR data reveal that one HEG group is bound on the boron center and that the protection group was removed by the harsh reaction conditions (see figure 9.12 on page 106). Absorption spectra of the product in acidic and basic environment (by adding a drop of trifluoroacetic acid or triethylamine, respectively) confirm that the protection group was removed which is visualized by a shift of the absorption maximum to higher wavelength upon deprotonation (figure 4.9).

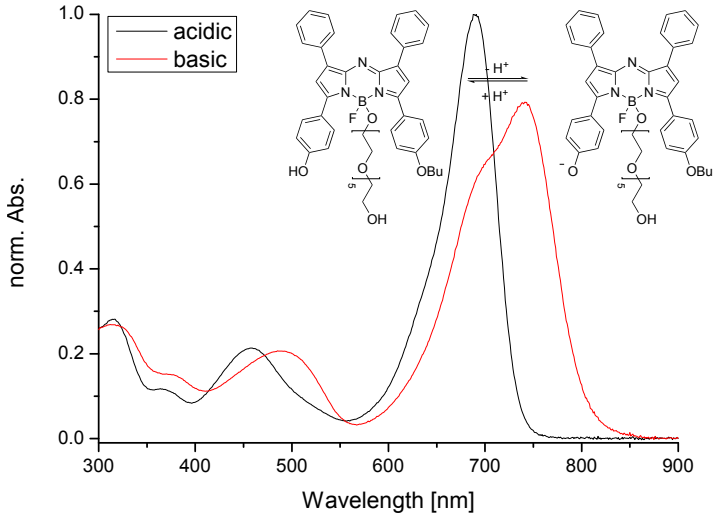


**Figure 4.9:** Absorption spectrum of the immobilization reaction of p-OH BuO azaBODIPY and HEG in MeOH in acidic and basic environment

**Coupling of azaBODIPYs to PAMcoHEAA**

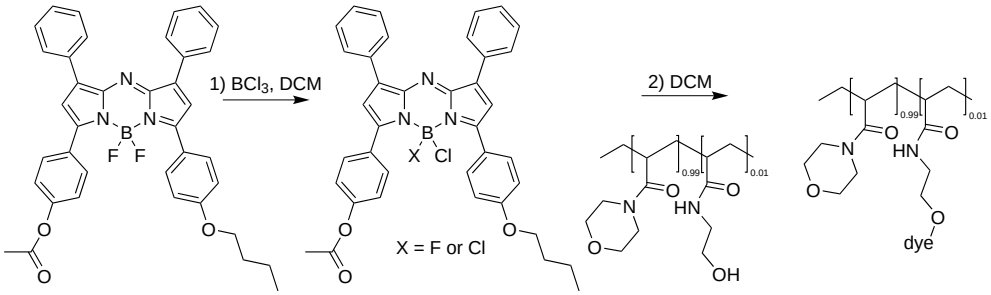


**Figure 4.10:** Reaction pathway of the coupling reaction of p-OH BuO azaBOIDPY on the polymer PAMcoHEAA with $BCl_3$

With these results immobilization reactions of the acetyl protected p-OH BuO azaBODIPY on the copolymer PAMcoHEAA according to the procedure in section 3.1.3 were examined (figure 4.10). First attempts were not successful: reaction with 10 eq $BCl_3$ (using a 1 M solution in DCM) and stirring for 10 min at 0 °C yields a pale green polymer. UV/VIS spectra however show an untypical broad band (figure 4.11 (a)). This broad absorption band may result from degradation of the dye or formation of a side product due to too high concentrations of the reactive Lewis acid $BCl_3$. Using only 2 eq of $BCl_3$ seems to work well. The product is a pale green polymer and absorption spectra show typical sharp peaks. Absorption bands exhibit a shoulder in basic environment at higher wavelength though, pointing out partial deprotection of the dye (figure 4.11 (b)). After using a new bottle of $BCl_3$ solution (1 M in DCM) deprotection and decomposition was observed again, even when small amounts of the $BCl_3$ solution were used (figure 4.11 (c)). Apparently $BCl_3$ is not stable over a long period of time and degrades when stored in DCM. This would explain why the reaction worked with large amounts of the old $BCl_3$ batch, but decomposition and deprotection takes place even when small volumina of the new $BCl_3$ solution were used.

It is assumed that $BCl_3$ is more stable as a solution in toluene, which is commercially available as well. Another advantage over DCM is its higher boiling point which makes the solution easier to handle. By using a 1 M solution of $BCl_3$ in toluene the reaction conditions were optimized to achieve a maximum of dye bound to the polymer while reducing the ratio of dye being deprotected during the reaction progress. For the coupling reaction of p-OH azaBODIPY to the polymer PAMcoHEAA the ideal reaction conditions were found to be activation of the B-F bond with 1.2 eq $BCl_3$ (1 M solution in toluene) for 20 min at room temperature in DCM, and reaction with a solution of PAMcoHEAA in DCM for 30 min at room temperature. Work up was done by partitioning between DCM and aqueous $NaHCO_3$ solution and multiple precipitation in CH : Tol 2 : 1 (figure 4.11 (d)). With this method a polymer with approximately 0.05 wt.% dye bound (relative to the polymer) could be synthesized.

The amount of dye bound to the polymer can be estimated via the molar absorption coefficient of the dye (assuming that the spectral properties of the dye remain unchanged after the immobilization) by dissolving a known amount of the obtained product in a known volume of DMSO and measuring its absorption. Moreover, the size of the shoulder in the absorption spectrum at higher wavelength in basic milieu indicates the ratio of deprotected (and therefore deprotonated) dye.

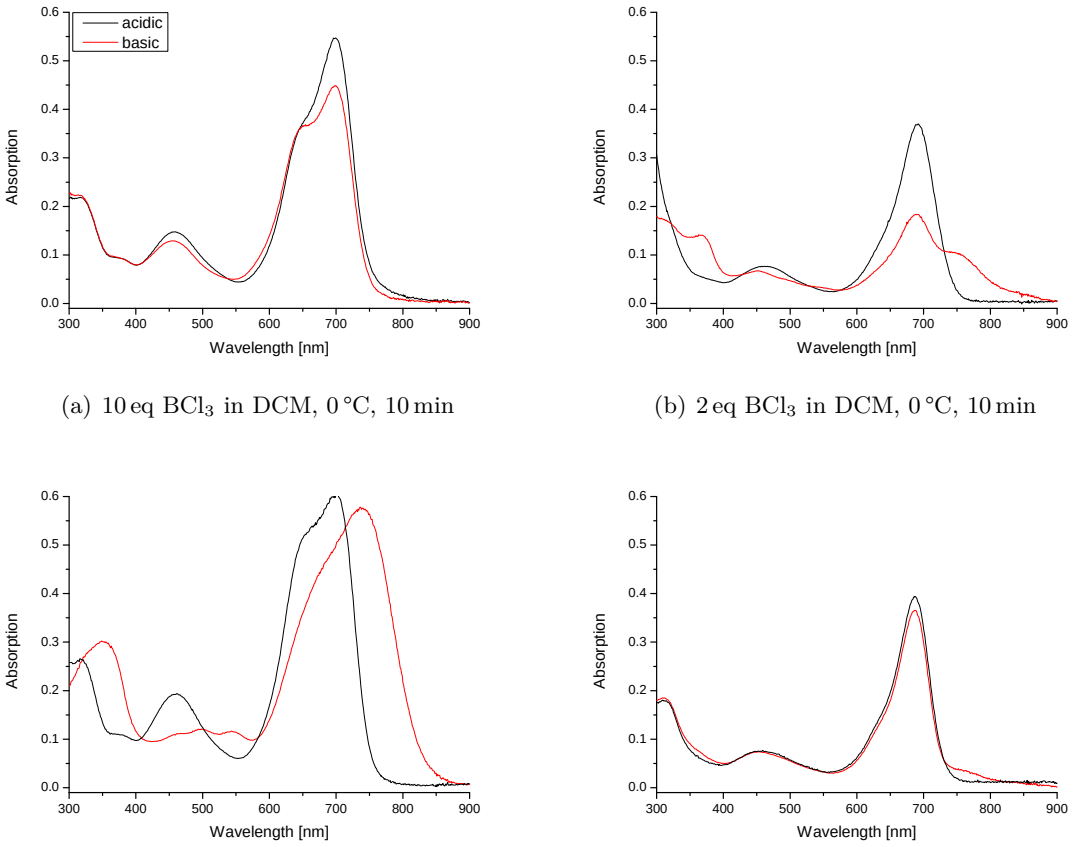


(a) 10 eq $BCl_3$ in DCM, 0 °C, 10 min

(b) 2 eq $BCl_3$ in DCM, 0 °C, 10 min

(c) 2 eq $BCl_3$ in DCM (new), 0 °C, 10 min

(d) 1.2 eq $BCl_3$ in Tol, RT, 20 min

**Figure 4.11:** Absorption spectra of the immobilization products of p-OH BuO azaBODIPY and PAMcoHEAA with $BCl_3$ in DMSO in acidic and basic environment

This procedure was adapted for immobilizing p-OH BuO azaBODIPY on PAMcoHEAA containing 2 % OH groups (see section 3.1.3). Other than expected, only slightly more dye could be immobilized (approximately 0.055 wt.%), even though twice the amount of hydroxy groups are available for immobilization in this polymer (figure 4.12 (a)).

With the same procedure the new dye m-OH diCl azaBODIPY (compound **3**) was immobilized as well. m-OH diCl azaBODIPY was coupled to PAMcoHEAA with 1 % hydroxy groups obtaining a pale green polymer with approximately 0.03 wt.% dye bound (figure 4.12 (b)).

Due to the meta-hydroxy substitution absorption spectra are pH independent. Therefore, degree of deprotection (deprotonation) is not apparent from the shown spectrum.

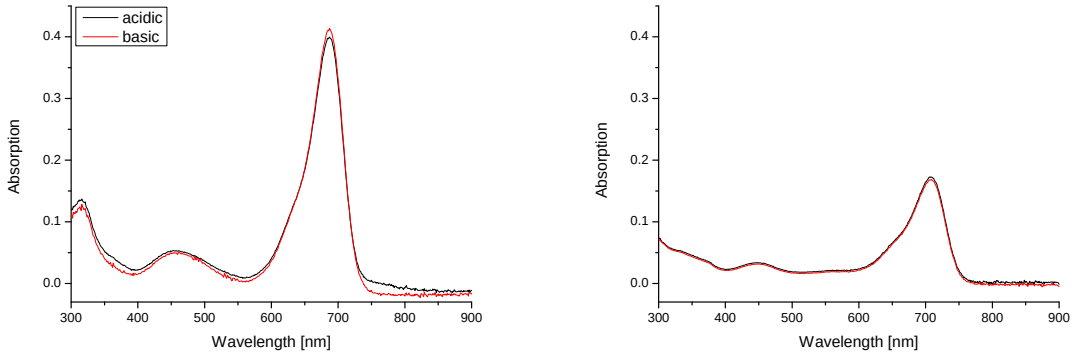


(a) 1.2 eq $BCl_3$ in Tol, RT, 20 min

(b) 1.2 eq $BCl_3$ in Tol, RT, 20 min

**Figure 4.12:** Absorption spectra of the immobilization reaction of (a) p-OH BuO azaBODIPY and PAMcoHEAA with 2 % OH groups in DMSO and (b) m-OH diCl azaBODIPY (compound **3**) and PAMcoHEAA with 1 % OH groups in DMSO in acidic and basic environment

### Coupling of azaBODIPYs to CAP

p-OH BuO azaBODIPY was coupled to cellulose acetate propionate (CAP) using a similar procedure. According to the manufacturer CAP has a hydroxyl content of 4.4 to 5.6 wt.%, to which the dye should bind.

For preparation of sensor films with CAP no crosslinking step is necessary. Therefore, more $BCl_3$ can be used for the coupling reaction because the protection groups do not have to stay intact. By using 5 eq $BCl_3$ a strongly stained polymer with approximately 0.3 wt.% immobilized dye was obtained (figure 4.13). However, a drawback of this matrix material is that CAP per se is too hydrophobic and $H^+$ permeability is too low to be used in pH sensors. Therefore, CAP must be hydrolyzed to convert it into cellulose which has a higher proton permeability. The harsh conditions of this preparation step of cellulose sensor films might cause decomposition of the dye molecules.

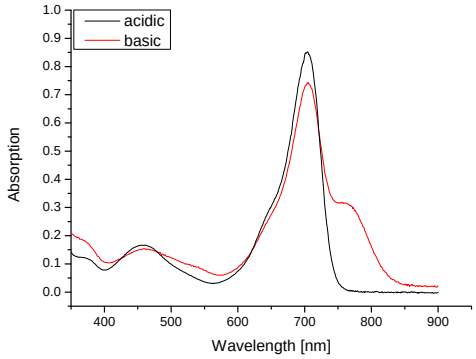


**Figure 4.13:** Absorption spectra of the immobilization reaction of p-OH BuO azaBODIPY and CAP in acetone in acidic and basic environment (5 eq $BCl_3$ in Tol, RT, 20 min)

An important factor influencing the coupling reaction is first of all the amount of $BCl_3$ used. There seems to be a thin line between deprotection/ decomposition of the dye and efficient coupling. Too high $BCl_3$ concentrations lead to degradation, whereas too little $BCl_3$ does not activate the B-F-bond efficiently. It is assumed that $BCl_3$ as a solution in DCM is not stable over an long time and degrades even when storing under inert atmosphere in the fridge. $BCl_3$ in toluene seems to be a better option. Due to toluene's higher boiling point it is easier to measure and add a reproducible amount of the solution to the reaction mixture. Nevertheless, it was difficult to obtain reproducible results from the previously described experiments. $BCl_3$ is a Lewis acid and is highly reactive towards water. In contact with water it hydrolyzes to hydrochloric acid and boronic acid. It also reacts with esters which leads to the cleavage of the acetyl protecting group. [58] Due to the high reactivity of $BCl_3$, only small amounts of residual water could have an impact on the efficiency of the coupling reaction, even when particular attention was paid to anhydrous and oxygen free reaction conditions.

Another important factor is the reaction temperature. The experiments were carried out either at 0 °C or at room temperature. Higher temperatures seem to enhance the reaction progress, however, also the degree of acetyl cleavage is enhanced at elevated temperatures. Concerning reaction times, it was found that the second reaction step (adding of a solution of PAMcoHEAA or CAP) increases with increasing reaction time up to 30 minutes. Between 30 and 120 min no further increase of reaction progress could be observed.

Size of the reaction batch turned out to have an impact as well. Better conversions with less deprotection were obtained when larger batches were used. $BCl_3$ reacts rapidly with residual water in the glass ware or syringe, therefore the negative impact of water gets less pronounced in larger reaction batches.

## 4.2 Photophysical characterization

The photophysical properties of the synthesized dyes **1-5** (see figure 4.7) are summarized in table 4.1 and will be discussed in the following sections.

**Table 4.1:** Photophysical properties of azaBODIPY dyes **1-5**

| Compound | $\lambda_{abs}$ (DCM) [nm] | $\lambda_{em}$ (EtOH/$H_2O$) [nm] | $\varepsilon$ (THF) [$M^{-1}$ $cm^{-1}$] | $\Phi_{rel}$ (THF) [%] | $pK_a$' (EtOH/$H_2O$) | $pK_a$' (D4) | $\tau_F$ (THF) [ns] |
|---|---|---|---|---|---|---|---|
| **1** m-OH | 696 | 723 | 83 205 | 24 | >11.5 | - | 2.54 |
| **2** m-OH Cl | 696 | 722 | 85 355 | 27 | 11.11 | 10.77 | 2.69 |
| **3** m-OH diCl | 689 | 721 | 80 705 | 26 | 7.77 | 7.53 | 2.56 |
| **4** m-OH diF | 693 | 719 | 73 292 | 27 | 10.25 | 10.29 | 2.67 |
| **5** m-OH OMe | 694 | 721 | 90 024 | 14 | - | >12 | 1.57 |

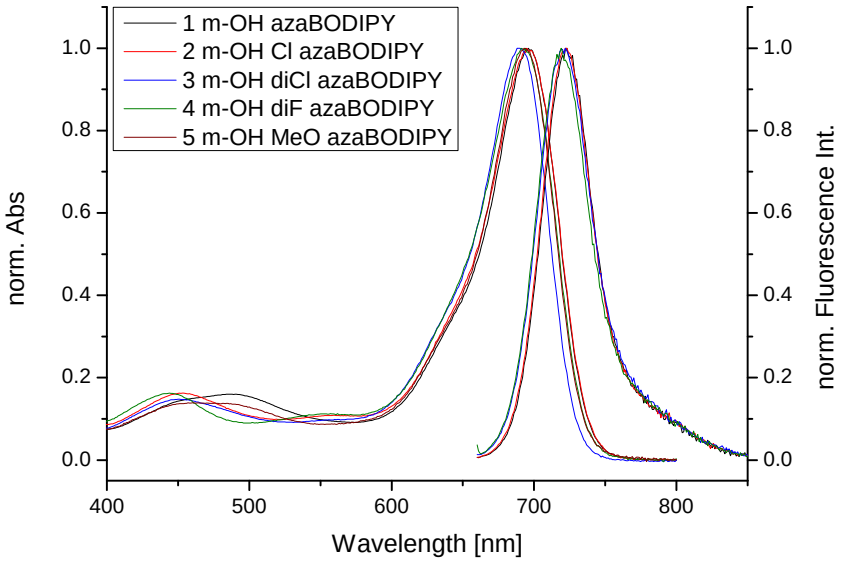


**Figure 4.14:** Absorption (in dichloromethane) and emission spectra (in EtOH/$H_2O$ 1 : 1) of the new azaBODIPYs **1-5**

### 4.2.1 Absorption

The synthesized azaBODIPYs **1-5** carry a pH sensitive group (a hydroxy group) in meta-position on the $Ar_1$. In consequence of the m-substitution, the hydroxy group is not connected to the $\pi$-system of the azaBODIPY core, resulting in a nearly pH independent absorption spectrum (see figure 4.15 bottom). In contrast to the novel dyes, previously synthesized azaBODIPYs had similar substitution pattern but a hydroxy group in para-position on an $Ar_2$ group. [5, 6] Thus, the hydroxy group is incorporated into the $\pi$-system of the fluorophore resulting in a wavelength shift from protonated to deprotonated state of the dye (see figure 4.15 top).

All five synthesized dyes have very similar absorption spectra with maxima ranging from 689 nm to 696 nm in dichloromethane (figure 4.14). Compared to other azaBODIPYs a slight bathochromic shift can be achieved with the new meta-hydroxy substitution. [6] Absorption in this region of the light is preferential for many applications because it lies in the so-called "optical window". Between 650 nm an 950 nm autoabsorption and autofluorescence as well as scattering of the light is reduced resulting in higher signal-to-noise ratios and less background noise.

Molar absorption coefficients of the dyes are in the range between 73 000 and 90 000 $M^{-1}\,cm^{-1}$ (in THF), which is typical for this class of dyes. [3, 5, 6]

Interestingly a shift of absorption maxima in the blue range (approximately 400 nm to 500 nm) can be observed. The absorption maxima of the dyes in the blue range and the molar absorption coefficients are summarized in table 4.2. The wavelengths of these "second" absorption maxima are important for e.g. blue light excitation of sensors.

**Table 4.2:** Absorption maxima (in the blue region) and molar absorption coefficients at the maxima (in the blue region) of dyes **1-5**

| Compound | $\lambda_{abs}$ [nm] | $\varepsilon$ [$M^{-1}\,cm^{-1}$] |
|---|---|---|
| **1** m-OH | 487 | 12 634 |
| **2** m-OH Cl | 453 | 11 814 |
| **3** m-OH diCl | 451 | 12 697 |
| **4** m-OH diF | 444 | 10 766 |
| **5** m-OH OMe | 471 | 13 820 |

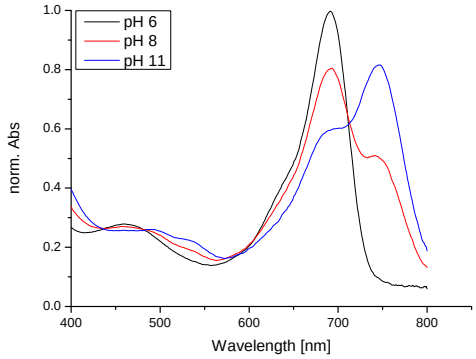


(a) Absorption spectrum of p-OH C12 azaBODIPY

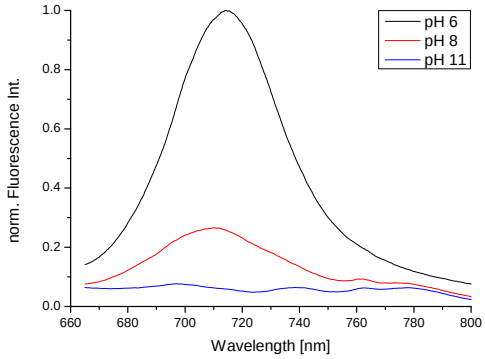


(b) Emission spectrum of p-OH C12 azaBODIPY

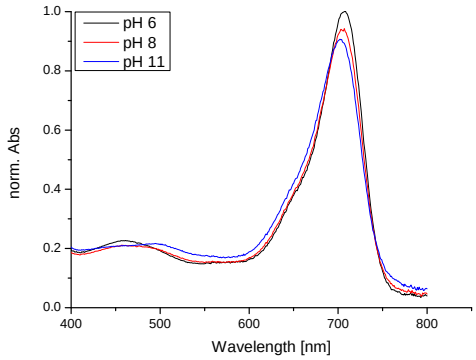


(c) Absorption spectrum of m-OH diCl azaBODIPY

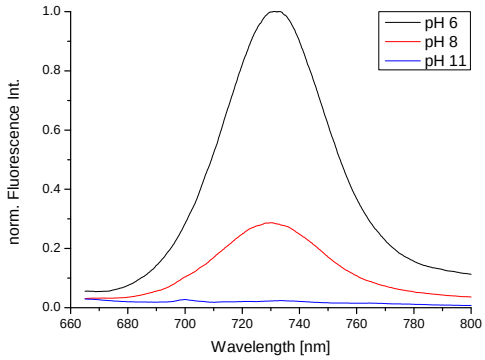


(d) Emission spectrum of m-OH diCl azaBODIPY

**Figure 4.15:** Comparison of absorption and emission spectra of para-OH substitution (p-OH C12 azaBODIPY) and meta-OH substitution (m-OH diCl azaBODIPY) depending on the pH

### 4.2.2 Fluorescence

As described in the theoretical part of this thesis, PET (photoinduced electron transfer) leads to quenching of fluorescence in the deprotonated state. An electron from the deprotonated oxygen is transferred to the $\pi$-system of the azaBODIPY core, which results in a radiationless decay to the ground state. In the protonated state however, this electron transfer is suppressed due to changes of the energy levels of the molecular orbitals, and the molecule relaxes under emission of fluorescent light. Consequently, fluorescence intensities, which reflect the concentration of the protonated dye in the excited state, change with changing pH of the surrounding medium (figure 4.16). The emission maxima of all five dyes are very similar, resembling the trend of the absorption maxima. The dyes emit in the NIR region of the light in a range from 719 nm to 723 nm (figure 4.14). Same as absorption maxima, the emission maxima are shifted a few nanometers to higher wavelengths compared to previously reported azaBODIPYs. [6]

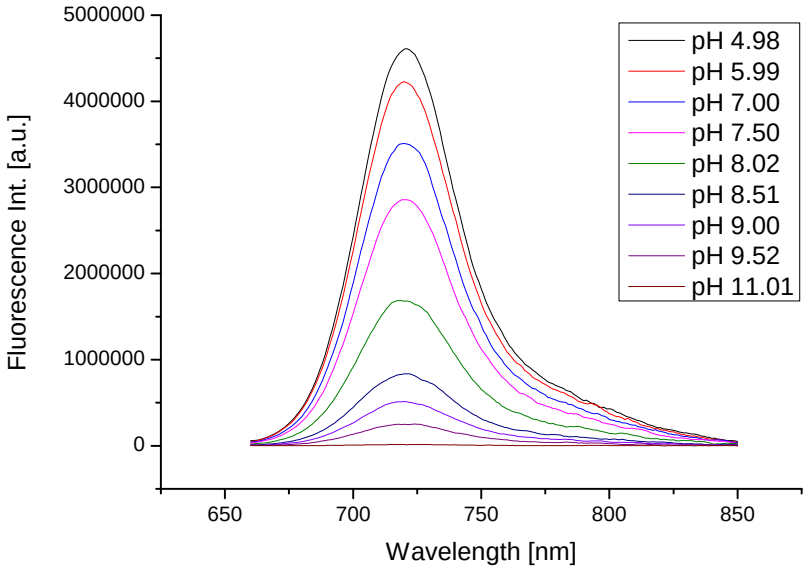


**Figure 4.16:** pH dependent emission spectrum of compound **3** at various pH values in EtOH/$H_2O$

### Quantum yields

Quantum yields measured in THF with the relative method range from 24 % to 27 %, with the exception of compound **5**, which has a significantly lower quantum yield of only 14 %. The quantum yields of compounds **1-4** are relatively high, compared to other compounds of this dye class. [6] A similar structure of an azaBODIPYs with meta-hydroxy group on the $Ar_2$ ring was reported, however, this dye has very low quantum yields of only 10 %. [5] By a structural modification of the dye, by relocating the position of the hydroxy group to $Ar_1$, the photophysical properties of the dye can be maintained but higher quantum yields can be achieved.

Additionally to the measurements in solution with the relative method, the quantum yield of m-OH diCl azaBODIPY (compound **3**) and p-OH C12 azaBODIPY with different concentrations between 0.05 % and 1 % in hydrogel D4 were measured with the absolute method. In D4 matrix lower quantum yields were determined. The QY of **3** in D4 calculated from the absolute method is 15 % (of the D4 sensor film with 0.05 % dye content), whereas in solution 26 % were measured. The quantum yields of compound **3** as well as of p-OH C12 azaBODIPY decrease with increasing concentration of dye in the hydrogel. This effect can be explained by FRET (Förster resonance energy transfer). The higher the concentration of the dye in the matrix, the smaller is the distance between each dye molecule. Therefore, FRET between two molecules in close proximity is enabled in higher dye concentrations. Inner filter effects (e.g. reabsorption of the emitted light) might be another factor decreasing the

quantum yields in sensor films with high dye concentrations. The relationship between dye concentration in hydrogel D4 and the measured quantum yields are illustrated in figure 4.17.

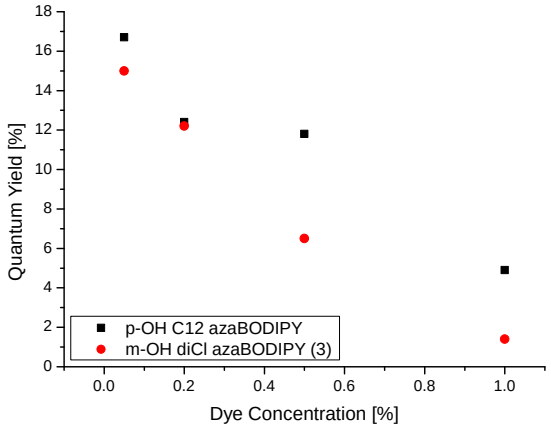


**Figure 4.17:** Relationship between the measured quantum yield of p-OH C12 azaBODIPY and m-OH diCl azaBODIPY (compound **3**) and the dye concentration in D4

### Fluorescence lifetime

The fluorescence lifetimes of dyes **1-4** measured in solution (in THF) via TCSPC range from 2.54 ns to 2.69 ns. No clear statement about the influence of the substitution pattern on the lifetime can be made. Compound **5** however makes an exception with a shorter lifetime of 1.57 ns. This finding agrees with the data obtained from quantum yield measurements, where compound **5** shows lower values as well. The results from lifetime measurements of **3** are shown in figure 4.18. The remaining results can be found in the appendix on page 112.

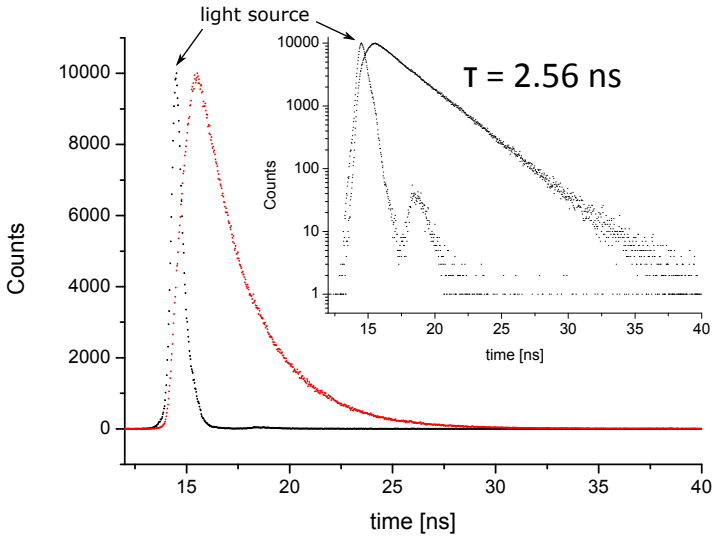


**Figure 4.18:** Lifetime of m-OH diCl azaBODIPY (**3**) in THF measured via TCSPC

Lifetime measurements of **3** and p-OH C12 azaBODIPY with different concentrations ranging from 0.05 % to 1 % in hydrogel D4 were investigated as well. The same trend as for quantum yields can be observed here: the lifetimes decrease with increasing dye concentration in the sensor layer (figure 4.19). Two phenomena could possibly explain these findings. On the one hand, FRET could decrease the lifetime due to energy transfer from the protonated form to the deprotonated form of the dye within the matrix. On the other hand, aggregation of the dye molecules within the matrix might cause the lifetime drop in higher concentrations. The issue of aggregation could be diminished by incorporating polar groups like hexaethylene glycol groups on the dye to enhance its solubility in the polymer matrix.

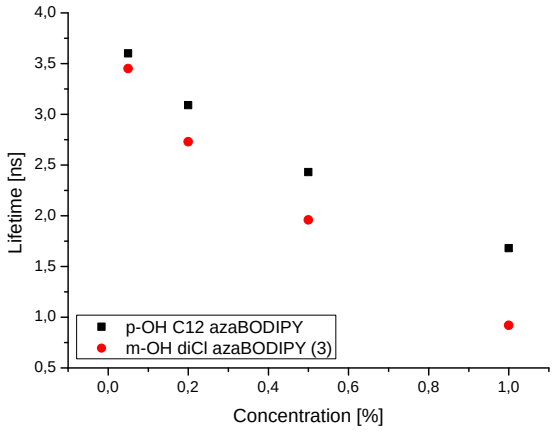


**Figure 4.19:** Relationship between the measured lifetime of p-OH C12 azaBODIPY and m-OH diCl azaBODIPY (**3**) and the dye concentration in D4

## 4.3 Sensing properties

### 4.3.1 pH sensing

From the fluorescence intensities the pH can be estimated with a sigmoidal calibration curve (equation 4.1). The measurements for $pK_a$ determination of previously reported azaBODIPYs (for example p-OH C12 azaBODIPY) are subjected to FRET (energy transfer from the protonated "on" state to the deprotonated "off" state) and therefore the $pK_a$ determined from emission measurements is reduced compared to the actual $pK_a$ of the dye. It might be that the $pK_a$ of the novel dyes is possibly affected by FRET as well, therefore the $pK_a$ calculated from emission will consequently be addressed as apparent $pK_a$ or $pK_a$'. The fitted calibration curves of compounds **1-4** in EtOH/$H_2O$ 1 : 1 can be seen in figure 4.20. It was not possible to measure a $pK_a$' of compound **5** because the dye was not sufficiently soluble in the solvent and seems to form aggregates resulting in a low emission intensity in the used medium. The shape of the calibration curve of compound **1** with its narrow transition range might suggest errors in the buffer preparation or bad buffer capacities of the buffer solutions used at high pH.

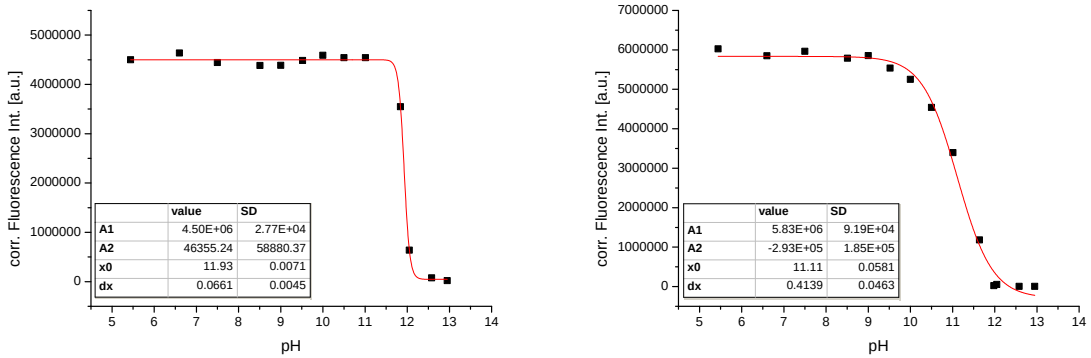


(a) m-OH azaBODIPY (**1**)

(b) m-OH Cl azaBODIPY (**2**)

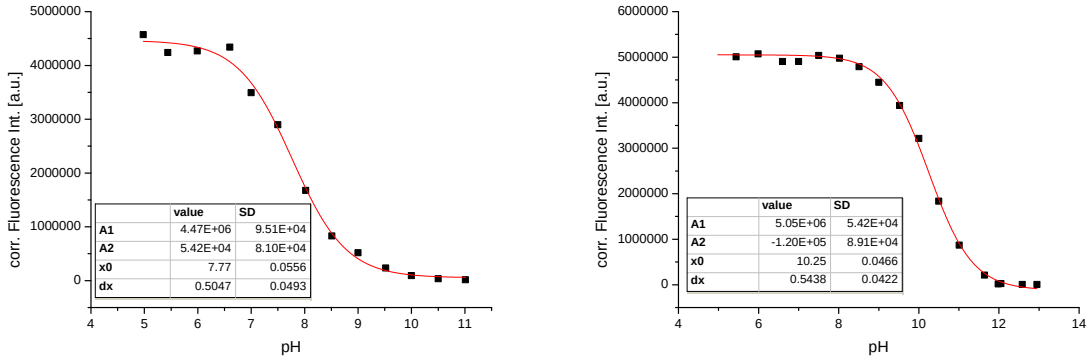


(c) m-OH diCl azaBODIPY (**3**)

(d) m-OH diF azaBODIPY (**4**)

**Figure 4.20:** pH calibration curves of compounds **1-4** in EtOH/$H_2O$ 1 : 1 (with a concentration of approximately $1.5 \cdot 10^{-6}$ M) based on emission spectra

The Boltzmann equation used for the calculation of the $pK_a$ is defined by

$$y = \frac{A_1 - A_2}{1 + e^{(x-x_0)/d_x}} + A_2 \tag{4.1}$$

where $A_1$ is the maximum, $A_2$ the minimum of the curve, $x_0$ represents the point of inflection and $d_x$ the slope at the point $x_0$. The point of inflection of the fitted curve represents the $pK_a$ of the dye.

Compounds **2-5** were incorporated in a hydrogel D4 matrix and sensor layers of this material were investigated as well. However, the measured data of compound **5** have to be treated with caution because the used buffer solutions were not in the optimal pH range for the sensor layer. Buffer solutions with higher pH would be necessary to make clear statements about the apparent $pK_a$ of **5** in a D4 matrix.

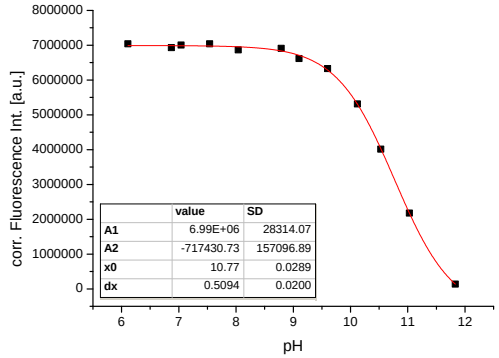


(a) m-OH Cl azaBODIPY (**2**)

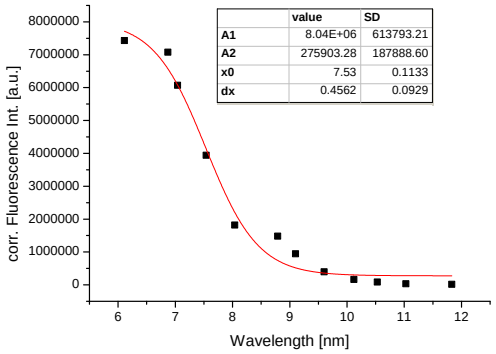


(b) m-OH diCl azaBODIPY (**3**)

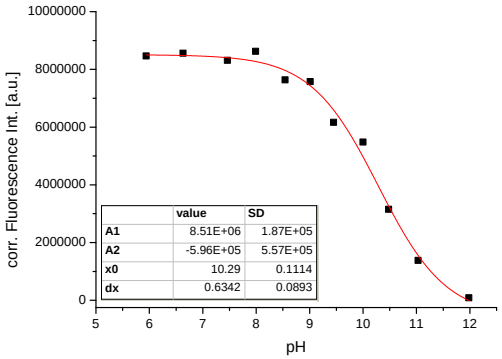


(c) m-OH diF azaBODIPY (**4**)

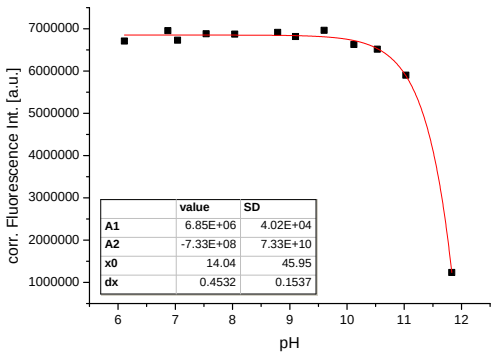


(d) m-OH MeO azaBODIPY (**5**)

**Figure 4.21:** pH calibration curves of compounds **2-5** entrapped in hydrogel D4 (containing 0.2 wt.% dye relative to the D4 matrix) based on emission spectra

Furthermore, a sensor layer consisting of compound **3** (m-OH diCl azaBODIPY) covalently immobilized on a polymer matrix PAMcoHEAA was investigated.

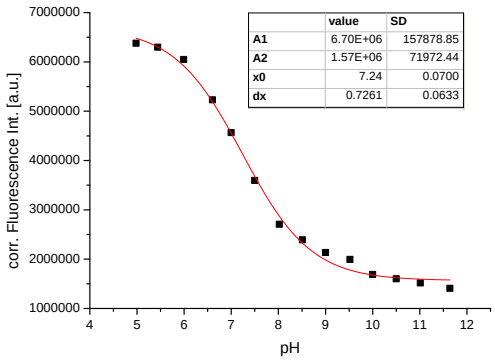


**Figure 4.22:** pH calibration curve of compound **3** (m-OH diCl azaBODIPY) covalently immobilized on PAMcoHEAA (containing approximately 0.03 wt.% dye relative to the polymer matrix) based on emission spectra

The measured $pK_a$' values of the dyes in solution (EtOH/$H_2O$ 1 : 1, with a concentration of approximately $1.5 \cdot 10^{-6}$ M), immobilized in a hydrogel D4 sensor layer (containing 0.2 wt.% dye relative to the D4 matrix) and covalently immobilized on a PAMcoHEAA polymer matrix (containing approximately 0.03 wt.% dye relative to the polymer matrix) are summarized in table 4.3.

**Table 4.3:** Measured $pK_a$' values of compounds **1-5** in solution (in EtOH/$H_2O$), immobilized in a hydrogel D4 matrix and covalently immobilized on a PAMcoHEAA polymer matrix

| Compound | $pK_a$' (EtOH/$H_20$) | $pK_a$' (D4) | $pK_a$' (PAMcoHEAA) |
|---|---|---|---|
| **1** m-OH | >11.5 | - | - |
| **2** m-OH Cl | 11.11 | 10.77 | - |
| **3** m-OH diCl | 7.77 | 7.53 | 7.24 |
| **4** m-OH diF | 10.25 | 10.29 | - |
| **5** m-OH OMe | - | >12 | - |

The general trend of the influence of electron donating and electron withdrawing functional groups on the $pK_a$ can be clearly observed: the higher the electron density in the aromatic ring, the higher the $pK_a$ and vice versa, the lower the electron density in the aromatic system, the lower the $pK_a$. Electron withdrawing substituents (like chlorine or fluorine) in ortho-position relative to the hydroxy group have the highest impact on the $pK_a$. This effect decreases with the following order ortho > meta > para.

Compound **3** with two electron withdrawing chlorine atoms has the lowest apparent $pK_a$ of 7.77 (in solution), whereas the electron donating group MeO as in compound **5** increases the electron density in the aromatic ring and increases the apparent $pK_a$ to more than 12. Compound **1** with no other substituents other than the hydroxy group has an apparent $pK_a$ of more than 11.5, which is surprisingly significantly higher than the $pK_a$ of phenol. The formation of the charged (deprotonated) form of the dye might be less favored when connected to the hydrophobic azaBODIPY core. This might explain the increased $pK_a$ compared to the $pK_a$ of phenol. Introduction of one ortho-chlorine (relative to the hydroxy group) decreases the apparent $pK_a$ to 11.11 (compound **2**). This is a surprisingly small $pK_a$ change compared to the large difference between phenol and o-chlorophenol ($pK_a$ 8.56). A second chlorine in o-position induces a remarkable $pK_a$ drop to 7.77 (compound **3**). The fluorine substituents decrease the $pK_a$ by 1.7 pH units. The same trend is observed in fluorine substituted phenols. The methoxy group increases the apparent $pK_a$, which might be explained by the enhanced electron density in the ring but also by the formation of a hydrogen bond between the hydrogen of the hydroxy group and the oxygen of the methoxy group and thus a stabilization of the acidic hydrogen. [59]

The decreased apparent $pK_a$ of m-OH diCl azaBODIPY in sensor matrixes like hydrogel D4 or in PAMcoHEAA in contrast to measurements in solution might be caused by a better stabilization of the negative charge of the deprotonated dye in the hydrophilic matrix material.

Dye **3** (m-OH diCl azaBODIPY) with its low $pK_a$' is promising for applications in biological or medical measurements because the pH of seawater and blood lies in the dynamic range of this indicator dye. Compounds **1**, **2**, **4** and **5** (m-OH, m-OH Cl, m-OH diF and m-OH MeO azaBODIPY) on the other side are promising candidates for $CO_2$ measurements in environmental analysis, marine monitoring or food packaging due to their high $pK_a$'. Only few "plastic type" $CO_2$ sensors based on azaBODIPYs have been reported so far and sensitivities of these sensor have been an issue [53] With the p-hydroxy substitution such high $pK_a$ values could not be obtained and since sensitivities of $CO_2$ sensors increases with increasing $pK_a$, the new azaBODIPYs with m-hydroxy substitution could overcome this problem (see section 4.3.4).

### 4.3.2 Concentration dependency

In contrast to previously reported azaBODIPYs, the novel azaBODIPY dyes with m-hydroxy substitution are purely based on PET-quenching and show a pH independent absorption spectrum. Consequently, the new dyes were expected to show less FRET, and thus a less pronounced concentration dependency of the emission signals and the apparent $pK_a$ than para-OH substituted azaBODIPYs.

However, as already found in quantum yield and fluorescence lifetime measurements, there seems to be a dependency on the dye concentration (see figures 4.17 and 4.19). To further investigate this assumption different concentrations of dye **3** and the reference dye p-OH C12 azaBODIPY (which is based on PET as well as on ICT) were entrapped in a D4 sensor matrix in concentrations ranging from 0.05 to 1 wt.% relative to the D4 matrix and emission intensities as well as $pK_a$' values of these sensor films were determined. The intensities of the sensor films with concentrations ranging from 0.05 % to 0.5 % dye content increase as expected with increasing dye concentration. However, at higher dye concentrations above 0.5 % the emission does no longer increase, but gets stagnant or even decreases for both, the p-OH and m-OH substituted dye (figure 4.23 (a)). The apparent $pK_a$ values of the two investigated dyes are reduced in higher concentrations in hydrogel D4 likewise (see figure 4.23 (b)). Quenching due to Förster resonance energy transfer takes place at higher rates in higher concentrations than in lower concentrations. Dye contents of 0.5 % and 1 % are quite high and FRET is facilitated in such high concentration where distances between the single dye molecules are reduced. However, FRET was expected to have only a small impact in the novel dyes (m-OH diCl azaBODIPY) compared to older azaBODIPY compounds (p-OH C12 azaBODIPY) due to the lack of ICT, but seems to significantly influence the emission intensity and the apparent $pK_a$ of the m-hydroxy substituted dye as well.

Another important factor which must be considered in this regard is inner filter effect. This effects causes reduction of the emission of light and get more pronounced in higher concentrations. Since absorption of the sensor films with concentrations of 0.5 % and 1 % are approximately 0.2 and 0.4, respectively, the inner filter effect may have caused considerable errors in this experiment. To reduce the influence of inner filter effect, sensor foils with reduced film thickens or lower dye concentrations should be used.

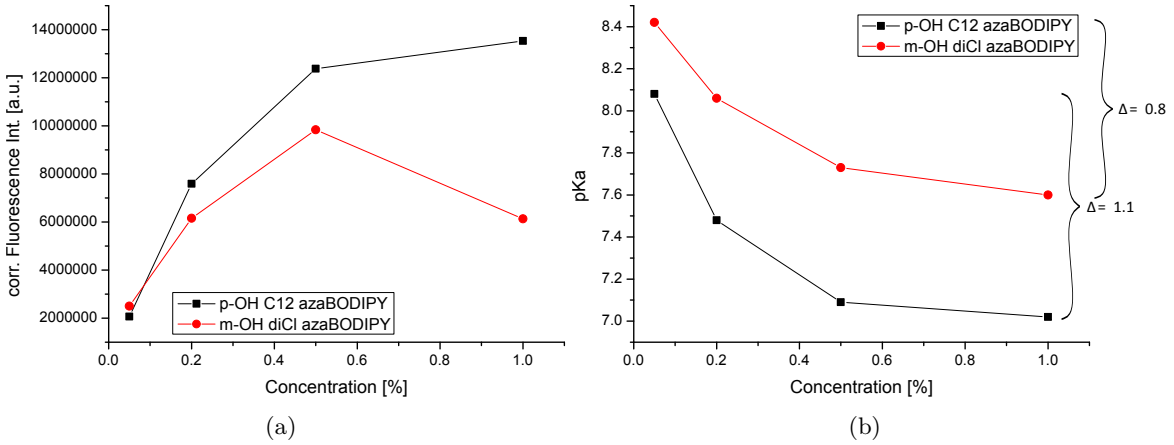


**Figure 4.23:** Relationship between the measured emission (a) and apparent $pK_a$ (b) and the dye concentration of p-OH C12 azaBODIPY and m-OH diCl azaBODIPY (compound **3**) in hydrogel D4

### 4.3.3 Light harvesting

Light harvesting is a versatile tool to enhance brightness of optical sensors, to improve the signal-to-noise ratio and to reduce background fluorescence in sensor films. This way, the film thicknesses of sensor films or particles sizes of sensor particles could be potentially decreased. By addition of a donor dye (antenna dye) with high brightness, more light gets absorbed. The excitation energy is transferred to a pH sensitive acceptor dye through energy transfer (ET), which in turn emits fluorescent light. For investigating fluorescence enhancement via light harvesting for compound **3** (m-OH diCl azaBODIPY) two different donor dyes were used: Donor 1, an unsubstituted azaBODIPY with four aryl groups with excitation maximum at 658 nm and emission maximum at 683 nm and donor 2, a rigid diCl tert-butyl BODIPY with excitation maximum at 635 nm and emission maximum at 640 nm (figure 4.24).

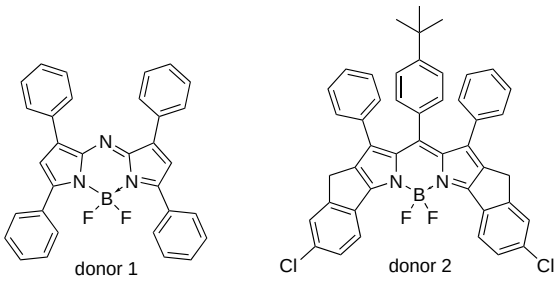


**Figure 4.24:** Structures of the used donor dyes for light harvesting

From the excitation spectra of the light harvesting sensor film containing donor 1 and m-OH diCl azaBODIPY recorded at pH 5 (figure 4.26 (a)) one can see, that the donor dye is better excitable at the donor's excitation maximum (658 nm) in the presence of an acceptor dye. Due to efficient energy transfer from the donor to the acceptor, emission of the acceptor is stronger in presence of donor dye than in absence of donor, even at lower acceptor dye concentrations (compare red and brown line in figure 4.26 (b)). The emission at approximately 725 nm (at the acceptor's emission maximum) increases with changing donor-to-acceptor ratios with excitation wavelength set to 624 nm. In a sensor film containing 0.2 % acceptor dye in the D4 matrix (red line), the emission intensity doubles by adding the same amount of donor (blue line). A fourfold increase of the emission could be achieved by using double the amount of donor and using a donor-to-acceptor ratio of 2 : 1 (green line). With 0.4 % donor and 0.1 % acceptor (brown line), the emission can be further increased, however, not all of the absorbed light is completely transferred to the acceptor and two emission bands, one at 683 nm and one at 725 nm, can be observed.

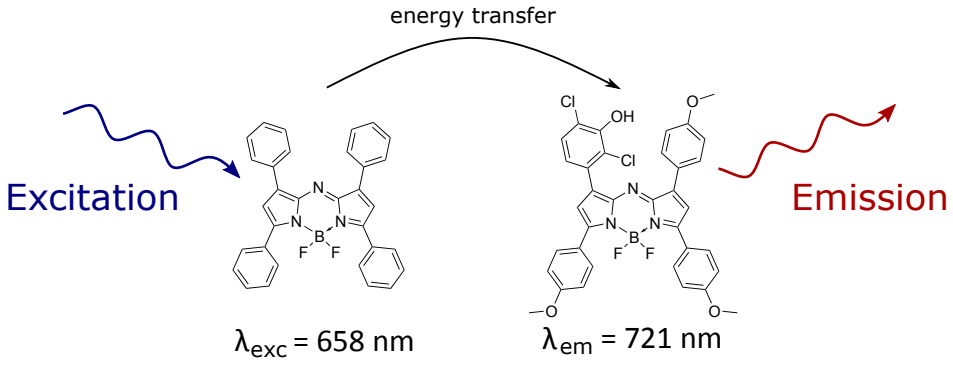


**Figure 4.25:** Scheme of energy transfer taking place in a light harvesting sensor containing donor 1 and m-OH diCl azaBODIPY (compound **3**)

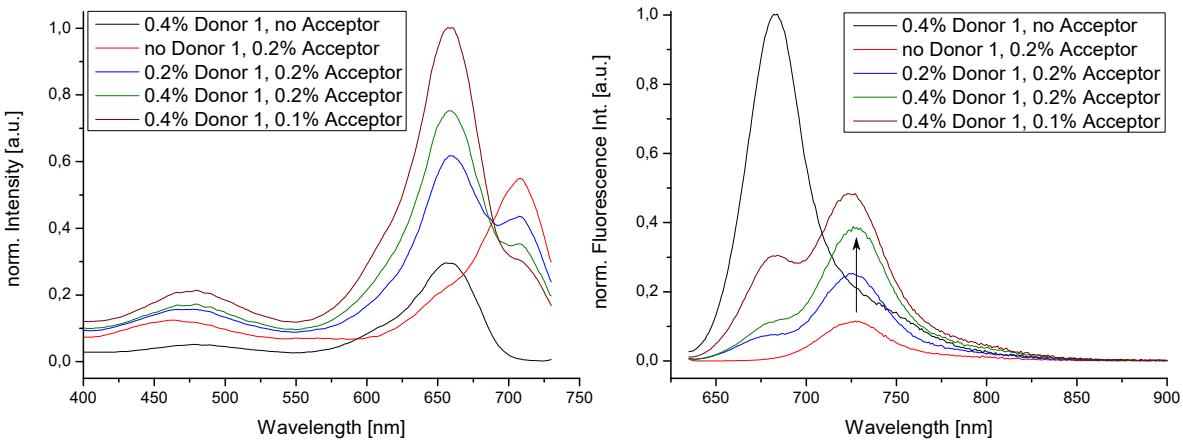


(a) Excitation at pH 5

(b) Emission at pH 5

**Figure 4.26:** Excitation spectra recorded at 740 nm (a) and emission spectra recorded at $\lambda_{exc}$ = 624 nm (b) of light harvesting sensor films containing donor 1 and m-OH diCl azaBODIPY (**3**)

Signal intensities of measurements of the sensor foils in the dry state with a FireStingO2 are summarized in the following table. Intensities can be significantly increased by addition of donor dyes. In both cases, using donor 1 and donor 2, best results were achieved with a donor-to-acceptor ratio of 2 : 1.

**Table 4.4:** Signal intensities of the sensor foils containing donor 1 or donor 2 and m-OH diCl azaBODIPY (compound **3**) measured with FireStingO2

| **Sensor composition** | **Signal Intensity Donor 1** | **Signal Intensity Donor 2** |
|---|---|---|
| no Donor, 0.2 % Acceptor | 47 | 47 |
| 0.2 % Donor + 0.2 % Acceptor | 128 | 192 |
| 0.4 % Donor + 0.2 % Acceptor | 190 | 225 |
| 0.4 % Donor + 0.1 % Acceptor | 190 | 218 |

Using donor 1 a strong enhancement of the emission can be achieved through energy transfer from donor to acceptor dye. By using a donor-to-acceptor ratio of 2 : 1 the emission can be increased fourfold. With this strong signal enhancement the layer thickness of sensor layers could potentially be decreased or particle sizes of sensor particles could be reduced. The Stokes shift is increased significantly from 32 nm to 63 nm because excitation is shifted to lower wavelength. This way, excitation filters can be adjusted to allow to pass through more excitation light. Moreover, the excitation wavelength can be shifted to wavelengths where alternative light sources can be employed. Concluding, light harvesting is a versatile tool to increase the emission of fluorescence. As described earlier, measurements of dye **3** in different concentrations in hydrogel D4 show that the intensity can not be enhanced endlessly by

increasing the concentration. Due to inner filter effect or quenching by FRET the emission intensity does not increase linearly with increasing dye concentration. By use of antenna dyes and light harvesting higher emissions can be achieved.

Donor 2 was chosen as donor due to its extremely high brightness. [60] In the spectra of the sensor films using donor 2 as antenna dye additional peaks at 698 nm in the excitation spectrum and at 706 nm in the emission spectrum were observed (see figure 4.27). These peaks are an indication for aggregation of the dye in the used matrix. Donor 2 may yet be a suitable candidate for light harvesting in combination with m-OH diCl azaBODIPY due to its spectral properties, however not in the used D4 matrix.

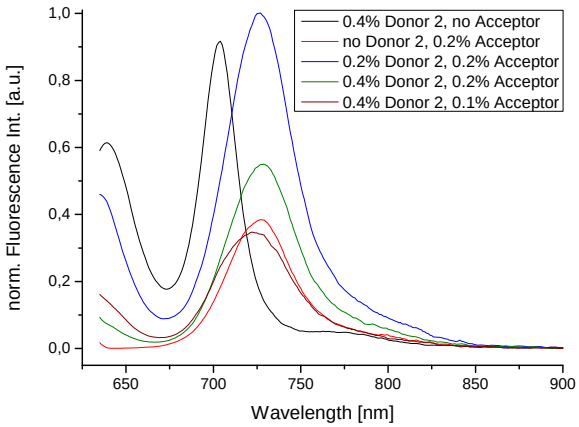


**Figure 4.27:** Emission spectra recorded at $\lambda_{exc} = 624$ nm of light harvesting sensor films containing donor 2 and m-OH diCl azaBODIPY (**3**)

### 4.3.4 $CO_2$ sensing

Carbon dioxide sensors of the so-called "plastic type" are based on the following principle: In the absence of $CO_2$ a pH sensitive dye exists in the deprotonated form and forms an ion pair with $TOA^+$, whereas presence of $CO_2$ which is in equilibrium with bicarbonate and carbonate ions induces protonation of the dye.

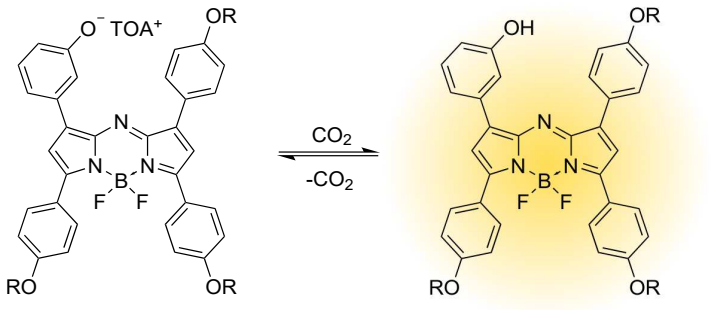


**Figure 4.28:** De-/protonation equilibrium of the pH sensitive m-OH azaBODIPY in absence/presence of carbon dioxide

Previously reported $CO_2$ sensors based on $BF_2$-chelated tetraarylazadipyrromethenes employed symmetrical azaBODIPYs carrying two hydroxy groups in para-positions. Presence of carbon dioxide causes protonation of the di-deprotonated form with two $TOA^-$ base pairs to the mono-deprotonated form. The sensitivity of the indicators could be tuned by electron donating or electron withdrawing groups to build sensors for various applications in different fields from food packaging to capnography. [53] These sensors are absorption based sensors, whose absorption spectra change upon $CO_2$ concentration changes. Emission is quenched in both states due to PET effect. Therefore, they require a complex inner-filter-DLR scheme for read-out. Asymmetric azaBODIPYs having only one hydroxy group were not applied in $CO_2$ sensors so far because the ion pair formed by the deprotonated dye and the tetraoctylammonium hydroxide base $TOA^+OH^-$ was too strong to re-protonate even at 100 % $CO_2$ exposure and could only be protonated by poisoning with HCl. However, mono-hydroxy azaBODIPYs have the advantage over di-hydroxy dyes. They are fluorescence-based and do not require an inner-filter-DLR scheme for read out. Working emission-based $CO_2$ sensors could be realized due to the high $pK_a$ of the novel dyes.

Using a Piccolo2-OEM modules from PyroScience a $CO_2$ calibrations of the $CO_2$ sensor layers of compounds **1**, **4** and **5** were conducted at room temperature with 100 % humidity using Egyptian blue as analyte-insensitive reference dye for DLR-based ratiometric read-out. Using test gas bottles with different $CO_2$ content (20 %, 5 % or 0.2 % $CO_2$) various sensitivities of the sensors towards carbon dioxide were investigated. As matrix ethyl cellulose and as protection layer Hyflon was chosen due to its simple handling.

Figure 4.29 shows $CO_2$ measurements of a sensor film of m-OH diF azaBODIPY (with a $pK_a$ of 10.25) in ethyl cellulose with $TOA^+OH^-$ base and a $CO_2$ permeable Hyflon protection layer on a PET support. The sensor layer response fast and reversible to $CO_2$ changes in the range from 0 to approximately 200 hPa carbon dioxide. However, a pronounced drift after multiple cycles can be observed.

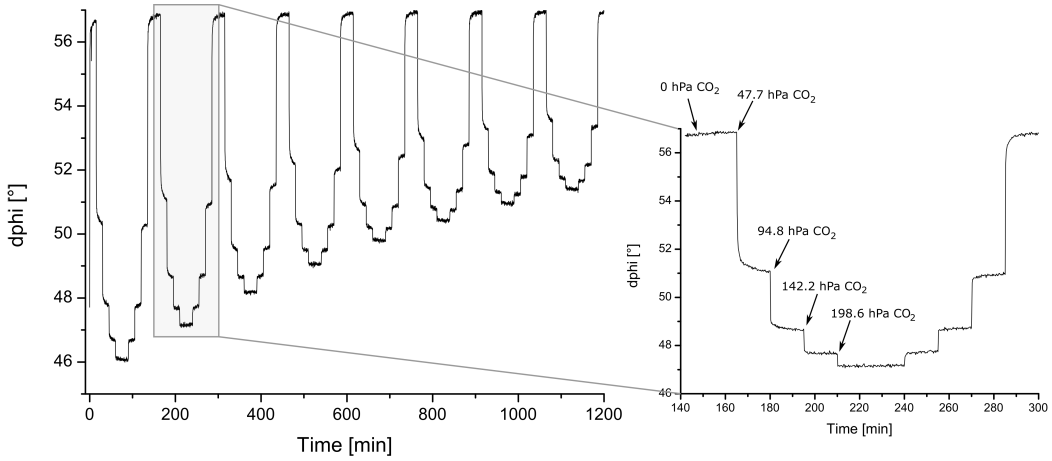


**Figure 4.29:** $CO_2$ measurements of a sensor film of m-OH diF azaBODIPY (**4**) in EC with $TOA^+OH^-$ on a PET support

m-OH azaBODIPY (**1**) ($pK_a$ >11.5) and m-OH MeO azaBODIPY (**5**) ($pK_a$ >12) are much more sensitive due to their higher $pK_a$. Both dyes show similar results. The following graph shows a measurement conducted with compound **1** in ethyl cellulose with $TOA^+OH^-$ on a PET foil in the range from 0 hPa to 100 hPa carbon dioxide. The sensor is not suitable for high $CO_2$ partial pressures and has long response times.

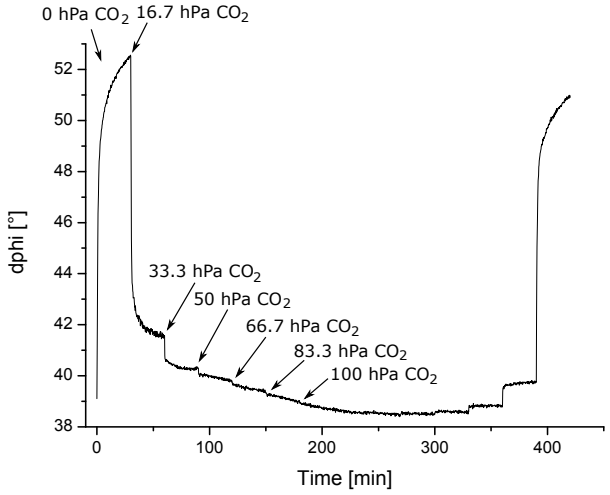


**Figure 4.30:** $CO_2$ measurements of a sensor film of m-OH azaBODIPY (**1**) in EC with $TOA^+OH^-$ on a PET support

Figure 4.31 shows the results of the same dye at lower carbon dioxide partial pressures up to only 50 hPa $CO_2$. From the graph it can be seen that the indicator would be better suitable for measuring even lower carbon dioxide concentrations of approximately 0 to 10 hPa $CO_2$.

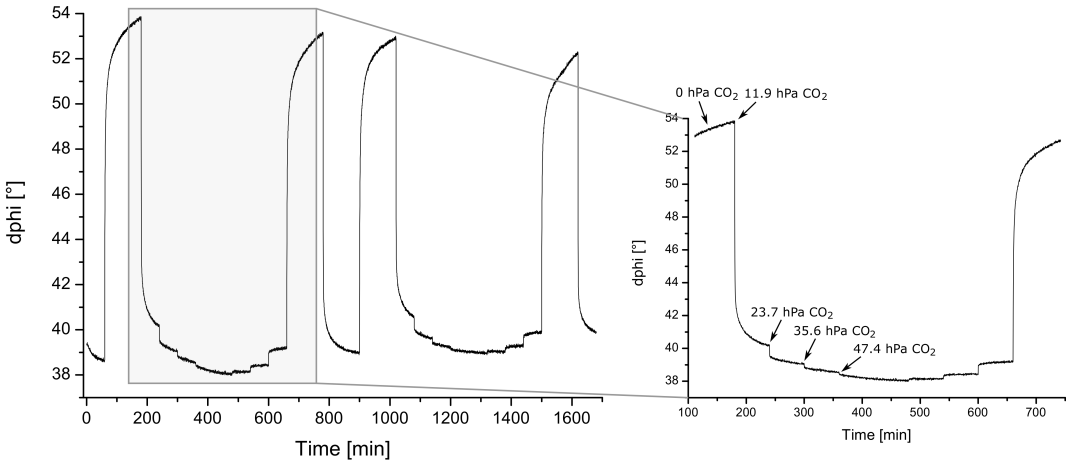


**Figure 4.31:** $CO_2$ measurements of a sensor film of m-OH azaBODIPY (**1**) in EC with $TOA^+OH^-$ on a PET support

The following data are obtained from a measurement of **1** and donor 1 (unsubstituted tetraphenyl azaBODIPY) in ethyl cellulose with $TOA^+OH^-$ and a Hyflon protection layer on

an untreated glass support (to realize a light harvesting sensor for increasing signal intensities and potentially reducing the film thickness of the sensor layer). The range of carbon dioxide partial pressure (ranging from 0 to approximately 2 hPa $CO_2$) seems to be suitable for the sensor. However, very long response times limit the application of such a sensor. Glass is broadly speaking a more suitable support material than PET because it has no carbon dioxide storage capacity. However, a drift of the signal may arise from a reaction of the base with the surface of the glass support. This issue may be reduced by pre-treatment (silanization) of the glass support.

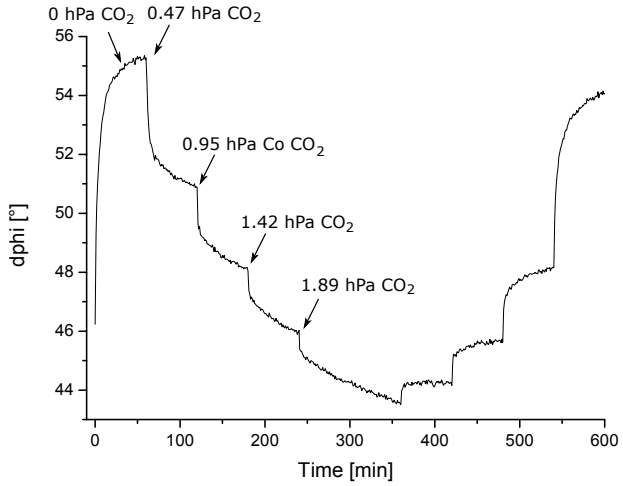


**Figure 4.32:** $CO_2$ measurements of a sensor film of m-OH azaBODIPY (**1**) in EC with $TOA^+OH^-$ on a glass support

To conclude, m-OH diF azaBODIPY with a $pK_a$ of 10.25 is a potentially suitable indicator for "plastic type" carbon dioxide sensors for applications in higher $CO_2$ concentrations, whereas m-OH azaBODIPY and m-OH MeO azaBODIPYs ($pK_a$ >11.5 and >12, respectively) are rather suitable in trace analysis of $CO_2$. PET as a support material is not universally applicable. A pre-treated glass support is preferable due to its better stability and no carbon dioxide uptake and storage. To further improve the performance of the $CO_2$ sensors, different matrix materials and protection layers should be examined to improve response time and reversibility.

# 5 Conclusion and Outlook

Within the scope of this work five new pH sensitive azaBODIPY dyes with different substitution patterns were synthesized successfully, starting from the corresponding benzaldehyde and acetophenone. The novel dyes exhibit good quantum yields (up to 27 %) and high molar absorption coefficients (approximately 73 000 to 90 000 $M^{-1}$ $cm^{-1}$). Absorption and emission spectra are in the far red/near infrared range with absorption maxima at approximately 690 nm and emission maxima at approximately 720 nm. Absorption and emission in this region of the light is preferential for many applications due to reduced background noise, higher signal-to-noise ratios and less scattering of excitation and emission light. [3, 51] The dyes exhibit pH independent absorption and emission spectra. pH sensing is enabled by PET (photoinduced electron transfer) quenching of fluorescence emission upon deprotonation of the hydroxy group of the indicator. These properties make the new PET-functionalized azaBODIPY dyes promising candidates for optical pH and carbon dioxide sensing for various applications in different pH and $CO_2$ ranges.

The $pK_a$' of the dyes was tuned by substitution with electron donating or electron withdrawing groups (including chlorine-, fluorine- and methoxy groups) on the phenyl group carrying the hydroxy group, resulting in dyes with $pK_a$' values ranging from approximately 7.8 to 12. The dyes with low $pK_a$', especially m-OH diCl azaBODIPY with a $pK_a$' of 7.8, represent ideal dyes for pH sensing in biology, marine monitoring or in medical applications. For further lowering the $pK_a$ of azaBODIPYs synthesis and characterization of trichloro or trifluoro dyes would have been interesting. However, synthesis of the corresponding benzaldehydes as educts was not successful.

The applicability of the new dyes as pH sensors was investigated in a hydrogel D4 matrix as well as covalently immobilized on a polymer matrix. A new strategy for immobilization of the dye on a copolymer (PAMcoHEAA) and on cellulose acetate propionate was achieved by activation of the B-F bond of the azaBODIPY core with boron trichloride and subsequent coupling to the polymer by formation of a new B-O bond. Substitution on the boron center of a similar class of dyes, of BODIPY dyes, can be found in multiple publications. [35–39] However, these reported reactions turn out to be less suitable for modifications of azaBODIPYs. Moreover, issues of reproducibility of the coupling reaction turned out to be a major problem. After optimization of the reaction conditions, PAMcoHEAA polymers with approximately 0.03 wt.% to 0.05 wt.% dye bound and cellulose acetate propionate with approximately 0.3 wt.% dye bound could be obtained by reaction of the dye with $BCl_3$.

The fluorescence properties of the new dyes were assumed to be less dependent on the concentration (compared to previously synthesized azaBODIPY dyes with similar structures [5, 6]) due to meta-hydroxy substitution and disconnection of the hydroxy group with the $\pi$-system of the azaBODIPY core. However, it was observed that fluorescence emission and $pK_a$ of the dyes is reduced when physically entrapped in higher concentrations in hydrogel D4. Quenching might be caused by FRET (Förster resonance energy transfer), however also errors caused by inner filter can not be neglected in this respect.

With a light harvesting approach of m-OH diCl azaBODIPY and a second (pH insensitive) antenna dye emission output could be increases significantly in a hydrogel matrix. Light is absorbed by a highly absorbing antenna dye (donor dye), the excitation energy is transferred to the pH sensitive acceptor dye, which in turn emits the light at higher wavelengths. By using a tetraphenyl azaBODIPY dye as donor and a donor-to-acceptor ration of 2 : 1 the emission can be increased fourfold in a D4 sensor film compared to a sensor film solely based on the acceptor dye m-OH diCl azaBODIPY. With this strategy emission output of sensors can be increased and extremely thin sensor layer with fast response times can be fabricated.

Compounds **1**, **4** and **5** (m-OH, m-OH diF and m-OH Meo azaBODIPY) turn out to be promising indicators in "plastic type" $CO_2$ sensors together with the quaternary ammonium compound tetraoctylammonium hydroxide due to their high $pK_a$ (>11.5, 10.25 and >12, respectively). Sensor films consisting of the dye and the base immobilized in a matrix of ethyl cellulose and a Hyflon protection layer show a reversible response to different $CO_2$ partial pressures. However, a pronounced drift of the signal can be observed. By optimizing the support material, matrix and protection layer compositions, hopefully better results could be achieved in the future.

# 6 References


1. Wencel, D., Abel, T. & McDonagh, C. Optical Chemical pH Sensors. *Analytical Chemistry* **86,** 15–29 (Jan. 2014).
2. McDonnell, S. O. & O'Shea, D. F. Near-Infrared Sensing Properties of Dimethlyamino-Substituted BF2-Azadipyrromethenes. *Organic Letters* **8,** 3493–3496 (Aug. 2006).
3. Killoran, J., McDonnell, S. O., Gallagher, J. F. & O'Shea, D. F. A substituted BF2-chelated tetraarylazadipyrromethene as an intrinsic dual chemosensor in the 650–850 nm spectral range. *New Journal of Chemistry* **32,** 483–489 (Mar. 2008).
4. Murtagh, J., Frimannsson, D. O. & O'Shea, D. F. Azide Conjugatable and pH Responsive Near-Infrared Fluorescent Imaging Probes. *Organic Letters* **11,** 5386–5389 (Dec. 2009).
5. Jokic, T., Borisov, S. M., Saf, R., Nielsen, D. A., Kühl, M. & Klimant, I. Highly Photostable Near-Infrared Fluorescent pH Indicators and Sensors Based on BF2-Chelated Tetraarylazadipyrromethene Dyes. *Analytical Chemistry* **84,** 6723–6730 (Aug. 2012).
6. Strobl, M., Rappitsch, T., Borisov, S. M., Mayr, T. & Klimant, I. NIR-emitting aza-BODIPY dyes – new building blocks for broad-range optical pH sensors. *Analyst* **140,** 7150–7153 (Oct. 2015).
7. Puligundla, P., Jung, J. & Ko, S. Carbon dioxide sensors for intelligent food packaging applications. *Food Control* **25,** 328–333 (May 2012).
8. Valeur, B. *Molecular fluorescence: principles and applications* (Wiley-VCH, Weinheim; New York, 2002).
9. Lakowicz, J. R. *Principles of fluorescence spectroscopy* 3rd ed (Springer, New York, 2006).
10. Albani, J. R. *Principles and applications of fluorescence spectroscopy* (Blackwell Science, Oxford; Ames, Iowa, 2007).
11. Zollinger, H. *Color chemistry: syntheses, properties, and applications of organic dyes and pigments* 3rd, rev. ed (Verlag Helvetica Chimica Acta; Wiley-VCH, Zürich, Weinheim, 2003).
12. Lakowicz, J. R. *Topics in fluorescence spectroscopy* (Springer, New York, 2002).
13. Crosby, G. A. & Demas, J. N. Measurement of photoluminescence quantum yields. Review. *The Journal of Physical Chemistry* **75,** 991–1024 (Apr. 1971).

14. Würth, C., Grabolle, M., Pauli, J., Spieles, M. & Resch-Genger, U. Relative and absolute determination of fluorescence quantum yields of transparent samples. *Nature Protocols* **8,** 1535–1550 (Aug. 2013).

15. Hulanicki, A., Glab, S. & Ingman, F. Chemical sensors: definitions and classification. *Pure and Applied Chemistry* **63,** 1247–1250 (1991).

16. Eggins, B. R. *Chemical sensors and biosensors* (J. Wiley, Chichester; Hoboken, NJ, 2002).

17. Cammann, K., Guibault, E. A., Hall, H., Kellner, R. & Wolfbeis, O. S. *The Cambridge definition of chemical sensors* in *Proceedings of the Cambridge workshop on chemical sensors and biosensors. Cambridge University Press, New York* (1996).

18. Gründler, P. *Chemische Sensoren: eine Einführung für Naturwissenschaftler und Ingenieure; mit 27 Tabellen* Softcover (Springer, Berlin, 2012).

19. Vasylevska, A. S., Karasyov, A. A., Borisov, S. M. & Krause, C. Novel coumarin-based fluorescent pH indicators, probes and membranes covering a broad pH range. *Analytical and Bioanalytical Chemistry* **387,** 2131–2141 (Mar. 2007).

20. De Silva, A. P., Moody, T. S. & Wright, G. D. Fluorescent PET (photoinduced electron transfer) sensors as potent analytical tools. *The Analyst* **134,** 2385–2393 (Dec. 2009).

21. Jung, H. S., Verwilst, P., Kim, W. Y. & Kim, J. S. Fluorescent and colorimetric sensors for the detection of humidity or water content. *Chemical Society Reviews* **45,** 1242–1256 (Feb. 2016).

22. Lee, M. H., Kim, J. S. & Sessler, J. L. Small molecule-based ratiometric fluorescence probes for cations, anions, and biomolecules. *Chemical Society Reviews* **44,** 4185–4191 (July 2015).

23. Wolfbeis, O. S. Materials for fluorescence-based optical chemical sensors. *Journal of Materials Chemistry* **15,** 2657–2669 (July 2005).

24. Kawabata, Y., Kamichika, T., Imasaka, T. & Ishibashi, N. Fiber-optic sensor for carbon dioxide with a ph indicator dispersed in a poly(ethylene glycol) membrane. *Analytica Chimica Acta* **219,** 223–229 (Jan. 1989).

25. Geddes, C. & Lakowicz, J. *Advanced Concepts in Fluorescence Sensing: Part A: Small Molecule Sensing* (Springer US, 2005).

26. Mills, A., Chang, Q. & McMurray, N. Equilibrium studies on colorimetric plastic film sensors for carbon dioxide. *Analytical Chemistry* **64,** 1383–1389 (July 1992).

27. Staudinger, C. & Borisov, S. M. Long-wavelength analyte-sensitive luminescent probes and optical (bio)sensors. *Methods and Applications in Fluorescence* **3,** 042005 (2015).

28. Huber, C., Klimant, I., Krause, C. & Wolfbeis, O. S. Dual lifetime referencing as applied to a chloride optical sensor. *Analytical Chemistry* **73,** 2097–2103 (May 2001).

29. Boniello, C., Mayr, T., Bolivar, J. M. & Nidetzky, B. Dual-lifetime referencing (DLR): a powerful method for on-line measurement of internal pH in carrier-bound immobilized biocatalysts. *BMC Biotechnology* **12,** 11 (Mar. 2012).

30. *New Trends in Fluorescence Spectroscopy Applications to Chemical and Life Sciences* (Springer Berlin Heidelberg, Berlin, Heidelberg, 2001).

31. Courtis, A. M., Santos, S. A., Guan, Y., Hendricks, J. A., Ghosh, B., Szantai-Kis, D. M., Reis, S. A., Shah, J. V. & Mazitschek, R. Monoalkoxy BODIPYs—A Fluorophore Class for Bioimaging. *Bioconjugate Chemistry* **25,** 1043–1051 (June 2014).

32. Goze, C., Ulrich, G., Mallon, L. J., Allen, B. D., Harriman, A. & Ziessel, R. Synthesis and Photophysical Properties of Borondipyrromethene Dyes Bearing Aryl Substituents at the Boron Center. *Journal of the American Chemical Society* **128,** 10231–10239 (Aug. 2006).

33. Goze, C., Ulrich, G. & Ziessel, R. Tetrahedral Boron Chemistry for the Preparation of Highly Efficient "Cascatelle" Devices. *The Journal of Organic Chemistry* **72,** 313–322 (Jan. 2007).

34. Gabe, Y., Ueno, T., Urano, Y., Kojima, H. & Nagano, T. Tunable design strategy for fluorescence probes based on 4-substituted BODIPY chromophore: improvement of highly sensitive fluorescence probe for nitric oxide. *Analytical and Bioanalytical Chemistry* **386,** 621–626 (Oct. 2006).

35. Lundrigan, T., M. Crawford, S., Stanley Cameron, T. & Thompson, A. Cl -BODIPYs: a BODIPY class enabling facile B -substitution. *Chemical Communications* **48,** 1003–1005 (2012).

36. Tahtaoui, C., Thomas, C., Rohmer, F., Klotz, P., Duportail, G., Mély, Y., Bonnet, D. & Hibert, M. Convenient Method To Access New 4,4-Dialkoxy- and 4,4-Diaryloxy-diaza-s-indacene Dyes: Synthesis and Spectroscopic Evaluation. *The Journal of Organic Chemistry* **72,** 269–272 (Jan. 2007).

37. Kubota, Y., Uehara, J., Funabiki, K., Ebihara, M. & Matsui, M. Strategy for the increasing the solid-state fluorescence intensity of pyrromethene–BF2 complexes. *Tetrahedron Letters* **51,** 6195–6198 (Nov. 2010).

38. Lundrigan, T. & Thompson, A. Conversion of F-BODIPYs to Cl-BODIPYs: Enhancing the Reactivity of F-BODIPYs. *The Journal of Organic Chemistry* **78,** 757–761 (Jan. 2013).

39. Tokoro, Y., Nagai, A. & Chujo, Y. Nanoparticles via H-aggregation of amphiphilic BODIPY dyes. *Tetrahedron Letters* **51,** 3451–3454 (June 2010).

40. Colbow, K. & Danyluk, R. P. Energy transfer in photosynthesis. *Biochimica et Biophysica Acta (BBA) - Bioenergetics* **440,** 107–121 (July 1976).

41. Nazeeruddin, M. K., Baranoff, E. & Grätzel, M. Dye-sensitized solar cells: A brief overview. *Solar Energy. Organic photovoltaics and dye sensitized solar cells* **85,** 1172–1178 (June 2011).

42. Masters, B. R. Paths to Förster's resonance energy transfer (FRET) theory. *The European Physical Journal H* **39,** 87–139 (Feb. 2014).

43. Mayr, T., Borisov, S. M., Abel, T., Enko, B., Waich, K., Mistlberger, G. & Klimant, I. Light Harvesting as a Simple and Versatile Way to Enhance Brightness of Luminescent Sensors. *Analytical Chemistry* **81,** 6541–6545 (Aug. 2009).

44. Ohkuma, S & Poole, B. Fluorescence probe measurement of the intralysosomal pH in living cells and the perturbation of pH by various agents. *Proceedings of the National Academy of Sciences of the United States of America* **75,** 3327–3331 (July 1978).

45. Han, J. & Burgess, K. Fluorescent Indicators for Intracellular pH. *Chemical Reviews* **110,** 2709–2728 (May 2010).

46. Hulth, S., Aller, R. C., Engström, P. & Selander, E. A pH plate fluorosensor (optode) for early diagenetic studies of marine sediments. *Limnology and Oceanography* **47,** 212–220 (Jan. 2002).

47. Ishihara, S., Labuta, J., Van Rossom, W., Ishikawa, D., Minami, K., Hill, J. P. & Ariga, K. Porphyrin-based sensor nanoarchitectonics in diverse physical detection modes. *Physical chemistry chemical physics: PCCP* **16,** 9713–9746 (June 2014).

48. Loudet, A. & Burgess, K. BODIPY Dyes and Their Derivatives: Syntheses and Spectroscopic Properties. *Chemical Reviews* **107,** 4891–4932 (Nov. 2007).

49. Loudet, A., Bandichhor, R., Wu, L. & Burgess, K. Functionalized BF2 chelated azadipyrromethene dyes. *Tetrahedron* **64,** 3642–3654 (Apr. 2008).

50. Ulrich, G., Ziessel, R. & Harriman, A. The chemistry of fluorescent bodipy dyes: versatility unsurpassed. *Angewandte Chemie (International Ed. in English)* **47,** 1184–1201 (2008).

51. Weissleder, R. A clearer vision for in vivo imaging. *Nature Biotechnology* **19,** 316–317 (Apr. 2001).

52. Ni, Y. & Wu, J. Far-red and near infrared BODIPY dyes: synthesis and applications for fluorescent pH probes and bio-imaging. *Organic & Biomolecular Chemistry* **12,** 3774–3791 (2014).

53. Schutting, S., Jokic, T., Strobl, M., M. Borisov, S., de Beer, D. & Klimant, I. NIR optical carbon dioxide sensors based on highly photostable dihydroxy-aza-BODIPY dyes. *Journal of Materials Chemistry C* **3,** 5474–5483 (2015).

54. Gorman, A., Killoran, J., O'Shea, C., Kenna, T., Gallagher, W. M. & O'Shea, D. F. In Vitro Demonstration of the Heavy-Atom Effect for Photodynamic Therapy. *Journal of the American Chemical Society* **126,** 10619–10631 (Sept. 2004).

55. Zach, P. W., Freunberger, S. A., Klimant, I. & Borisov, S. M. Electron-Deficient Near-Infrared Pt(II) and Pd(II) Benzoporphyrins with Dual Phosphorescence and Unusually Efficient Thermally Activated Delayed Fluorescence: First Demonstration of Simultaneous Oxygen and Temperature Sensing with a Single Emitter. *ACS Applied Materials & Interfaces* **9,** 38008–38023 (Nov. 2017).

56. Hall, M. J., McDonnell, S. O., Killoran, J. & O'Shea, D. F. A Modular Synthesis of Unsymmetrical Tetraarylazadipyrromethenes. *The Journal of Organic Chemistry* **70,** 5571–5578 (July 2005).

57. Grossi, M., Palma, A., McDonnell, S. O., Hall, M. J., Rai, D. K., Muldoon, J. & O'Shea, D. F. Mechanistic Insight into the Formation of Tetraarylazadipyrromethenes. *The Journal of Organic Chemistry* **77,** 9304–9312 (Oct. 2012).

58. Gerrard, W. & Lappert, M. F. Reactions Of Boron Trichloride With Organic Compounds. *Chemical Reviews* **58,** 1081–1111 (Dec. 1958).

59. Liptak, M. D., Gross, K. C., Seybold, P. G., Feldgus, S. & Shields, G. C. Absolute pKa Determinations for Substituted Phenols. *Journal of the American Chemical Society* **124,** 6421–6427 (June 2002).

60. Müller, B. J., Borisov, S. M. & Klimant, I. Red- to NIR-Emitting, BODIPY-Based, K+-Selective Fluoroionophores and Sensing Materials. *Advanced Functional Materials* **26,** 7697–7707 (Nov. 2016).

61. Borisov, S. M., Würth, C., Resch-Genger, U. & Klimant, I. New life of ancient pigments: application in high-performance optical sensing materials. *Analytical Chemistry* **85,** 9371–9377 (Oct. 2013).

# 7 List of Figures

# 8 List of Tables

# 9 Appendix

## 9.1 Chemicals and materials

**Table 9.1:** Used chemicals

| chemicals | abbr. | supplier | CAS number |
|---|---|---|---|
| 2,4-dichloro-3-hydroxybenzaldehyde | | Fluorochem | 56962-13-1 |
| 2,6-difluoro-3-hydroxybenzaldehyde | | Fluorochem | 152434-88-3 |
| 2-chloro-3-hydroxybenzaldehyde | | Sigma-Aldrich | 56962-10-8 |
| 3-hydroxybenzaldehyde | | TCI | 100-83-4 |
| 4'-butoxyacetophenone | | TCI | 5736-89-0 |
| 4'-methoxyacetophenone | | TCI | 100-06-1 |
| 4-acryloylmorpholine | | Sigma-Aldrich | 5117-12-4 |
| acetyl chloride | | Fluka | 75-36-5 |
| ammonium acetate | | Merck | 631-61-8 |
| boron trichloride (1.0 M solution in toluene) | $BCl_3$ | Sigma-Aldrich | 10294-34-5 |
| boron trifluoride diethyl etherate | | Sigma-Aldrich | 109-63-7 |
| cellulose acetate propionate | CAP | Acros Organics | 9004-39-1 |
| DESMODUR N 75 MPA/X | DESMODUR | Covestro | |
| di-n-butlydilauryltin | | ABCR | 77-58-7 |
| hexaethylene glycol | HEG | Sigma-Aldrich | 2615-15-8 |
| hydrochloric acid | HCl | Merck | 7647-01-0 |
| isovanillin | | TCI | 621-59-0 |
| *N*,*N*-diisopropylethylamine | | TCI | 7087-68-5 |
| *N*-hydroxyethyl acrylamide | | Sigma-Aldrich | 7646-67-5 |
| nitromethane | | Sigma-Aldrich | 75-52-5 |
| *p*-anisaldehyde | | TCI | 123-11-5 |
| poly(1-vinylpyrrolidone-co-styrene) | | Sigma-Aldrich | 25086-29-7 |
| potassium hydroxide | KOH | Merck | 1310-58-3 |
| potassium peroxodisulfate | | Roth | 7727-21-1 |
| sodium chloride | NaCl | Merck | 7647-14-5 |
| sodium hydrogen carbonate | $NaHCO_3$ | Merck | 144-55-8 |
| sodium hydroxide | NaOH | Merck | 1310-73-2 |
| sodium sulfate | $Na_2SO_4$ | Merck | 7757-82-6 |
| tetraoctylammonium hydroxide solution (20 % in MeOH) | $TOA^+OH^-$ | Sigma-Aldrich | 17756-58-0 |
| triethylamine | TEA | Roth | 121-44-8 |
| trifluoroacetic acid | TFA | Fluka | 76-05-1 |
| trimethylsilyltrifluormethansulfonat | TMSOTf | Sigma-Aldrich | 27607-77-8 |

**Table 9.2:** Used solvents

| solvents | abbr. | supplier | CAS number |
|---|---|---|---|
| 1-butanol | BuOH | TCI | 71-36-3 |
| acetone | | VWR Chemicals | 67-64-1 |
| chloroform-d | $CDCl_3$ | Euriso-top | 865-49-6 |
| cyclohexane | CH | VWR Chemicals | 110-82-7 |
| dichloromethane | DCM | Fisher Chemical | 75-09-2 |
| dioxane | dioxane | Fluka | 123-91-1 |
| dimethyl sulfoxide | DMSO | Sigma-Aldrich | 67-68-5 |
| ethanol | EtOH | VWR Chemicals | 64-17-5 |
| ethyl acetate | EA | VWR Chemicals | 141-78-6 |
| methanol | MeOH | VWR Chemicals | 67-56-1 |
| perfluordecalin | PFD | ABCR | 306-94-5 |
| tetrahydrofuran | THF | Roth | 109-99-9 |
| toluene | Tol | VWR Chemicals | 108-88-3 |

Dry, water-free solvents were prepared by storage under inert atmosphere over 4 Å molecular sieve.

**Table 9.3:** Used buffer substances

| buffer | supplier | CAS number |
|---|---|---|
| bis-TRIS | Roth | 6976-37-0 |
| CAPS | Roth | 1135-40-6 |
| CHES | Roth | 103-47-9 |
| MES | Roth | 4432-31-9 |
| piperazine | Sigma-Aldrich | 110-85-0 |
| TRIS | Merck | 77-86-1 |

**Table 9.4:** Used gases

| gas | supplier |
|---|---|
| $CO_2$ | Linde gas |
| test gas (20 % $CO_2$, rest $N_2$) | Linde gas |
| test gas (5 % $CO_2$, rest $N_2$) | Linde gas |
| test gas (0.2 % $CO_2$, rest $N_2$) | Linde gas |
| $N_2$ | Linde gas |

**Table 9.5:** Used materials

| **chemicals** | **abbr.** | **supplier** |
|---|---|---|
| ALUGRAM® aluminium sheets, Alox N/UV$_{254}$, 0.20 mm | | Macherey-Nagel |
| aluminum oxide, neutral, Brockmann I, 50 - 200 µm, 60 Å | Alox | Acros |
| aluminum TLC plates, silica gel 60 F$_{254}$ | | Merck |
| ethyl cellulose (ethyloxy content 50 %) | EC | Scientific Polymer |
| hydromed® D4 | D4 | AdvanSource biomaterials |
| hyflon® AD 60 | hyflon | Solvay |
| PET foil Melinex® 125 µm | | Pütz Folien |
| silica gel 60 (0.04 - 0.063 mm, 60 Å) | | Roth |

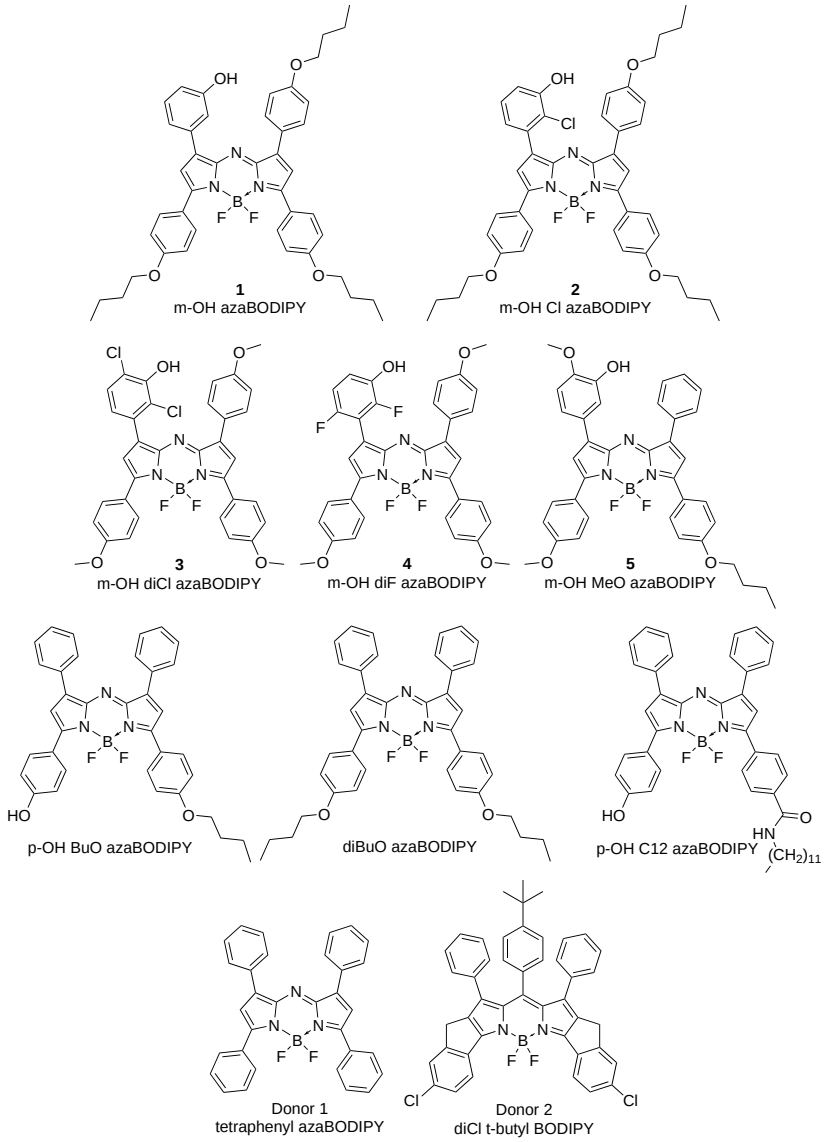


**Figure 9.1:** Structures of all synthesized dyes (compounds **1-5**) and used BODIPY and azaBODIPY dyes*

**Table 9.6:** Used dyes

| **dye** | **abbr.** |
|---|---|
| m-OH azaBODIPY | compound 1 |
| m-OH Cl azaBODIPY | compound 2 |
| m-OH diCl azaBODIPY | compound 3 |
| m-OH diF azaBODIPY | compound 4 |
| m-OH MeO azaBODIPY | compound 5 |
| p-OH BuO azaBODIPY* | |
| diBuO azaBODIPY* | |
| p-OH C12 azaBODIPY* | |
| tetraphenyl azaBODIPY* | donor 1 |
| diCl t-butyl BODIPY* | donor 2 |
| Egyptian blue* | |

*Dyes p-OH BuO azaBODIPY, diBuO azaBODIPY, p-OH C12 azaBODIPY and tetraphenyl azaBODIPY were synthesized by Martin Strobl according to literature [6], diCl t-butyl BODIPY was synthesized by Matthias Schwar according to literature [60]. Egyptian blue was synthesized according to literature [61].

## 9.2 NMR data

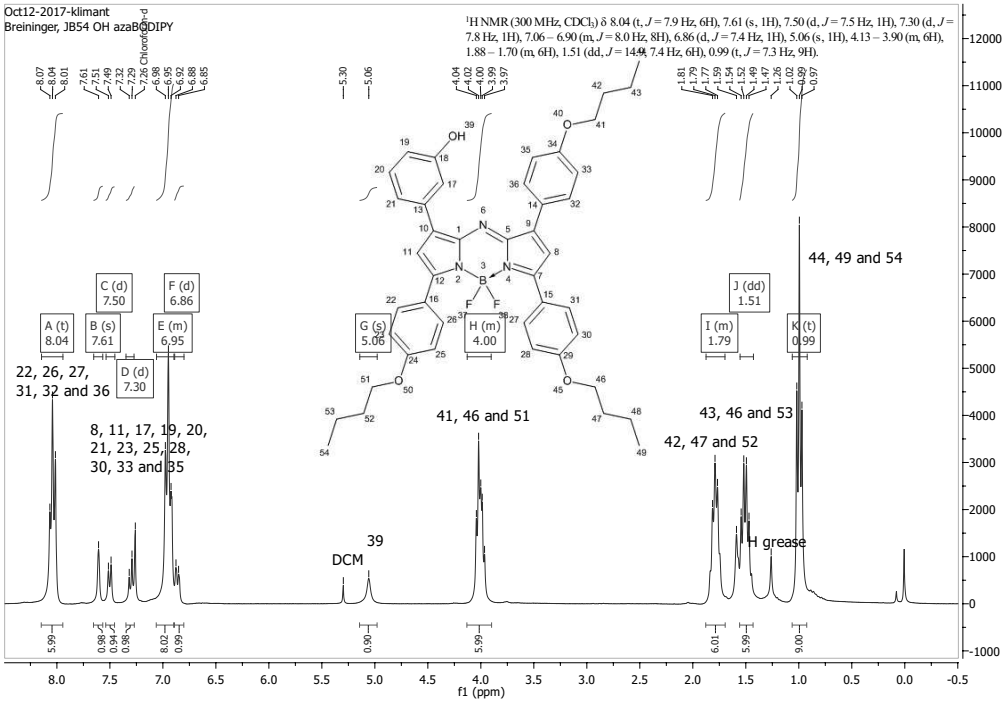


**Figure 9.2:** $^{1}$H NMR spectrum of compound **1** (m-OH azaBODIPY) in chloroform-d

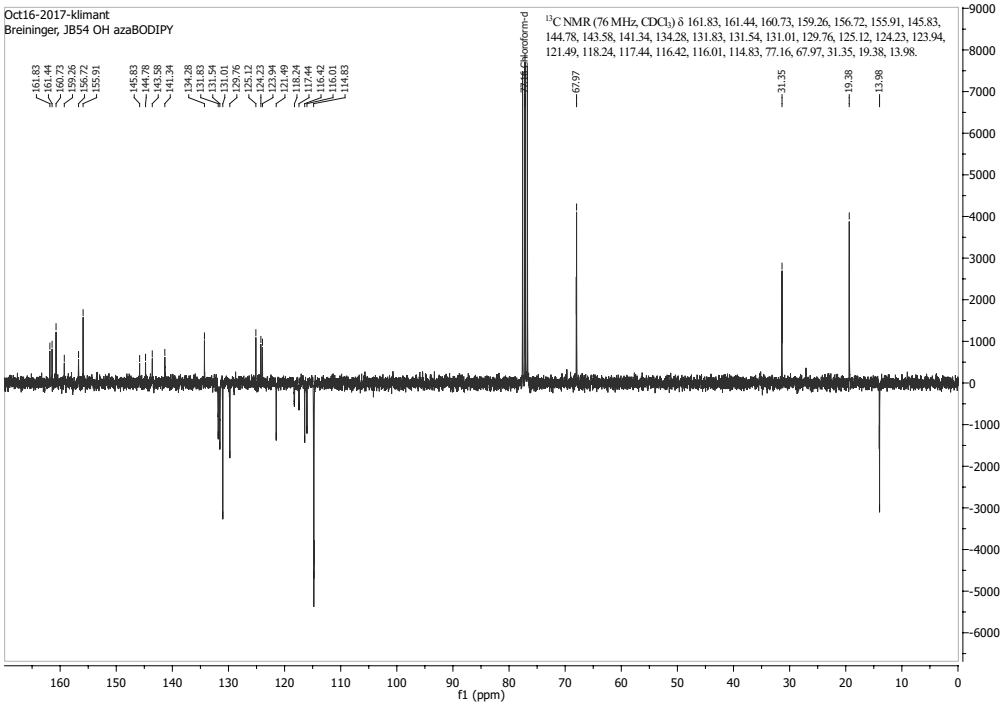


**Figure 9.3:** APT NMR spectrum of compound **1** (m-OH azaBODIPY) in chloroform-d

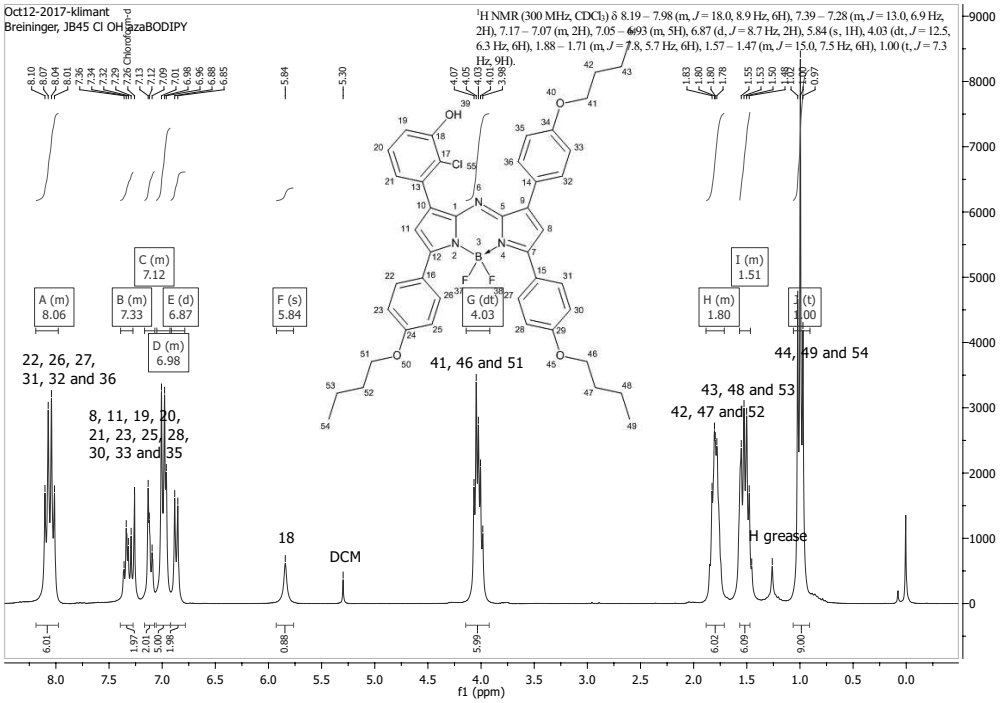


**Figure 9.4:** $^{1}$H NMR spectrum of compound **2** (m-OH Cl azaBODIPY) in chloroform-d

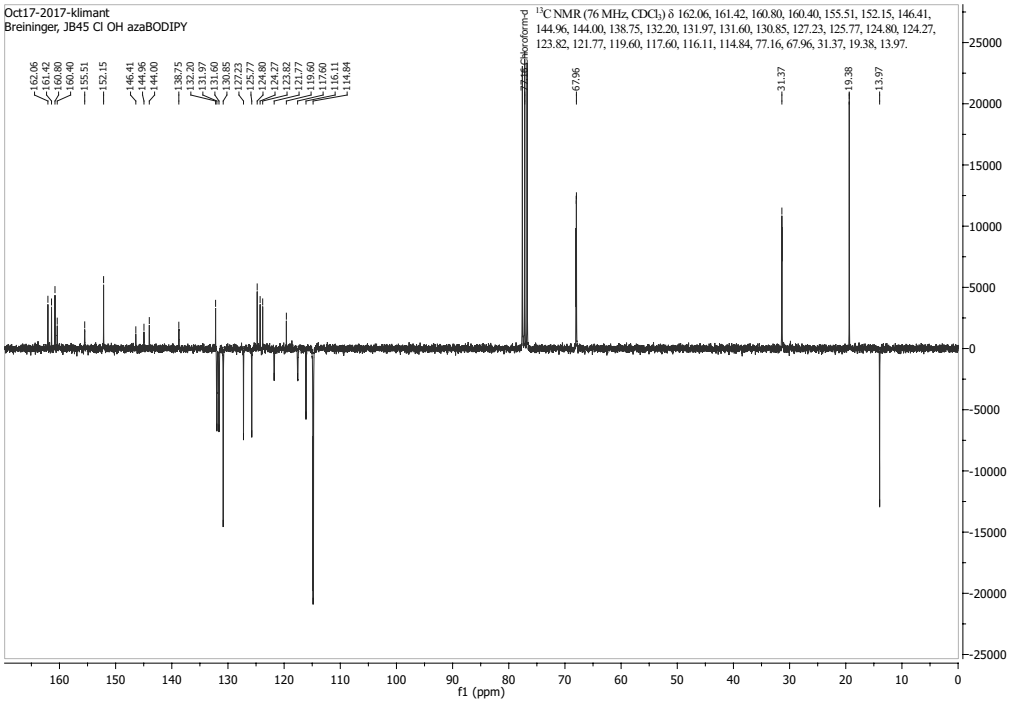


**Figure 9.5:** APT NMR spectrum of compound **2** (m-OH Cl azaBODIPY) in chloroform-d

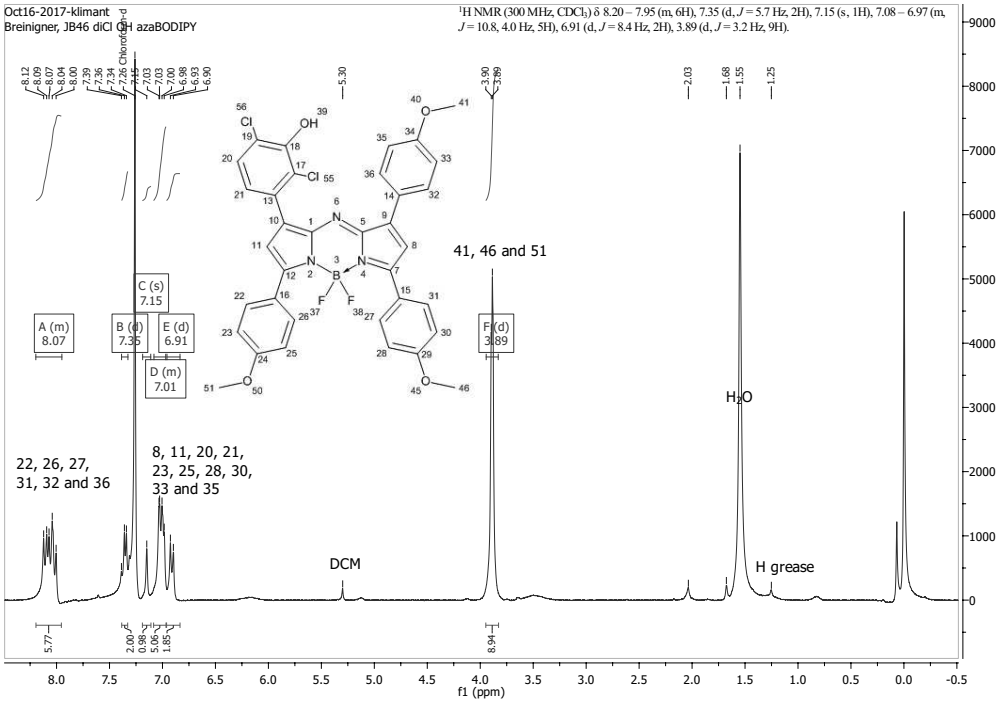


**Figure 9.6:** $^1$H NMR spectrum of compound **3** (m-OH diCl azaBODIPY) in chloroform-d

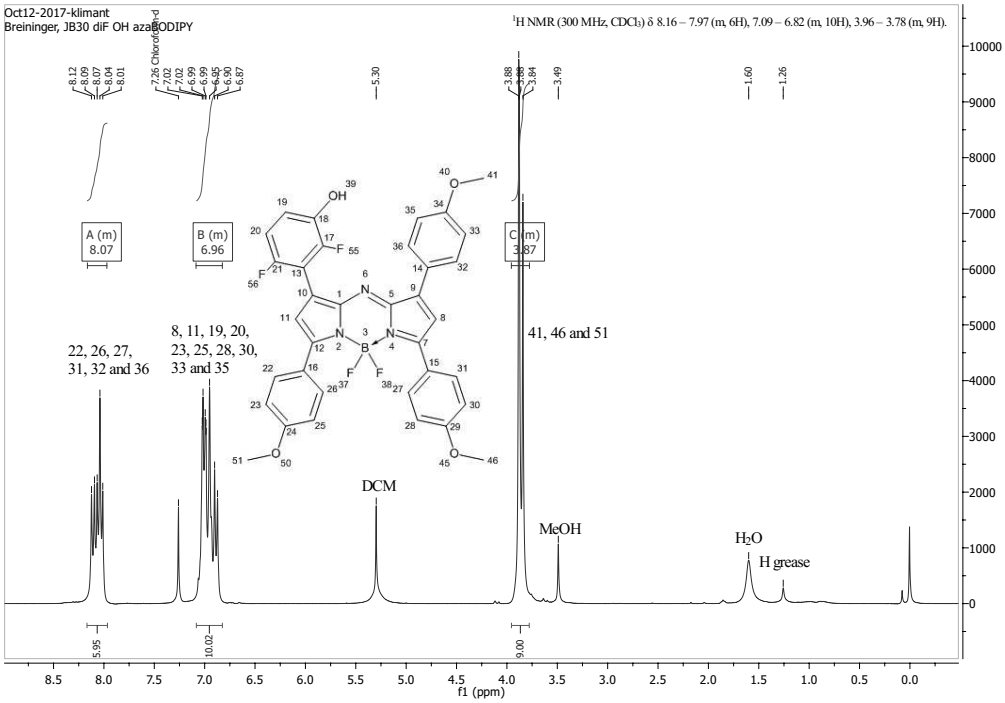


**Figure 9.7:** $^1$H NMR spectrum of compound **4** (m-OH diF azaBODIPY) in chloroform-d

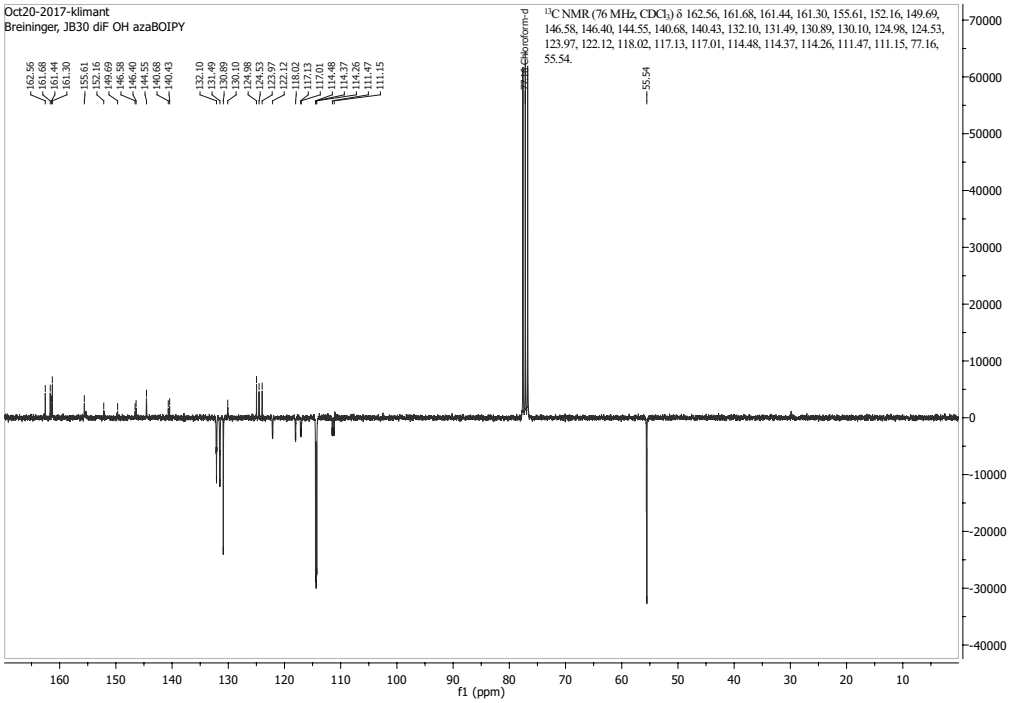


**Figure 9.8:** APT NMR spectrum of compound **4** (m-OH diF azaBODIPY) in chloroform-d

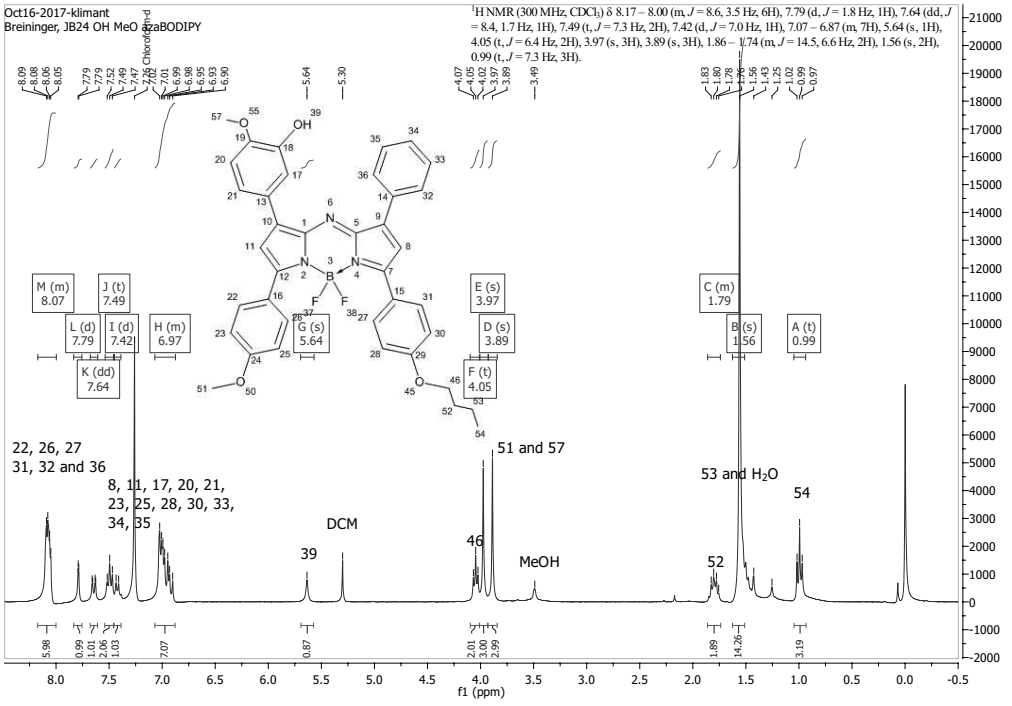


**Figure 9.9:** $^{1}$H NMR spectrum of compound **5** (m-OH MeO azaBODIPY) in chloroform-d

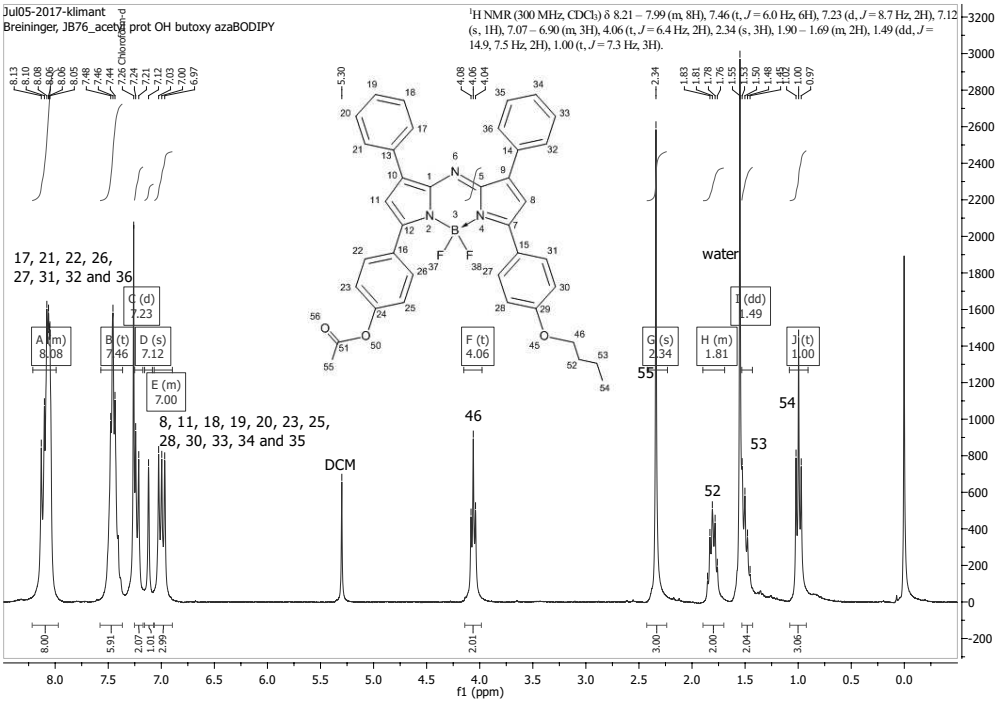


**Figure 9.10:** $^1$H NMR spectrum of acetyl protected p-OH BuO azaBODIPY in chloroform-d

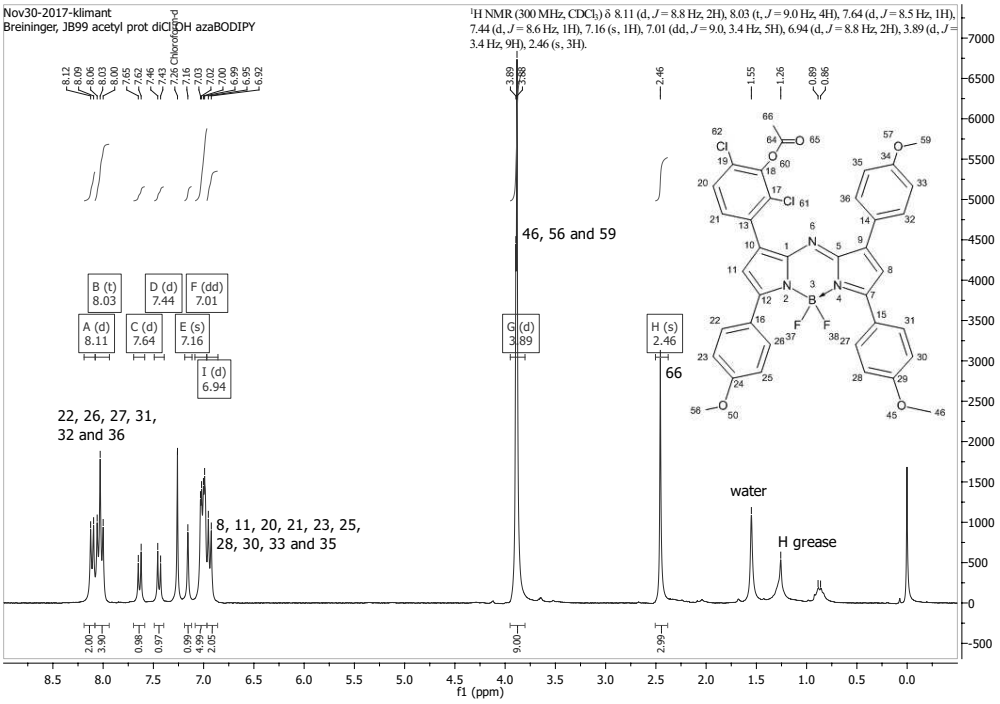


**Figure 9.11:** $^1$H NMR spectrum of acetyl protected m-OH diCl azaBODIPY in chloroform-d

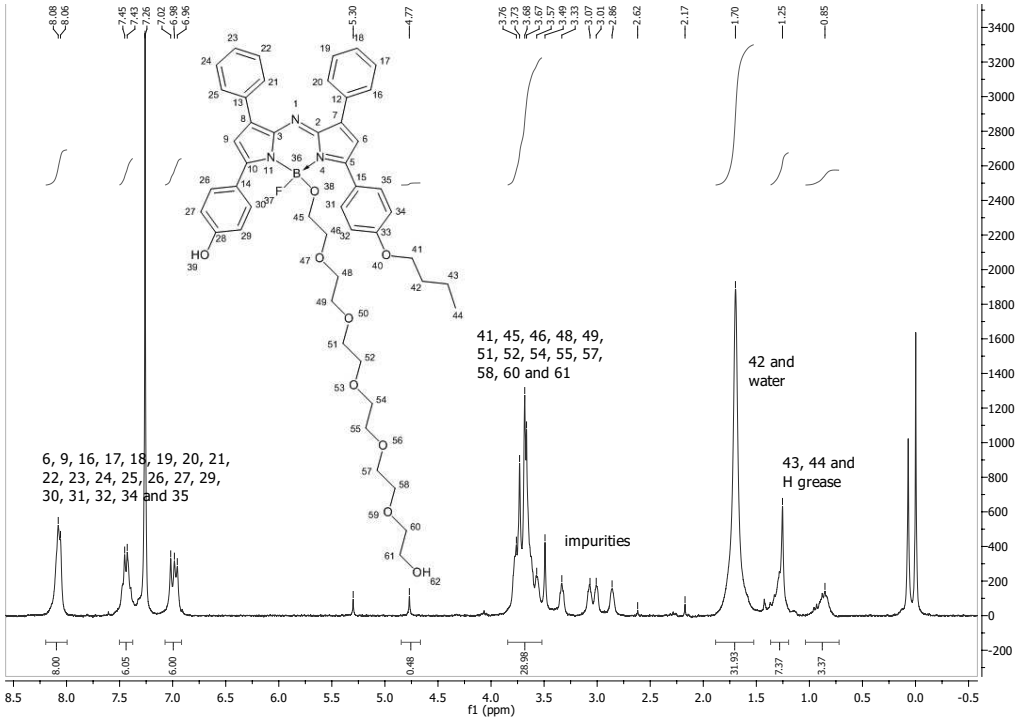


**Figure 9.12:** $^{1}$H NMR spectrum of the coupling product of OH BuO azaBODIPY with HEG in chloroform-d

## 9.3 HR-MS data

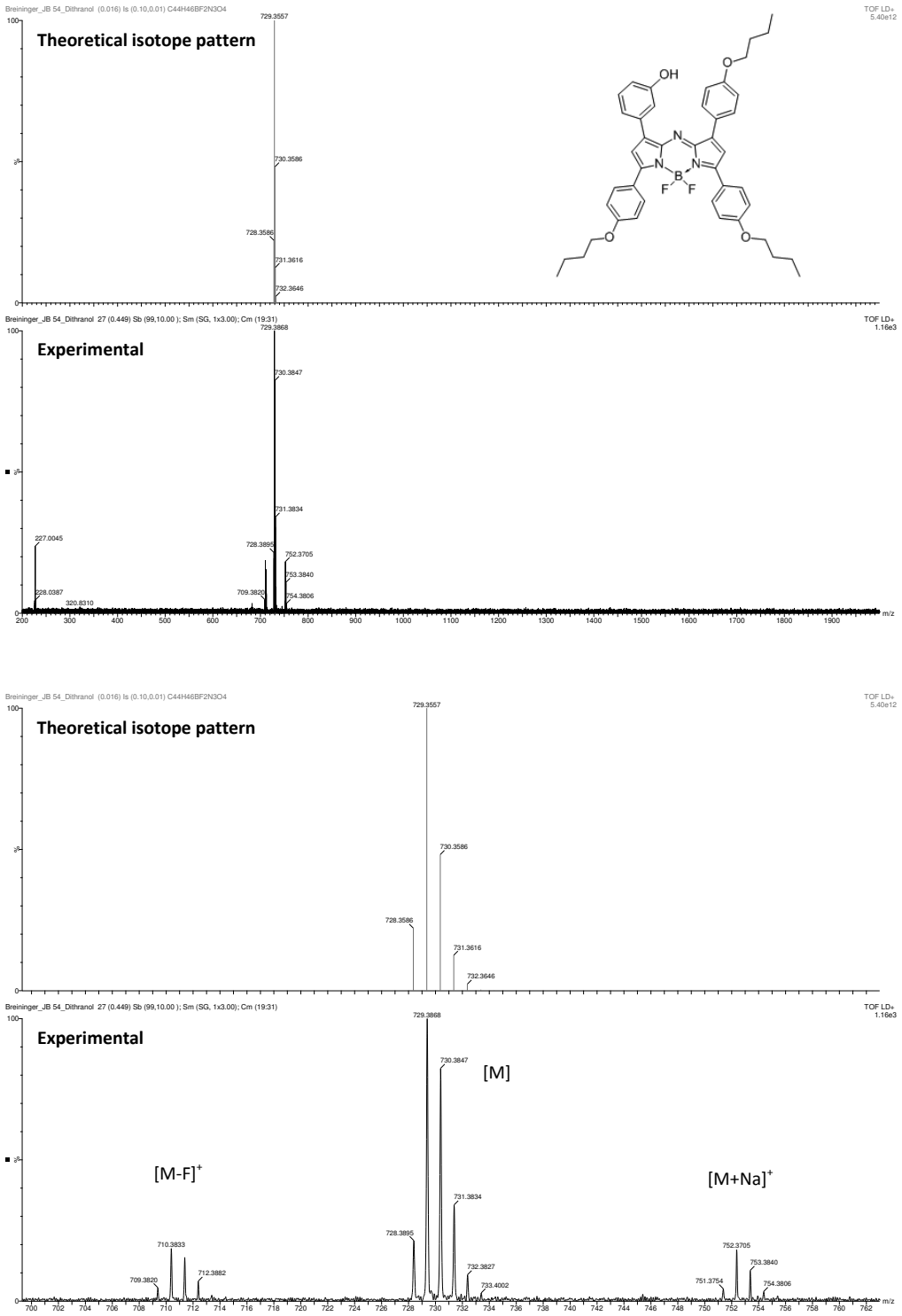


**Figure 9.13:** MALDI-TOF spectrum of compound **1** (m-OH azaBODIPY) in a dithranol matrix with the corresponding isotope pattern

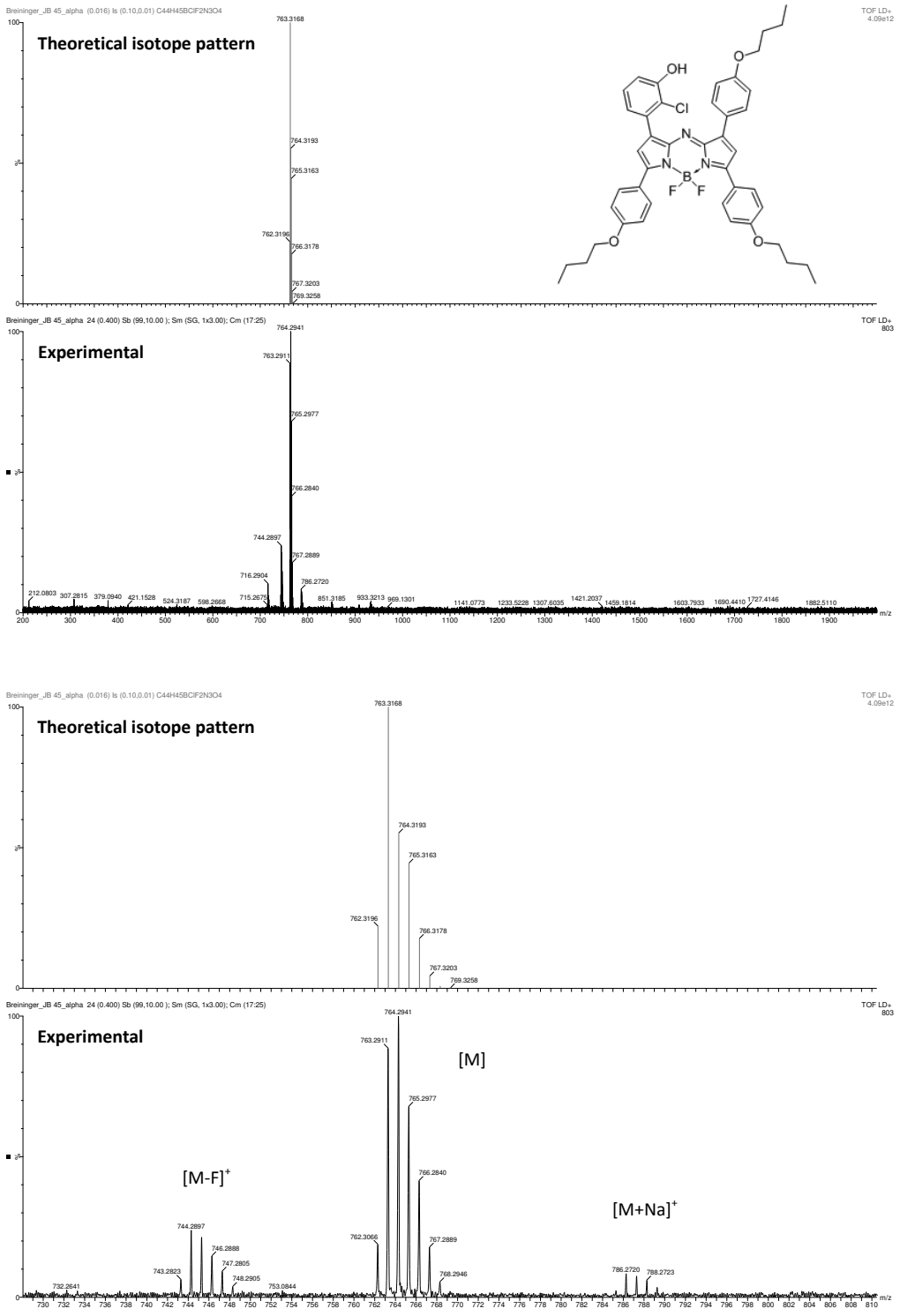


**Figure 9.14:** MALDI-TOF spectrum of compound **2** (m-OH Cl azaBODIPY) in a dithranol matrix with the corresponding isotope pattern

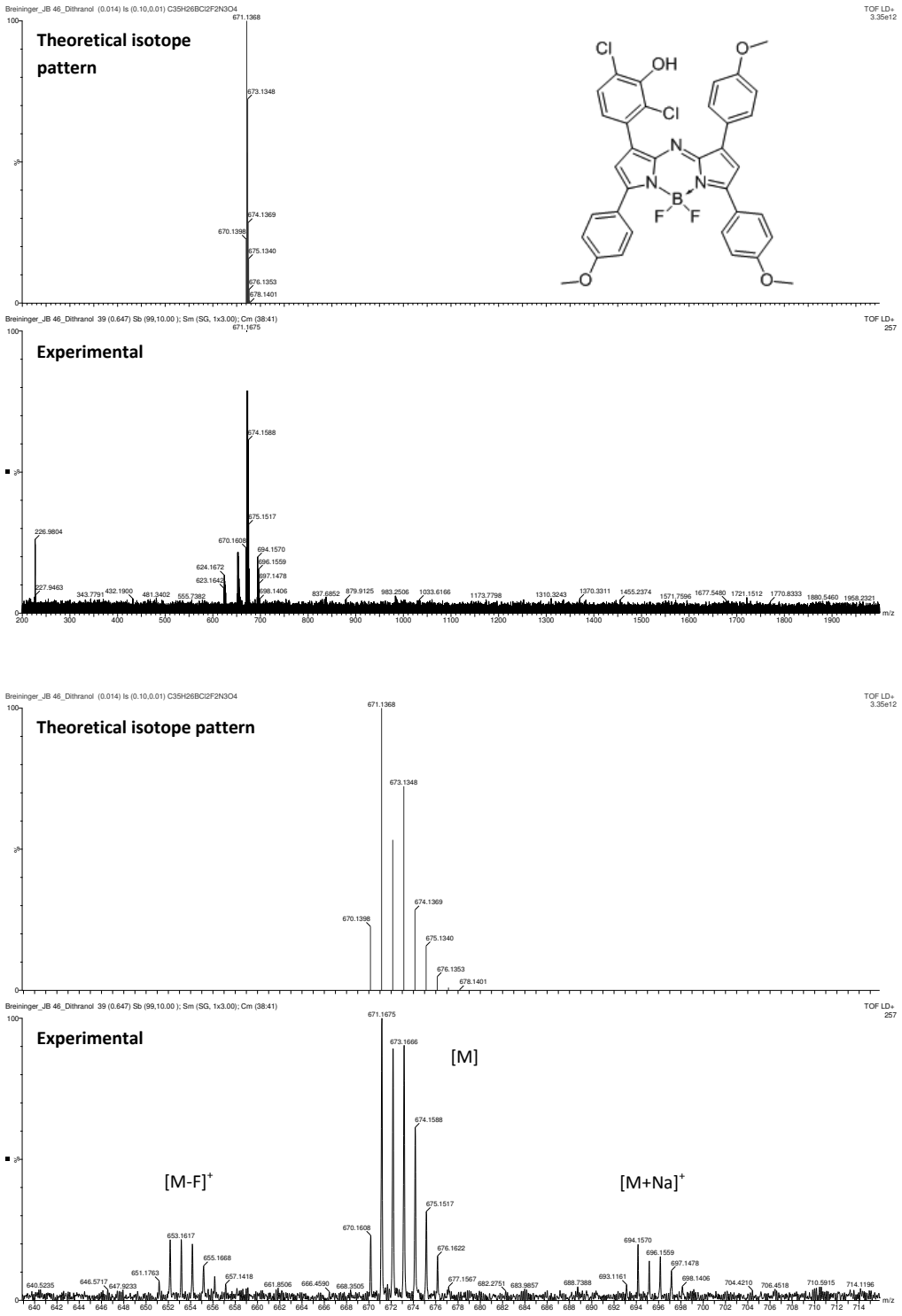


**Figure 9.15:** MALDI-TOF spectrum of compound **3** (m-OH diCl azaBODIPY) in a dithranol matrix with the corresponding isotope pattern

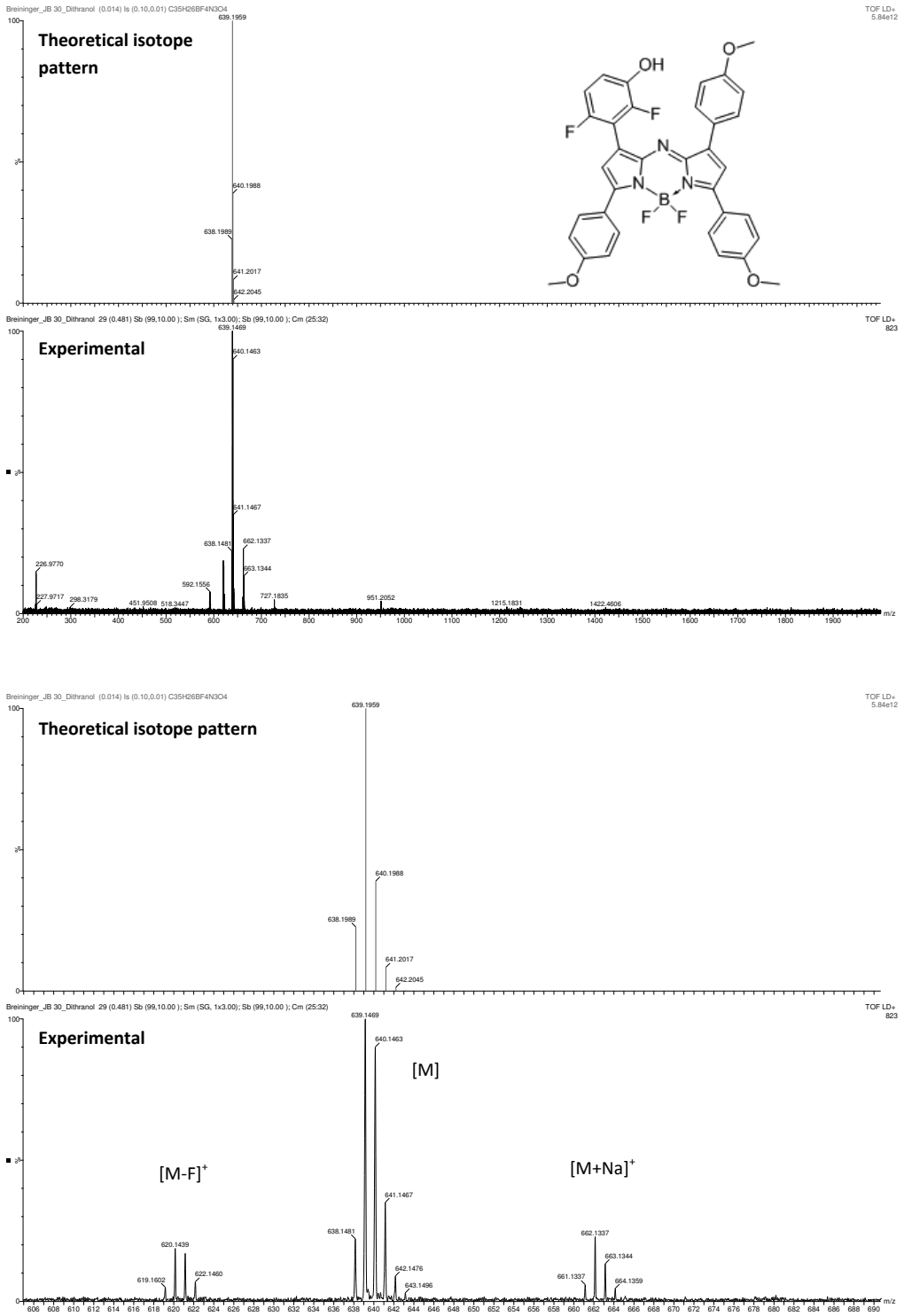


**Figure 9.16:** MALDI-TOF spectrum of compound **4** (m-OH diF azaBODIPY) in a dithranol matrix with the corresponding isotope pattern

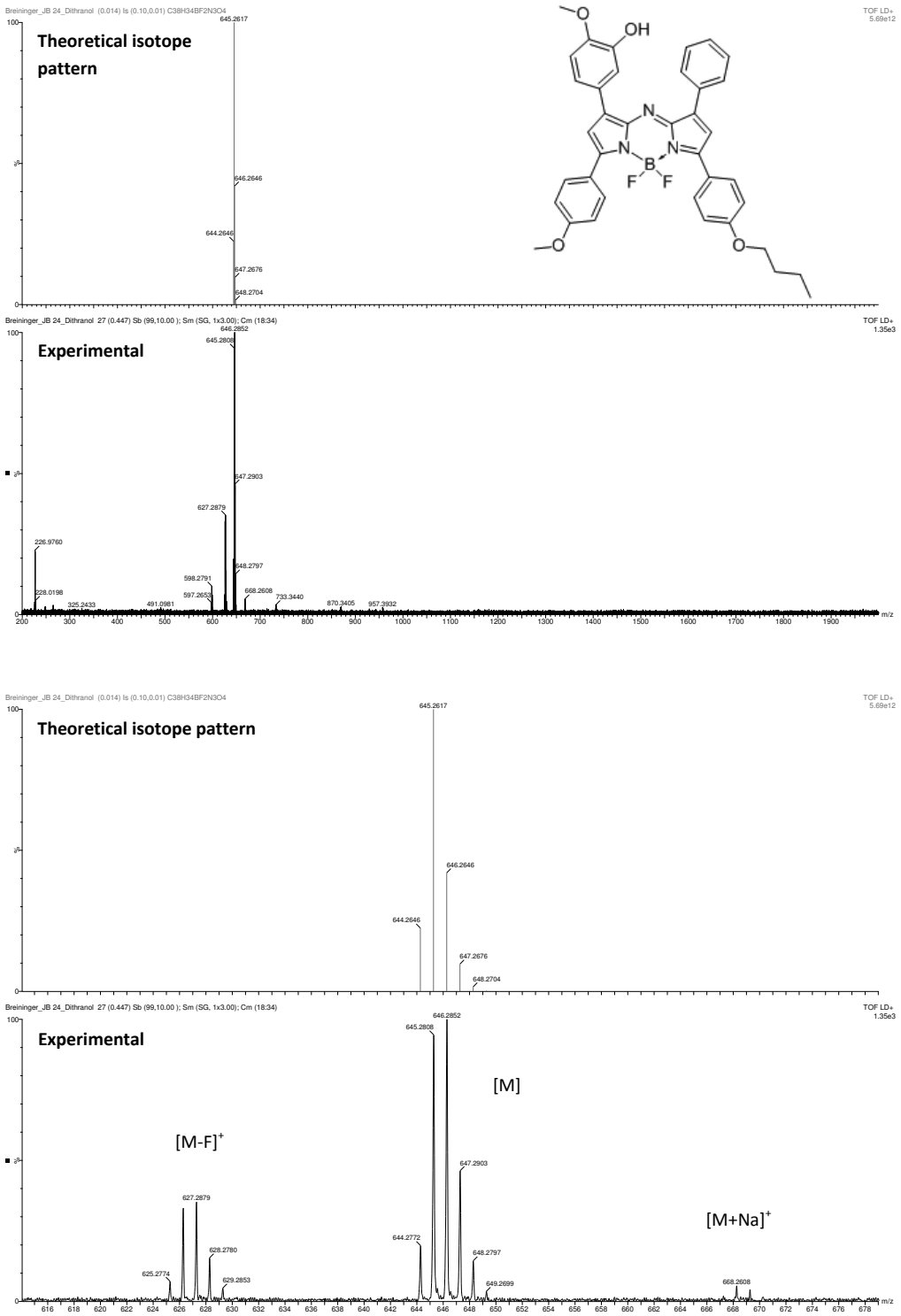


**Figure 9.17:** MALDI-TOF spectrum of compound **5** (m-OH MeO azaBODIPY) in a dithranol matrix with the corresponding isotope pattern

## 9.4 TCSPC lifetime measurements

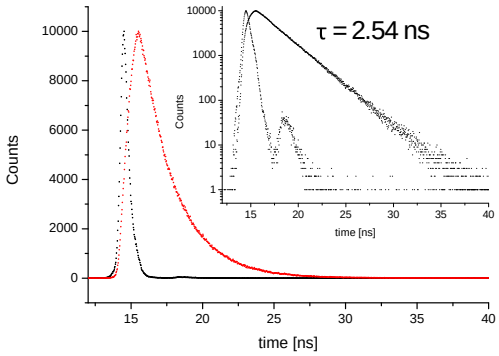


(a) Lifetime of compound **1** in THF

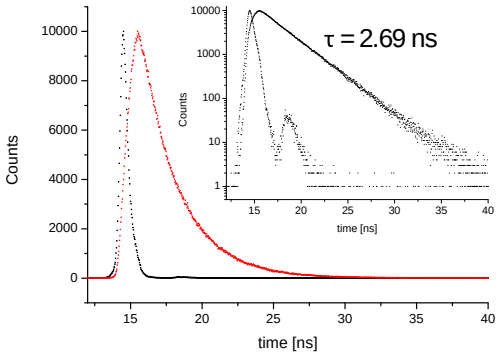


(b) Lifetime of compound **2** in THF

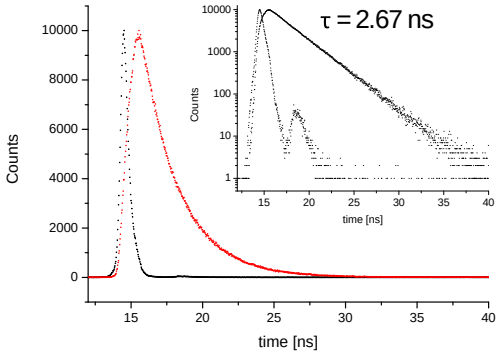


(c) Lifetime of compound **4** in THF

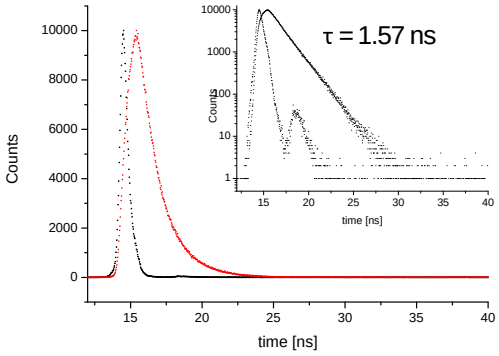


(d) Lifetime of compound **5** in THF

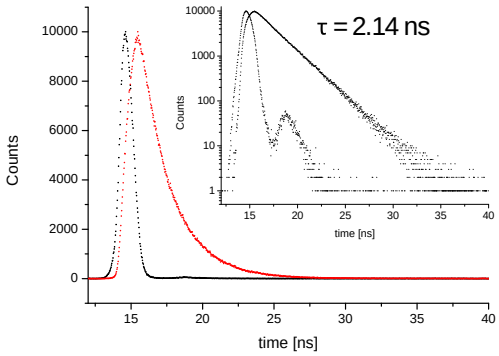


(e) Lifetime of compound p-OH C12 azaBODIPY in THF

**Figure 9.18:** Lifetimes of compound **1**, **2**, **4**, **5** and p-OH C12 azaBODIPY in THF measured via TCSPC

## 9.5 Other spectra

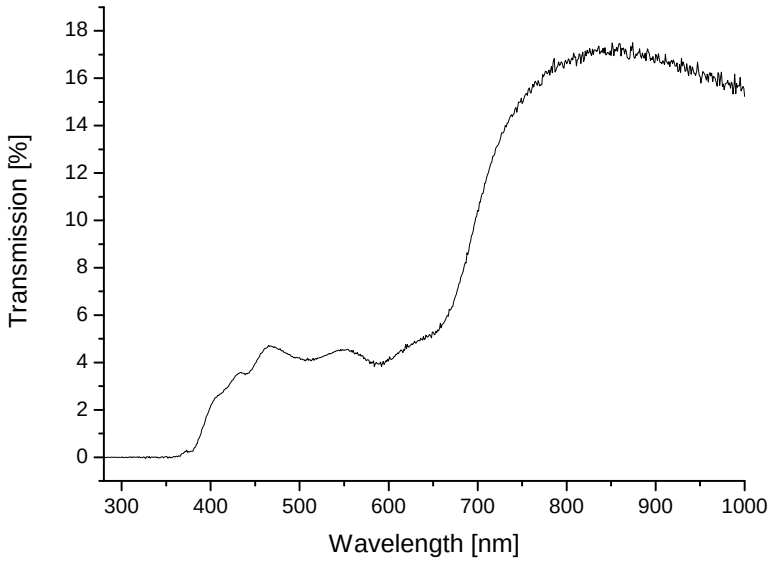


**Figure 9.19:** Actual transmission of the used neutral density 5 % transmission filter